MOLECULAR RECOGNITION EVENTS IN POLYMER-BASED SYSTEMS

By RABIA MATEEN, B.Sci., M.A.Sc

A Thesis Submitted to the School of Graduate Studies in Partial Fulfillment of the Requirements for the Degree
Doctor of Philosophy
McMaster University
©Copyright by Rabia Mateen, January 2019

McMaster University DOCTOR OF PHILOSOPHY (2019) Hamilton, Ontario (Biomedical Engineering)

TITLE: Molecular Recognition Events in Polymer-Based Systems

AUTHOR: Rabia Mateen, B.Sc, M.A.Sc (McMaster University)

SUPERVISOR: Professor Todd Hoare

NUMBER OF PAGES: xx, 164

Lay Abstract

This thesis describes the development of polymer-based materials that exploit molecular recognition events for drug delivery and biosensing applications. First, cyclodextrins (CDs) are molecules that are capable of binding a wide range of small molecules. A comprehensive analysis of the complexation properties of CD derivatives revealed critical insight regarding their application in polymer-based drug delivery vehicles. Second, a printable hydrogel platform was developed to support the immobilization and activity of biomolecules and establish a biosensing interface that facilitates the diffusion of small molecules but not molecular aggregates. A microarray-based assay was developed by employing the printed hydrogel interface for the screening of inhibitors of the model enzyme, β-lactamase, and the detection of DNA hybridization events.

Abstract

Molecular recognition is an important tool for developing tunable controlled release systems and fabricating biosensors with increased selectivity and sensitivity. The development of polymer-based materials that exploit molecular recognition events such as host-guest complexation, enzyme-substrate and enzyme-inhibitor interactions and nucleic acid hybridization was pursued in this thesis. Using polymers as an anchor for molecular recognition can enhance the affinity, selectivity, and the capacity for immobilization of recognition units, enabling the practical use of affinity-based systems in real applications.

To introduce the potential for immobilization while preserving or enhancing the affinity of small molecule recognition units, the affinity of derivatized cyclodextrins for the hydrophobic drug, dexamethasone, was investigated. Cyclodextrins (CDs) are molecules that possess a hydrophilic exterior and a hydrophobic cavity capable of accommodating a wide range of small molecule guests. Analysis of the solubilization capacities, thermodynamic parameters and aggregative potentials of carboxymethyl and hydrazide derivatives of CDs established the dextran-conjugated βCD derivative as an ideal carrier of hydrophobic drugs and the hydrazide βCD derivative as an optimal solubilizer of lipophilic pharmaceuticals, both alone and when incorporated in a polymer-based drug delivery vehicle.

To enable non-covalent immobilization and stabilization of biomacromolecular recognition units, a printed layer hydrogel was investigated as a selective diffusion barrier for analyte sensing and enzyme inhibitor recognition. A printable hydrogel platform was developed from an established injectable system composed of aldehyde- and hydrazide-functionalized poly(oligoethylene glycol methacrylate) polymers. The printed layer hydrogel effectively immobilized a wide range of enzymes and protected enzyme activity against time-dependent and protease-induced denaturation, while facilitating the diffusion of small molecules. Furthermore, to demonstrate the potential of the printed film hydrogel immobilization layer to enhance the selectivity of the target, the printable hydrogel platform was used to develop a microarray-based assay for the screening of inhibitors of the model enzyme, β-lactamase. The assay was able to accurately quantify dose-response relationships of a series of established inhibitors, while reducing the required reagent volumes in traditional drug screening campaigns by 95%. Most significantly,

the assay demonstrated an ability to discriminate true inhibitors of β-lactamase from a class of non-specific inhibitors called promiscuous aggregating inhibitors.

Finally, to enable non-covalent immobilization of DNA recognition units, the printable hydrogel-based microarray was tested for its ability to immobilize DNA recognition sites and promote the detection of DNA hybridization events. A long, concatameric DNA molecule was generated through rolling circle amplification and was used as a sensing material for the detection of a small, fluorophore labeled oligonucleotide. The printable hydrogel was able to effectively entrap the rolling circle amplification product. Properties of the printable hydrogel were investigated for their ability to support the detection of DNA hybridization events.

Acknowledgements

I would like to thank Professor Todd Hoare for the support and guidance provided over the course of my PhD research. Over the years, your recommendations have helped advance my abilities as both a researcher and technical writer.

Drs. Yingfu Li and Carlos Filipe are acknowledged for the advice given during my supervisory committee meetings. Thank you to Dr. Monsur Ali for your helpful suggestions that contributed to the success of the hydrogel microarray project. Dr. Glynis de Silveira is acknowledged for acquiring the SEM images that were used in this project, as well as for the profound discussions on research and graduate student life. I would also like to thank Dr. Kha Tram for designing the sequences in the RCA printing project and for kindly providing the necessary training for the experimental procedures.

Thank you to members of the Hoare lab for your kindness and technical assistance. In particular, I would like to acknowledge Fei Xu for generously helping me with the high-throughput robot and confocal microscope. Thank you to the original Hoare lab members (Scott Campbell, Daryl Sivakumaran, Trevor Gilbert, Mathew Patenaude and Mayra Tzoc) for the meaningful friendships that we have developed throughout the years.

This thesis is dedicated to my late father, who would always say: “all’s well that ends well”.

Table of Contents

List of Figures

Chapter 1

Chapter 2

Chapter 2 Appendix

Chapter 3

Chapter 3 Appendix

Chapter 4

Chapter 4 Appendix

Chapter 5

Chapter 5 Appendix

List of Tables

.

List of Abbreviations and Symbols

AA: Acrylic acid

ADH: Adipic acid dihydrazide

AIBME: 2,2-azobisisobutryic acid dimethyl ester

Ald: Aldehyde

1,8-ANS: 8-anilino-1- naphthalenesulfonic acid ammonium salt

AP: Alkaline phosphatase

ATR-FTIR: Attenuated total reflection-Fourier transform infrared spectroscopy

β-Lac: β-Lactamase

βCD: β-Cyclodextrin

BSA: Bovine serum albumin

CM: Carboxymethyl

CD: cyclodextrin

CDT: Circular DNA template

CE: Complexation efficiency

dPAGE: Denaturing polyacrylamide gel electrophoresis

Dex: Dexamethasone

Dex-βCD: Dextran conjugated with βCD

DIW: Deionized water

DLS: Dynmaic light scattering

DMAEMA: N,N-dimethylaminoethyl methacrylate

DMSO: Dimethyl sulfoxide

EDGMA: Ethylene glycol dimethacrylate

EDC: N-3-dimethylaminopropyl-N-ethyl carbodiimide

5-FITC: 5-fluorescence isothiocyanate

FTIR: Fourier-transform infrared spectroscopy

GPC: Gel permeation chromatography

Hzd: Hydrazide

HCl: Hydrochloric acid

HPLC: High performance liquid chromatography

$IC_{50:}$ Half maximal inhibitory concentration

ITC: Isothermal titration calorimetry

M_n: Number average molecular weight

$M_{w:}$ Mass average molecular weight

NaCl: Sodium chloride

NaOH: Sodium hydroxide

NHS: N-hydroxysuccinimide

NMR: Nuclear magnetic resonance spectrometry

NTA: Nanoparticle tracking analysis

OEG: oligo(ethylene glycol)

PBS: Phosphate buffered saline

PBST: Phosphate buffered saline with Tween-20

PDI: Polydispersity index

PEG: Poly(ethylene glycol)

PNIPAM: Poly(N-isopropylacrylamide)

PNK: Polynucleotide kinase

PO: Poly(oligoethylene glycol methacrylate)

POA: Aldehyde-functionalized poly(oligoethylene glycol methacrylate)

POH: Hydrazide-functionalized poly(oligoethylene glycol methacrylate)

RCA: Rolling circle amplification

SSC: Saline-sodium citrate

TGA: Thioglycolic acid

TP: Template primer

Ur: Urease

UV: Ultraviolet

XPS: X-ray photoelectron spectroscopy

Declaration of Academic Achievement

The majority of the work described in this thesis was conceived, carried out, analyzed and written by the author, in consultation with Dr. Todd Hoare, except for the following:

Chapters 3 and 4: Dr. Monsur Ali suggested using chromatography to validate the hydrogel printing protocol, employing a wax-printed nitrocellulose template for hydrogel printing and a protocol to test for enzyme immobilization. Dr. Glynis de Silveira (Canadian Center for Electron Microscopy, McMaster University) is acknowledged for acquiring the SEM images. Dr. Danielle Covelli (Biointerfaces Institute) collected the XPS measurements.

Chapter 5: Dr. Kha Tram designed the sequences and protocols for rolling circle amplification product synthesis.

Chapter 1: Introduction

1.1.1 Molecular recognition events

Molecular recognition events govern vital biological processes such as gene expression, signal transduction, the immune response, and enzyme-substrate interactions. The association of a receptor with its cognate ligand is primarily regulated by non-covalent interactions such as hydrogen bonding, aromatic-aromatic interactions, and van der Waals forces[1, 2]. In addition to the weak intermolecular forces that mediate receptor-ligand interactions, solvent effects influence the thermodynamics of binding events while molecular diffusion and conformational fluctuations influence the kinetics of these interactions[3]. The binding affinity between two molecules is determined by the differences in non-covalent bonding between the free and bound states[4]. Upon reaching equilibrium, complexes held together by non-covalent forces tend to dissociate and generate a blend of free and associated molecules. One way of calculating the strength of the molecular interaction is to measure the concentration of the free and complexed species at equilibrium[5]. Molecular binding affinity can also be determined experimentally by measuring changes in enthalpy that arise from complexation[6].

1.1.2 Thermodynamics of molecular recognition events

The binding affinity of a receptor (R) and ligand (L) interaction can be described by the equation (Eq. 1.1):

$$(\text{Eq. } 1.1)\ R + L \rightleftharpoons R \cdot L$$

The equilibrium constant or the association constant (K_A) of the receptor-ligand complex (R·L) is (Eq. 1.2):

$$(\text{Eq. } 1.2)\ \ K_A = \frac{[R \cdot L]}{[R][L]}$$

where [R·L] is the concentration of the receptor-ligand complex, [R] is the concentration of the free receptor, and [L] is the concentration of the free ligand. The strength of the binding reaction is more commonly expressed as a dissociation constant, K_D (Eq. 1.3)[7]:

$$(\text{Eq. } 1.3)\ \ K_D = \frac{[R][L]}{[R \cdot L]}$$

Biologically important non-covalent interactions, such as those between an enzyme and substrate, possess dissociation constants that range from picomolar to nanomolar (10^{-12}-10^{-9}) for the strongest interactions to millimolar (10^{-3}) for the weakest interactions[8].

Binding affinity can also be described as the standard free energy or Gibbs free energy change upon binding (Eq. 1.4)[9]:

$$\text{(Eq. 1.4)}\quad \Delta G^{\circ}_{binding} = RTlnK_D$$

where R is the gas constant and T is the temperature. In this equation, a more negative $\Delta G^{\circ}_{binding}$ corresponds to a larger binding constant (K_D) and a spontaneous transformation. In biological recognition systems, the standard free energy changes upon binding are approximately -50 kJ mole^{-1} for the strongest interactions (i.e., an inhibitor binding to an enzyme) and -17 kJ mole^{-1} for the weakest interactions (i.e., ATP binding to a protein kinase).[8] Assessing the change in Gibbs free energy can reveal the effects of changes in bonding ($\Delta H^{\circ}_{binding}$) and changes in the entropy (in terms of $T\Delta S^{\circ}_{binding}$) within the system.[4] For most association reactions, enthalpy effects dominate at high temperatures while entropy effects influence complex formation at lower temperatures.[10] An exception to this rule is hydrophobic interactions, in which complex formation is driven by the minimization of contact area between hydrophobic domains and water molecules. The effect is mostly entropy driven at room temperature, apart from specific cases where the presence of water molecules in the binding cavity interfere with receptor-ligand interactions.[4]

Analyzing experimental values of $\Delta H^{\circ}_{binding}$ and $\Delta S^{\circ}_{binding}$ can be problematic since minor changes made to a receptor-ligand association event often correspond with inconsistent shifts in enthalpy and entropy values[11]. Modest changes to the system can also induce an enthalpy and entropy compensation effect that has a negligible influence on the overall change in free energy.[12] Although experimentally derived values of $\Delta H^{\circ}_{binding}$ and $\Delta S^{\circ}_{binding}$ can reveal important structural insights into receptor-ligand interactions, they are usually not informative of binding affinities.[13] Both thermodynamic parameters can be determined by investigating the temperature dependence of the affinity constant, or changes in enthalpy or entropy can be ascertained through microcalorimetry.[9]

1.1.3 Experimental determination of binding affinity

An affinity constant can be experimentally determined from a binding isotherm: a curve representing the amount of ligand adsorbed onto a receptor as a function of the concentration or partial pressure of the ligand at a fixed temperature.[14] There are many different ways of measuring the free or bound ligand in a binding assay.[8]

1.1.3.1 Binding isotherms

A signal that is proportional to the concentration of the receptor-ligand complex must be measured in order to generate a binding isotherm[14]. The signal can be spectroscopic, calorimetric, or functional (as is the case of enzyme inhibition by an associated ligand) in origin. The binding isotherm gives the fraction of the receptor (R) that is bound with ligand (L), *r*, at equilibrium (Eq. 1.5):[15]

$$\text{(Eq. 1.5)}\quad r = \frac{C_{RL}}{C_R + C_{RL}} = \frac{KC_L}{1 + KC_L}$$

where C_{RL} is the concentration of the receptor-ligand complex, C_R is the concentration of the receptor, C_L is the concentration of the free ligand, and K is the binding constant. Once the experimental data is collected, the binding constant is determined by fitting the data to a theoretical model that best fits the complexation system. Disagreement between the experimental data and the theoretical model can however raise uncertainty about whether binding is occurring under equilibrium conditions or the suitability of the chosen signal.[8]

Binding assays can be homogenous in design or they can incorporate the separation of bound and unbound ligand.[14] For example, a ligand and receptor at a known concentration can be separated by a dialysis membrane that is permeable only to the ligand. Once equilibrium binding is reached, the concentrations of ligand are measured on both sides of the membrane. The presence of ligand in the compartment containing the receptor is indicative of a receptor-ligand association event.[5, 16]

Although equilibrium methods are most commonly employed in binding assays, kinetic experiments can also be performed in order to gain insight into the dynamics of a complexation system.[17] In a typical kinetic experiment, the equilibrium concentrations of the receptor, ligand and the receptor-ligand complex are measured over a range of concentrations of either the receptor or the ligand. From these experimental data, both values of the rate constants for the forward and reverse reactions as well as the equilibrium constant (equivalent to the ratio of the forward and reverse rate constants) can be derived.[5]

Many binding assays are based on absorbance or fluorescence readout methods, where the difference in the absorption or fluorescence intensity of the complexed product is compared to that of one of the reactants. Specific fluorescence techniques such as fluorescence anisotropy, fluorescence resonance energy transfer (FRET) and polarity-sensitive fluorescent probes can be employed when the ligand and/or receptor are tagged with a fluorophore.[18, 19] Fluorescence anisotropy measures the rotational diffusion of a molecule.[20] A receptor-ligand complex has a lower rotational diffusion coefficient than the individual reactants and thus a higher fluorescence anisotropy. FRET occurs when excitation energy is transferred between donor and acceptor fluorophore tags that are present on both reactants.[21] Specialized fluorescent probes can monitor changes in the surrounding hydrophobicity by exhibiting an induced shift in the emission spectrum or a decrease in fluorescence intensity upon encountering regions of increased polarity.[22]

Functional assays can be employed to assess the activity of a reactant in a complexation system. These assays are useful in investigating the efficacy of pharmaceuticals that act as enzyme inhibitors.[23] In this context, the association constant, K_A, is described as the inhibition constant, K_I, which is derived from an experiment in which the rate of the enzymatic reaction is measured for a range of substrate concentrations against one concentration of inhibitor. Multiple concentrations of inhibitor are studied, generating up to 100 rate measurements in a typical experimental setup[17]. Evaluating drug inhibition using inhibition constants can thus be onerous, especially when analyzing the thousands of compounds that are required for an average drug discovery screen. The half maximal inhibitory concentration (IC_{50}) value is more frequently used as a measure of drug efficacy in pharmaceutical research.[24] Compared to the evaluation of K_I, determining the IC_{50} value of a drug requires about 15–20% as many data points since it is acquired from an experimental setup that measures enzymatic activity over a range of inhibitor

concentrations at one specific concentration of substrate.[23] The IC_{50} value is calculated by applying logistic regression to a non-linear plot of the percent of enzymatic activity remaining as a function of the log concentration of inhibitor (Fig. 1.1). Although the IC_{50} is a relative value for a drug compound that depends on the substrate concentration chosen for the assay, it remains a widely used measure of drug potency.[24]

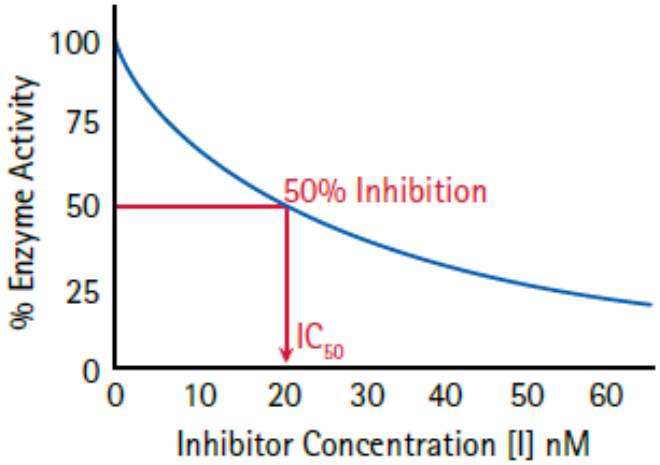

Fig. 1.1 IC_{50} determination from enzyme activity as a function of inhibitor concentration. Figure reproduced from Mohan et al.[25]

1.1.4 Experimental determination of enthalpy and entropy values

Estimating changes in enthalpy and entropy values associated with binding systems typically involve indirect methodologies. An example of this is van't Hoff analysis, in which the enthalpy and entropy of binding (ΔH_b° and ΔS_b°) are calculated via measurements of binding constants at different temperatures.[11] The relationship between the thermodynamic parameters and the binding constant are described in the van't Hoff equation (Eq. 1.6):[26]

$$(Eq.\ 1.6)\ \ln(K_D) = \frac{\Delta H_b^\circ}{RT} - \frac{\Delta S_b^\circ}{R} = \frac{\Delta G_b^\circ}{RT}$$

Plotting $\ln(K_D)$ as a function of inverse temperature generates a linear relationship in which the slope and y-intercept of the plot give estimates of ΔH_b° and ΔS_b°, respectively. The limitation of this estimate arises from the assumption that these parameters are independent of temperature.[27] Since many of the properties of enzymes and ligands (as well as their respective aqueous

microenvironments) are temperature dependent, this assumption is untenable for most biorecognition systems. Estimates of ΔH_b° determined via van't Hoff analysis are burdened with errors that are large relative to the magnitude of ΔG_b° and subsequently result in large errors in ΔS_b° due to an observed form of enthalpy-entropy compensation that is often not grounded in physical meaning.[11]

Conversely, calorimetry allows for independent estimates of ΔH_b° and ΔG_b° based on nonlinear fits to plots of heat generated as a function of the molar ratio of ligand titrated into the receptor solution.[28] The difference in these two parameters yields a value of ΔS_b° (Eq. 1.7):

$$(Eq.\ 1.7) \quad -T\Delta S_b^\circ = \Delta G_b^\circ - \Delta H_b^\circ$$

1.1.4.1 Isothermal titration calorimetry (ITC)

Isothermal titration calorimetry (ITC) measures binding interactions by detecting the heat absorbed or released during complexation, which directly corresponds to the change in binding enthalpy ΔH_b° (Fig. 1.2).[29] A typical ITC experiment can be performed with unmodified forms of the reactants and in the absence of a separation step that is often required in equilibrium assays. Binding affinities that range from the nanomolar to millimolar scale can be measured directly via ITC, although detecting sufficient binding heats necessitates the use of reactant concentrations at the micromolar level.[30] In order to generate estimates of binding affinities and thermodynamic parameters of a complexation system, the ITC data must be fitted to either a simple independent single-site or two-site binding model. These models are based on the assumption that the receptor does not experience a ligand-induced conformational change and/or exhibit self-association behaviour.[31] These potential properties of the binding system are determined prior to ITC data analysis by performing separation experiments on the reactants and products via analytical ultracentrifugation or gel filtration chromatography.[32, 33]

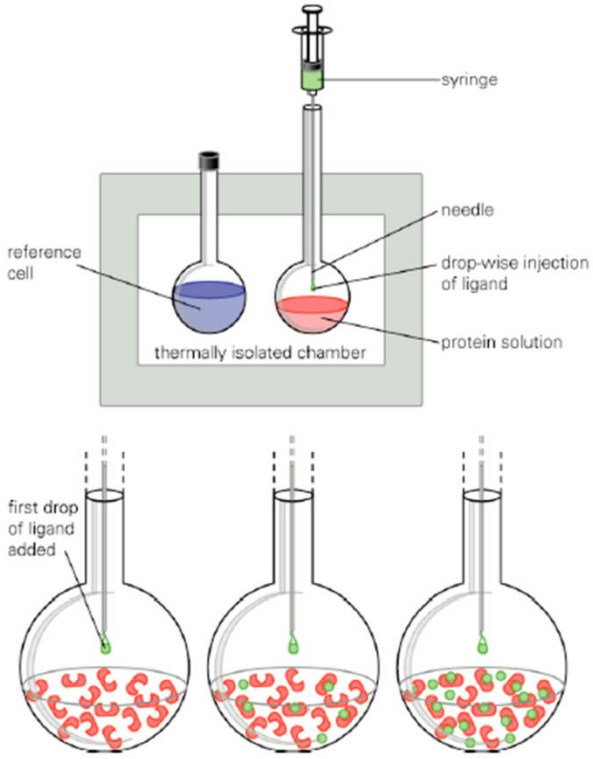

Fig. 1.2 Isothermal titration calorimetry (ITC). A syringe slowly titrates a ligand into a vessel containing a receptor (i.e. a protein). Receptor-ligand binding will either release or absorb heat. The heat released or absorbed by the complexation system is correlated to the amount of power required to maintain equal temperatures between the reference and sample cells. Figure adapted from Kuriyan et al.[8]

1.2 Types of molecular recognition events

The recognition of small molecules presents itself in a variety of contexts in both natural and synthetic systems. Many polymer-based technologies exploit molecular recognition events in order to fabricate materials with novel properties that can support enhanced compound solubility, the controlled release of pharmaceuticals, and the identification and separation of compounds at the analytical level. Thus, developing pharmaceutical formulations, drug delivery vehicles, and biosensors all require in-depth knowledge and optimization of the relevant binding systems. This review will focus on supramolecular events (specifically, host-guest interactions), enzyme-substrate and enzyme-inhibitor interactions, as well as nucleic acid hybridization (Fig. 1.3).

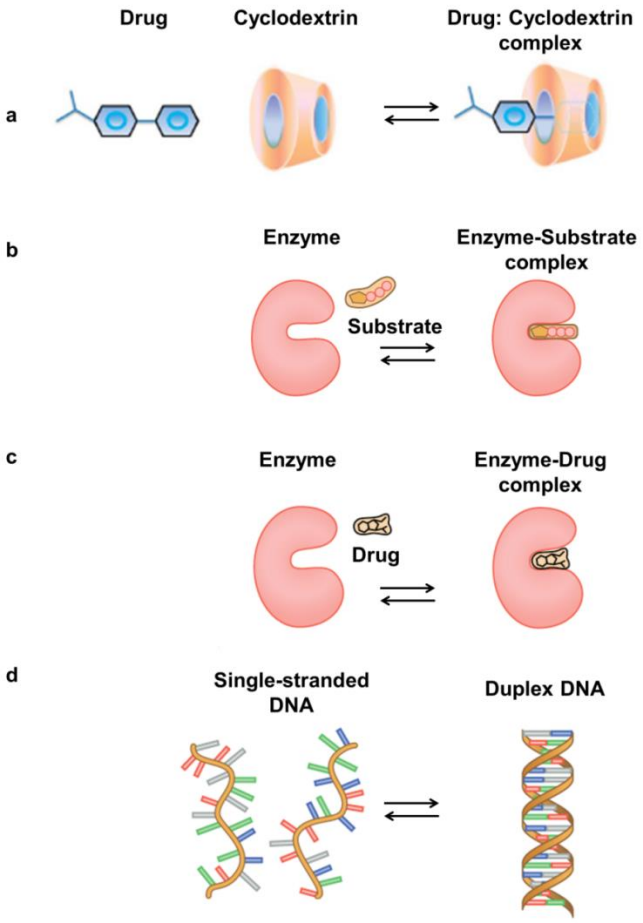

Fig. 1.3 Types of molecular recognition events (a) An example of host-guest association; cyclodextrin-drug complexation. **(b)** Enzyme-substrate complexation. **(c)** Enzyme-drug complexation. **(d)** Duplex DNA formation. Figure adapted from Kuriyan et al. and Dahab et al.[8, 34]

1.2.1 Supramolecular chemistry: host-guest complexation

Supramolecular chemistry describes complexation systems that are mediated by non-covalent intermolecular forces.[35] An example of supramolecular chemistry is host-guest complexation, a unique structural relationship in which the binding sites of two molecules unite due to a combination of geometric fit and complementary interactions including hydrogen bonding, ion pairing, π-backbonding, metal:ligand binding, van der Waals attractive forces, solvent reorganization, and partial covalent bonding resembling a transition state.[36] Most examples of host-guest chemistry are complexes that are formed between binding sites that are oriented inwards or towards a cavity, in which case the host is called an endo-receptor;[37] alternately, when the binding sites of a host-guest complex are located on an outward surface, the host is

referred to as an exo-receptor.[38] Host-guest complexation often involves multiple binding sites that can increase the strength of the interaction in an additive manner, a phenomenon referred to as the multi-valency chelate effect.[39] Examples of host molecules include crown ethers (heterocycles containing repeating units of ethyleneoxy that selectively bind cationic compounds), calixarenes (cyclic molecules composed of repeating phenolic units or phenolic derivatives that can bind many neutral organic molecules and heavy metal ions), porphyrins (macrocyclic compounds consisting of four pyrrole rings linked by methine bridges that associate with metal ions) and cyclodextrins (cyclic oligosaccharides containing repeating units of glucopyranose that tend to bind hydrophobic compounds).[40, 41, 42, 43] Cyclodextrins are particularly widely-investigated as model systems for biological receptors.[2]

1.2.1.1 Cyclodextrins

Cyclodextrins (CDs) are synthesized through the degradation of starch by amylase derived from the microbe, *Bacillus macerans*.[43] There are three main types of CDs: the six glucose-membered αCD, the seven glucose-membered βCD, and the eight glucose-containing γCD.[44] These molecules possess a toroidal shape with a slightly hydrophobic inner cavity and hydrophilic exterior.[45] The hydrophobicity of the CD cavity is attributed to the presence of carbons arising from the constituent glucose residues and the relatively higher polarity of the primary and secondary hydroxyl groups located on the outer rims of the toroid. The overall polarity of the molecule has been described to be similar to that of an ethanol/water solution.[46] CDs can form inclusion complexes with compounds that are physically compatible with the internal binding pocket and less polar than the surrounding medium. The three main types of underivitized CDs possess different cavity sizes.[47] For example, the cavity of αCD is too small to form an inclusion complex with most drug molecules, while βCD and γCD possess cavities that are large enough to accommodate most small molecule pharmaceuticals. βCDs are frequently used in pharmaceutical formulations, personal care products, as well as a component of food additives.[43] A significant drawback associated with all three parent CDs is their low water solubility, attributed to intramolecular hydrogen bonding that occurs between the secondary hydroxyl groups within the molecule.[48] The synthesis of CD derivatives is pursued not only to increase the aqueous solubility of CDs but also to enhance their capacity to bind guest molecules and potentially integrate them into polymer based materials.[49] Specifically, CDs can be incorporated in polymer conjugates, hydrogels, or molecularly imprinted polymers to enable the solubilization

of lipophilic agents, the separation of isomeric mixtures, the enhancement of detection sensitivity, microdialysis, and/or solid/liquid phase extractions.[50]

1.2.2 Enzyme-substrate and enzyme-inhibitor interactions

Enzymes are catalytic agents that accelerate a reaction by decreasing its activation energy. In order to carry out its function, the binding site of an enzyme must accommodate the initial and transition states of the substrate along with the reaction product.[51] There are two foundational theories that attempt to explain how enzymes bind their respective substrates. In Fischer's lock-and-key model, the conformation of the free enzyme remains unchanged following ligand binding (Fig. 1.4).[52] Thus, the fixed morphology of the enzyme requires the substrate to specifically fit inside the binding cavity. In Koshland's induced fit model, the conformation of the substrate-bound enzyme differs from that of the free enzyme (Fig. 1.4).[53] Upon substrate recognition, the active site of the enzyme undergoes a morphological change that accommodates the binding of the substrate. Although experimental data supports the conformational difference between the substrate-bound enzyme and the native state of the enzyme, there are limitations of the induced fit model, including the requirement of a minimal degree of substrate specificity.[54] Because compounds can interact with an enzyme despite being structurally incompatible with the active site, alternative mechanistic descriptions of enzyme-substrate interactions are warranted. Kinetic experiments have demonstrated that binding events are more likely dictated by conformational selection from a large population of substrate bound enzymes that differ slightly in morphology from one another.[55]

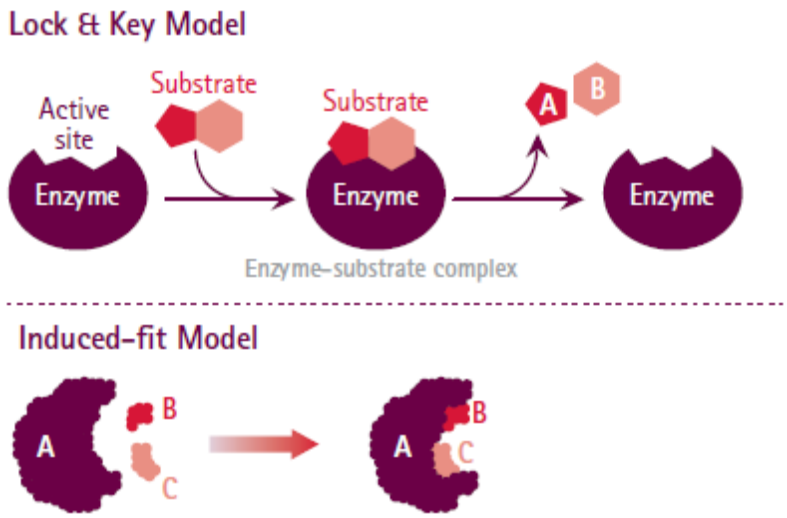

Fig. 1.4 Illustrations of Fischer's Lock and Key and Koshland's Induced-fit models. Figure reproduced from Mohan et al.[25]

Reversible inhibitors behave similarly to substrates, although they form highly stable complexes with enzymes and consequently possess low dissociation constants.[56] Weak non-covalent interactions mediate binding between reversible inhibitors and enzymes. Irreversible inhibitors form covalent bonds with the enzyme active site, modifying critical residues that are involved in catalytic activity.[57] There are three main types of reversible inhibitors: competitive, non-competitive and uncompetitive inhibitors.[58] Similar to substrates, competitive inhibitors bind to the active site of enzymes. Uncompetitive inhibitors interfere with substrate binding by associating with the enzyme-substrate complex. Non-competitive inhibitors can bind to the enzyme alone or the enzyme-substrate complex, typically interacting with a site on the enzyme that is not involved in catalysis to induce a conformational change in the enzyme that reduces its affinity for the substrate. There is also an added class of reversible non-specific inhibitors called promiscuous aggregating inhibitors that are highly problematic in affinity screening interactions.[59] Such inhibitors have a tendency to form colloidal aggregates in solution and inhibit the activities of a wide range of enzymes by promoting the adsorption of enzymes onto the aggregate surface,[60, 61] representing a form of steric inhibition of the enzyme active site.

1.2.3 Nucleic acid hybridization

Complementary nucleic acid strands can form stable hybrid complexes by annealing to one another according to the Watson–Crick rules of base pairing, dictating that specific nucleotides are held together by hydrogen bonds. The stacking of base pairs on top of one another is driven by van der Waals interactions that also reinforce the double stranded DNA complexes.[62] These hydrophobic interactions between bases are favoured since the more polar functionalities of the DNA duplex are exposed to the surrounding aqueous medium.[63] The stability of the annealed complexes is determined by the temperature at which the complex will dissociate, also known as the melting temperature (T_m). T_m is calculated using a formula that describes the thermodynamic parameters of annealing oligonucleotides in a reference buffer.[64] For an oligonucleotide that is 17-24 base pairs in length, the presence of each adenine-thymine (A-T) base pair contributes 2°C to the T_m while each guanine-cytosine (G-C) base pair contributes 4°C to the T_m.[65] Additional factors such as the ionic strength/pH of the medium, length of the complementary oligonucleotide, G–C content, and the presence of mismatched base pairs can also significantly influence the stability of double-stranded DNA complexes.[66]

1.3 Molecular recognition in polymer-based systems

Molecular recognition can be incorporated in polymer-based materials as a tool that promotes self-assembly and introduces functionality to the material. For example, polymers functionalized with complementary host and guest molecules can be cross-linked via inclusion complex formation[67], an example of which is shown in Fig. 1.5.

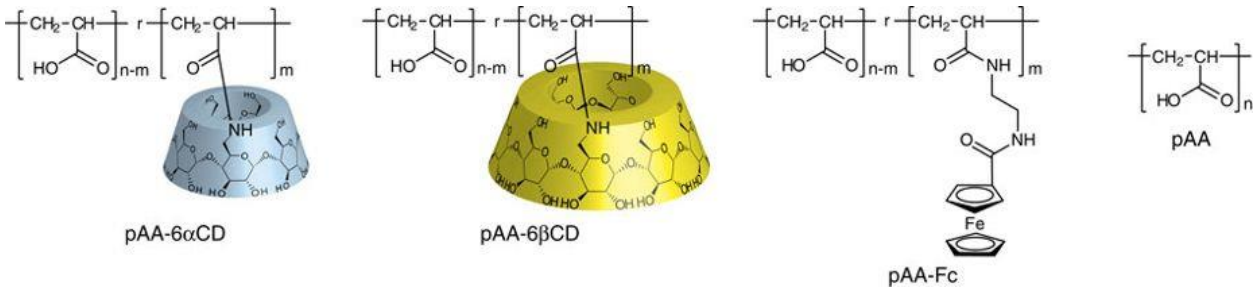

Fig. 1.5 Examples of a host polymers (poly(acrylic acid) functionalized with cyclodextrins (CDs)) and a guest polymer (poly(acrylic acid) functionalized with ferrocene (Fc)). Complexation between the CD and Fc units results in the formation of a supramolecular hydrogel. Figure reproduced from Nakahata et al.[68]

Hydrogels, defined as networks of cross-linked water soluble polymers, are often fabricated in this manner by exploiting the interaction between CD polymers and water-soluble polymers bearing potential guest molecules such as cholesterol, azobenzene , ferrocene and adamantyl groups[68, 69, 70, 71, 72]. Hydrogels can also be generated from inclusion complexes that form between linear water-soluble polymers such as polyethylene oxide (PEO) and α-CD. PEO penetrates the binding cavity of α-CD much like beads strung onto a necklace, creating cross-linking sites and driving physical gelation.[73] In addition to driving the self-assembly of hydrogels, host-guest complexation can impart materials with interesting properties such as the ability to self-heal or autonomously restore mechanical integrity following internal damage.[74] For example, Wang et al. fabricated hydrogels from the UV-induced polymerization of a "three-arm" triacrylate monomer containing an inclusion complex of β-CD with an adamantyl group, generating materials with covalent cross-links that are further strengthened by inclusion complexes.[75] Damage incurred to the hydrogel material resulted in dissociated host-guest complexes that were able to re-connect when the cut sites were brought into close contact. Molecular recognition can also serve specific functions in the design of polymer-based materials, including analyte sensing and drug delivery. For example, chemoreceptors that act as hosts for phosphate-based analytes have been entrapped in hydrogels formed from supramolecular interactions, leading to the fabrication of an array-type sensor chip that detected small molecule analytes in a high-throughput fashion.[76] Yhaya et al. synthesized micelles from β-CD functionalized block copolymers for the delivery of the poorly soluble anti-cancer drug albendazole, greatly enhancing the drug-loading capacity of the micelle and offering a potentially promising drug release platform.[77] The following section will discuss in depth how molecular recognition is specifically exploited in the development of pharmaceutical excipients, drug delivery, sensing, and separations applications of polymer conjugates and hydrogels.[78]

1.3.1.1 Polymer conjugates

Biomolecules and drugs exhibit sensitivity towards fluctuations in temperature and pH as well as a tendency to denature in both aqueous and organic solvents. Peptides, proteins or drugs can be protected by conjugation with water-soluble polymers that act as an intermediate between the biomolecule and its respective environment.[79] For example, many small molecule pharmaceuticals have been conjugated to polyethylene glycol (PEG) in a method referred to as

PEGylation[80], effectively increasing the molecular weight of a drug and thus reducing kidney clearance and increasing functional half-life.[81] A PEG-pharmaceutical conjugate can also experience an increased biocirculation time due to the ability of PEG to prevent immune-mediated elimination of the drug.[82]

There are many synthetic routes for developing polymers that are conjugated to biomolecules or molecular receptors. Biomolecules can be coupled to the polymer covalently or non-covalently and in a random or site-specific fashion.[83] Attachment of the biomolecule can occur to a fully synthesized polymer via reactive coupling or affinity strategies.[84] In contrast, a "grafting from" approach employs a biomolecule that has been derivatized with a polymerizable functional group.[85] The functionalized biomolecule can be co-polymerized with an additional monomer to generate a polymer in which the tethered biomolecule is randomly distributed throughout its backbone.[86] The most common coupling chemistry employed in the synthesis of polymers conjugated to biomolecules is the covalent coupling of amine groups and activated esters.[87] Biotin-streptavidin binding is the most frequently utilized non-covalent coupling strategy,[88] by which a polymer is functionalized with biotin or streptavidin and the respective binding partner is attached to a biological or molecular receptor.

Polymers conjugated to proteins or molecules that act as receptors for a specific ligand can serve as agents that promote the solubilization, stability and controlled release of pharmaceuticals as well as facilitate analyte sensing and separation. For example, Hoffman and Stayton developed comprehensive techniques to covalently couple stimuli responsive polymers, such as poly(N-isopropylacrylamide) (PNIPAM), to proteins and biomolecules for a wide range of applications.[89] The temperature sensitivity of PNIPAM allows a conjugated receptor to transition between a soluble and collapsed state, isolating a bound ligand from solution and demonstrating potential utility in bioseparation applications.[90] Hoffman and Stayton also developed a reversible biotin binding system in which they conjugated a mutated version of streptavidin to PNIPAM in a site-specific manner. Biotin binding was reversibly blocked when the polymer was in a collapsed state, also releasing biotin that was associated with the streptavidin-PNIPAM complex.[91] This demonstration of triggered binding and release established stimuli-responsive polymer conjugates as a potential platform for biosensing.[79]

1.3.1.2 Pharmaceutical excipients and drug delivery

Pharmaceutical excipients are inert substances added to drug formulations in order to stabilize or solubilize active drug compounds.[92, 93] In particular, poor drug solubility is a significant issue as an increasing number of drug candidates exhibit low aqueous solubility.[94] For example, free cyclodextrin is often utilized as a pharmaceutical excipient in derivatized forms (i.e. hydropropyl β-CD) and can optionally be grafted onto polymers to generate soluble drug carriers. [46, 95] Alternatively, conjugating a lipophilic drug to a water-soluble polymer can greatly enhance the aqueous solubility of the pharmaceutical.[96] Combining polymer conjugation with host-guest complexation can improve drug solubility while establishing a controlled release system. Zhang et al. functionalized hyperbranched polyglycerol with β-CD moieties and developed a self-assembled micellar delivery system for the hydrophobic anti-cancer agent paclitaxel. The micelles demonstrated high loading efficiencies and controlled release profiles that could be modulated by adjusting the composition of the β-CD conjugate polymer.[97] Namgung et al. developed a conjugate co-polymer of β-CD with maleic anhydride and a complementary co-polymer composed of maleic anhydride and paclitaxel.[98] The two resulting conjugate polymers (pCD and pPTX) assembled into nanostructures, driven by inclusion complex formation between paclitaxel and β-CD, that dispersed well in an aqueous medium and demonstrated excellent stability, drug encapsulation, cancer cell uptake and efficient release rates. Interestingly, molecular dynamics simulations indicated that the pCD/pPTX complex dissociated at a much lower rate than the monomeric paclitaxel/ β-CD inclusion complex, a phenomenon attributed to the reduced exposure of hydrophobic paclitaxel to the surrounding aqueous medium when grafted to the polymer. Additionally, the entropic gain that results from the dissociation of the PTX/CD complex in solution is much larger in comparison to the dissociation of the inclusion complex conjugated to a polymer chain. These observations demonstrate that the properties of molecular recognition events can change in a polymeric system, often increasing the thermodynamic stability of inclusion complexes and imparting significant functional advantages.

1.3.1.3 Biosensors

Polymers conjugated or associated with biomolecules (such as enzymes or oligonucleotides) are often incorporated in biosensing devices. For example, Doré et al. reported on the fabrication of a solution based assay consisting of a cationic polymer (polythiophene) that can form polyelectrolyte complexes with anionic oligonucleotide probes, allowing for the specific detection of nucleic acid target sequences.[99] The polythiophene polymer/DNA complex tends to form aggregates in solution, quenching the inherent fluorescence of the polymer. Polythiophene fluorescence was recovered when the complexed oligonucleotide hybridized with a complementary oligonucleotide probe.

There are also many examples of the use of conducting polymers in the development of biosensors that operate based on electronics detection. For example, Rahman et al. developed a sensor for the detection of the neurotransmitter L-glutamate.[100] A platinum electrode was coated with layers of a conducting polymer, the surface of which was subsequently functionalized with the enzyme glutamate oxidase via EDC coupling chemistry. Rat brains were injected with cocaine and the resulting glutamate release was measured by monitoring changes in amperometric responses. Lee et al. developed a biosensor capable of detecting base-pair mismatches in DNA sequences.[101] Similar to the work of Rahman et al., a glassy carbon electrode was coated with a conducting polymer and the external polymer coating was functionalized with an oligonucleotide via EDC coupling chemistry. The degree of hybridization of DNA samples to the immobilized oligonucleotide was correlated to the difference in measured impedance before and after hybridization.

1.4.1 Hydrogels

Hydrogels, networks of cross-linked water soluble polymers, have attracted particular interest as a platform for the controlled release of pharmaceuticals and as functional interfaces in biosensing devices. They typically exhibit low toxicity and high cytocompatibility due to their ability to swell in water, as well as their mechanical and chemical similarities to biological tissues.[102] The polymer networks can be covalently cross-linked (via UV photopolymerization or other methods of chemical cross-linking) or physically cross-linked (via hydrogen bonding, electrostatic or hydrophobic interactions).[103] For most biosensing and drug delivery applications, chemical cross-linking strategies are preferable given their more controllable degradability. For this

purpose, water-soluble polymers are often derivatized with moieties that exhibit complementary reactivity. For example, polymers that contain alcohol, amine or hydrazide groups can be cross-linked with polymers functionalized with aldehydes.[104] Aldehyde-hydrazide cross-linking is specifically attractive since the resulting hydrazone bonds form quickly and demonstrate increased hydrolytic stability in comparison to other Schiff bases.[105] Hydrogels synthesized through hydrazone cross-linking tend to be amenable to administration via injection and enable stable encapsulation of biomolecules.[106, 107]

Hydrogels can be adapted in a number of ways to fit the desired application. For example, hydrophobic binding sites or CDs can be incorporated in hydrogels for the delivery of lipophilic pharmaceuticals.[108, 109] A major limitation of conventional hydrogels is their inability to effectively load and release hydrophobic pharmaceuticals.[110] Introducing functionalities that form favourable interactions with lipophilic ligands can prevent the aggregation of drug molecules that is often responsible for the collapse of a gel network, reducing the average pore size of the hydrogel and restricting the diffusion limited release of the drug. Hydrogels have also been adapted to suit the demands of interfacial coatings for biosensing devices.[111, 112] Advantages associated with hydrogels such as deformability as well as their ability to swell lend themselves to the development of surface film coatings for miniaturized devices.[113] Although grafted polymer layers have also been used in sensing interfaces, hydrogels fare better in this application as they form stable, free-standing films that have multiple points of association with substrates and are able to encapsulate and stabilize biomolecules that can act as molecular recognition agents.[114]

1.4.1.1 Hydrogel films

Reducing the dimensions of a bulk hydrogel can significantly improve mass transfer limitations that are often encountered in reaction-based applications of macroscale hydrogels as well as reduce the response times of hydrogels to changes in their environment.[115]. There are many ways to fabricate interfacial hydrogels including dip-coating[116], spray deposition[117], spin-coating[118] and drop on demand printing[119]. Printing is an advantageous deposition technique since it is amenable to dispensing small volumes, can localize materials in specific patterns, as well as fabricate materials with ease and potential for scale-up. On account of its capacity to

stably entrap and deposit biological agents in a controlled manner, hydrogel printing has been investigated thoroughly and received significant attention in biomaterials research.[120, 121, 122]

Hydrogel films have been utilized as mediums for the catalysis of chemical reactions as both the kinetics and demand for product isolation can be supported by this hydrogel morphology.[123, 124] For example, Suri et al. developed a continuous glucose sensing system consisting of a quencher derivatized with a boronic acid functional group and an anionic fluorescent dye immobilized in a hydrogel film.[125] Boronic acids reversibly bind to glucose in aqueous environments; when functionalized with a dye, they can influence the fluorescence as a function of glucose concentration.[126] The sensor was able to detect glucose in the physiological range via visible changes in fluorescence. The binding affinities between the boronic acid functionalized fluorescent dye and glucose, fructose and galactose were determined in isolation and when immobilized in the hydrogel film. Not only did the dye sensor exhibit greater selectivity for glucose when immobilized in the hydrogel, the binding constant also increased upon incorporation in a polymer matrix.

The ability of hydrogels to function as membranes that exercise size selectivity has also been widely investigated.[127] For example, Sadeghi et al. synthesized an ultra-thin hydrogel on a commercial ultrafiltration membrane through a technique called interfacially initiated free radical polymerization. In this synthetic strategy, the support membrane is saturated in aqueous monomer and the photoinitiator is dispersed in the oil phase, generating a hydrogel layer that is formed at the oil−water interface that coats the surface of the support membrane.[128] The hydrogel membrane exhibited antifouling properties and the ability to separate proteins based on size.

1.4.1.2 Drug delivery

Molecular recognition events are commonly incorporated in hydrogel materials for the controlled release of biological agents and pharmaceuticals, typically to facilitate triggered release when a particular affinity agent is present in the gel environment and/or alter the kinetics of diffusion-based release from hydrogels. As an example of the former, Yamaguchi et al. developed a hydrogel that was cross-linked via non-covalent associations between heparin modified star PEG polymer and vascular endothelial growth factor (VEGF). [129] In the presence of VEGF receptors,

the VEGF mediated cross-links were broken, triggering the release of the growth factor. As an example of the latter, Soontornworajit et al. incorporated an acrydite-modified aptamer into the synthesis of polyacrylamide hydrogels with the aim of developing a controlled release system for anti-platelet-derived growth factor-BB (anti-PDGF-BB). The aptamer functionalized hydrogels exhibited a continuous release profile for a duration of 6 days, in comparison to an unmodified hydrogel which presented a conventional burst release profile in a 48 hour time period.[130]

1.4.1.3 Biosensors

The physicochemical, mechanical, electrical and optical properties of hydrogels render them excellent candidates for biosensing interfaces.[131] Hydrogels offer specific advantages for the detection of analytes in complex biological assays, including the ability to resist non-specific adsorption, promote the selective diffusion of analytes in and out of the hydrogel barrier, as well as the capacity to stably entrap biomolecules in the absence of covalent modification. There are many examples of biosensing devices that have exploited these specific properties of hydrogels. For example, Deng et al. fabricated a paper-based sensing device with a hydrogel film interface deposited through a dip-coating process[116]. The hydrogel was composed of reactive poly(oligoethylene glycol methacrylate) precursor polymers functionalized with aldehyde and hydrazide moieties that are capable of rapidly forming a gel upon mixing or contact. The sensor was validated as a platform for an enzyme-linked immunosorbent assay (ELISA) and the hydrogel interface demonstrated the ability to resist the non-specific adsorption of IgG antibodies, resulting in more effective passivation than traditional blocking agents like bovine serum albumin or skim milk. Tan et al. reported on the development of a graphene oxide-based hydrogel immobilizing fluorescently-labeled aptamers designed to selectively bind to the antibiotic tetracycline. Due to the fluorescence quenching properties of graphene oxide, the aptamers lost their fluorescence signal upon entrapment in the graphene oxide hydrogel matrix, which was physically cross-linked via electrostatic interactions with adenosine. Upon exposure to tetracycline, the aptamer recovered its fluorescence signal and was able to detect quantities of tetracycline in a dose-dependent manner and with high sensitivity.[132] Alev-Tuzuner et al. reported on the fabrication of a paper-based urea sensor with a polyethylene glycol (PEG) hydrogel interface.[133] A mixture of mono- and diacrylate PEG containing urease was cast onto a litmus strip and photopolymerized into a transparent, hydrogel film upon exposure to UV light to

immobilize urease onto the paper substrate. When a urine or saliva sample was applied to the sensor, the pH indicator paper changed colour depending on the concentration of urea present in the sample.

1.4.1.3.1.2 Microarrays

Microarrays are two-dimensional arrays consisting of a collection of immobilized biomolecules that act as miniaturized sensors. Hydrogels have been implemented in many microarray applications, particularly drug screening and hybridization assays.[134, 135] Immobilized biomolecules are supported by the well hydrated hydrogel microenvironment, rendering hydrogel interfaces an attractive development in the microarray-based screening for pharmaceuticals. In one of the first demonstrations of drug screening performed via a hydrogel microarray, Kiyonaka et al. developed a supramolecular hydrogel that entrapped enzymes and was able to discriminate enzymatic inhibitors from compounds exhibiting little to no inhibitory activity.[136] Given that the microarray format is conducive to high-throughput analyses, this platform is easily translatable to assays performed in drug discovery.

Microarrays are also useful in the context of DNA sensing. In a typical hybridization assay, a labeled oligonucleotide probe anneals to an immobilized DNA-based sensing material. A critical aspect of this assay is the requirement for separating free labeled probe from the hybridized probe. A hydrogel interface can act as a membrane that facilitates the diffusion of oligonucleotide probes to and from the entrapped sensing material. As an example, Beyer et al. developed a hydrogel microarray for in-gel DNA detection in which hybridization events were monitored visually by a colour change caused by the deposition of silver nanoparticles.[137] Amino-functionalized DNA was covalently incorporated into the hydrogel via a synthetic polymerization strategy that was initiated by exposure of the monomer solution to visible light. The fabricated hydrogel interface was porous enough to allow for the efficient diffusion and association of labeled DNA probes, generating a quantitative and sensitive assay for the detection of hybridization events.

1.5 Objectives of research

Based on the demonstrated promise of affinity-based hydrogels in different applications, the objective of this thesis was to develop and investigate novel polymer-based technologies that exploit molecular recognition phenomena for pharmaceutical and biosensing applications. In particular, the thesis focuses on strategies to better integrate affinity tags into hydrogel structures and then apply those integrated affinity tags for pharmaceutical and biosensing applications. More specifically, the results presented in this thesis demonstrate that incorporating molecular recognition in polymeric systems can enhance the affinity, selectivity and capacity for immobilization of the recognition units to either enhance their function or introduce new functionality into the recognition system to expand their potential applications.

Although there are many examples of pharmaceutical excipient and delivery systems based on cyclodextrins, there are a few key areas that have remained unexplored. Chapter 2 focuses on a detailed comparison of the binding capacity and stability of a dexamethasone complex with free functionalized CDs relative to polymer-immobilized CDs. Specifically, βCDs were modified with varying densities of a small, negatively charged moiety (carboxyls) and a large, neutral moiety (hydrazides), with the solubilization capacities, thermodynamic parameters and aggregative potential of these host–guest interactions subsequently studied. In view of the frequency with which CDs are incorporated in controlled release systems, this investigation is warranted as the binding characteristics of CDs when functionalized with different reactive functional groups can provide critical insight into the rational design of polymer-based affinity delivery systems.

Molecular recognition in a biosensing context was studied through the development of a printable hydrogel film that demonstrates utility as a platform for the screening of enzyme inhibitors and specific oligonucleotide probes. Chapter 3 describes the fabrication of a printable hydrogel based on the injectable, *in situ* gelling, aldehyde and hydrazide functionalized poly(oligoethylene glycol methacrylate) (PO) polymers. This is the first description of a method to print a covalently cross-linked hydrogel in the absence of ultraviolet (UV) photopolymerization to initiate gelation. The printed hydrogel was examined for its capacity to immobilize biomolecules and enzymes of varying sizes and facilitate the efficient transport of small molecule substrates. Chapter 4 describes the translation of the printable hydrogel to a

sensing interface for microarray applications. Firstly, the ability of the hydrogel to stabilize entrapped enzymes against proteases and time-dependent denaturation was investigated in order to establish its utility as a biosensing interface. A microarray-based assay was developed for the screening of β-lactamase inhibitors, a critical compound in antibiotic therapies. The assay was able to accurately quantify the dose–response relationships of the inhibitors while using 95% less sample than required for a solution assay. More excitingly, the assay platform prevented the occurrence of false-positive hits by non-specific inhibitors, a critical bottleneck in the drug discovery process. Chapter 5 examines the application of this printable hydrogel-based microarray in a hybridization assay. A long concatameric DNA molecule was used as an immobilized sensing material for the detection of a small fluorophore-labeled oligonucleotide. The properties of the printable hydrogel were investigated in the context of its ability to support the development of this assay.

The work presented in this thesis describes novel strategies to integrate molecular recognition units into polymer-based systems, demonstrating significant improvements in a wide range of applications including the controlled release of pharmaceuticals, drug discovery and the detection of biological analytes.

Chapter 2: Carboxymethyl and hydrazide functionalized β-cyclodextrin derivatives: A systematic investigation of complexation behaviours with the model hydrophobic drug dexamethasone

Preface

This chapter and its appendix are reproduced from the publication describing the complexation behaviours of β-cyclodextrins derivatized with carboxymethyl and hydrazide functional groups and a dextran conjugate. Complexation with dexamethasone was investigated via phase solubility studies, continuous variation method (Job's method), isothermal titration calorimetry and nanoparticle tracking analysis.

Rabia Mateen[1] and Todd Hoare[1,2*]
[1]School of Biomedical Engineering, McMaster University, Hamilton, Ontario L8S 4K1, Canada.
[2]Department of Chemical Engineering, McMaster University, 1280 Main St. W, Hamilton, Ontario, Canada L8S 4L7

In *International Journal of Pharmaceutics* 472.1-2 (2014): 315-326. Reproduced with permission from Elsevier.

Abstract

Cyclodextrins (CDs) are typically functionalized to increase their solubility or provide reactive functional groups suitable for grafting onto polymer supports designed for controlled release applications. In this work, a systematic investigation was performed on the binding behaviour of the model drug dexamethasone with βCD derivatives functionalized with a small, negatively charged moiety (carboxyl groups, CM) and a large, neutral, reactive moiety (hydrazide groups, Hzd), both free and grafted to dextran. Solubilization capacities and thermodynamic parameters were examined through phase solubility analysis, the method of continuous variation, and isothermal titration calorimetry. Alternate mechanisms of solubilization were also investigated by probing aggregation of both free and complexed βCD derivatives using nanoparticle tracking analysis. CM/βCD and Hzd/βCD derivatives exhibited similar complexation behaviours with dexamethasone: 1:1 stoichiometry, linear phase solubility profiles, and consistent binding enthalpies. Increased functionalization reduced the complex stability constant as well as the complexation efficiency, while polymer grafting resulted in no significant change in binding properties. CM/βCD derivatives complexed with dexamethasone formed more and larger aggregates, while Hzd/βCD derivatives formed significantly fewer, smaller aggregates and dextran grafted βCD did not aggregate. Such characterization of βCD derivatives provides a framework for designing βCDs as pharmaceutical excipients or drug binding sites in drug delivery vehicles.

2.1 Introduction

Cyclodextrins (CDs) have been widely applied both academically and industrially as host molecules for enhancing the bioavailability of poorly soluble drugs.[46, 138] Parent (unmodified) cyclodextrins (CDs) tend to exhibit a higher binding affinity for compounds with low aqueous solubility and have been safely and effectively used in oral delivery systems, given that CDs can be metabolized by the gastrointestinal system.[46] However, the inherently low water solubility of unmodified CDs in aqueous media, attributed to intramolecular hydrogen bonding between the secondary hydroxyl groups in the molecule,[139] significantly limit their use in other types of delivery systems, particularly for injectable or intravenous drugs. Intravenous administration of drug complexes prepared with the most widely-used CD variant, β-cyclodextrin (βCD), has been reported to frequently lead to precipitation of the complex either locally or at another site in the body, such as the kidney.[46, 140] βCDs can also induce haemolysis by disturbing the lipid composition of the cell membrane.[141]

Introducing new functional groups to βCDs is typically pursued to (1) increase the water solubility of βCD (2) increase the capacity of βCDs to form complexes with guest molecules,[142] and/or (3) to provide functional group tethers permitting grafting of βCD to a polymeric support (e.g. a linear polymer, a hydrogel, or a nanoparticle).[143, 144, 145] Because βCD has 21 possible hydroxyl groups that can be modified, an astronomical number of possible homologues and isomers of a derivative can be generated.[146] It has been demonstrated that selectively functionalizing βCD generates products with a tendency towards rapid crystallization whereas statistically modified products with low degrees of substitution give rise to an amorphous product with significantly lower toxicity.[147] Introducing different functionalities to βCD can also impart other advantageous properties to the molecule. For example, ionic groups can reduce the tendency of βCD to extract cholesterol and other important membrane components.[141, 142]

The stability of inclusion complexes of lipophilic molecules with the non-polar environment of the CD cavity is significantly influenced by size/shape matching between host and guest molecules, weak hydrophobic interactions between the substrate and the CD cavity interior, steric hindrance, hydrogen bonding, and the lipophilicity of both the host and guest.[148] CD complexation events are usually investigated by measuring a chemical or physical property of

the guest molecule, since these properties will change according to whether the guest is free or bound to the host. While inclusion complexes are routinely assumed to account for the majority of CD/guest interactions, such interactions do not exclusively occur through inclusion complexation[149]; indeed, a number of native and derivitized CDs display self-associative behavior that leads to aggregation of multiple CD-drug binding pairs into a particle form. Understanding the mechanism of CD self-assembly is thus critical in the development of CD-based injectable formulations, ophthalmic solutions, and other non-oral dosage forms from both a pharmokinetic and safety perspective.[150]

A number of βCD derivatives have been reported to be safely incorporated into injectable pharmaceutical formulations, with hydroxypropylated βCD (HPβCD) and sulfobutyl ether βCD (SBE-βCD) being the most popular.[46] HPβCD is the most widely used and accepted CD-based excipient due to its high aqueous solubility and minimal toxicity. The acute toxicity of native βCD in rats was reported to be 450 mg/kg, while its hydroxypropyl functionalized counterpart had an LD_{50} greater than 2000 mg/kg.[151] Furthermore, the reactivity of the functional group on functionalized CDs permits grafting of CDs on a variety of polymeric drug delivery systems. In this case, the functionalization serves two purposes: one pharmaceutical (to increase solubility and/or drug binding capacity) and another chemical (to optimize the number of graft sites and/or tune the stability of the cross-link between the CD derivative and the polymeric support). This latter issue is critical since the number of functional handles on a single CD molecule will largely determine whether CD behaves as a cross-linker or a graft in any given polymer preparation.

Given the importance of functionalized CDs for expanding the scope of CD use and, more broadly, the capacity to deliver hydrophobic drugs effectively in an aqueous environment, significant work has been performed on investigating the drug binding behavior of functionalized CDs in their independent state for a variety of drugs.[152, 153, 154, 155, 156] The complexation behaviour of CDs incorporated in hydrogel networks with dexamethasone have been investigated, providing insight into achieving efficient drug loading in CD based delivery networks.[157] More specifically, understanding the influence of functional group type and degree of substitution on the solubilization capacity, inclusion complex stability, and aggregative

potential of CD derivatives can help establish a framework for developing new or better CD derivatives that can be in used in a variety of pharmaceutical contexts.

In this study, the complexation behavior of carboxymethylated βCD (CM/βCD), hydrazide-functionalized βCD (Hzd/βCD) and a βCD functionalized dextran polymer (Dex-βCD) were investigated, using the moderately hydrophobic drug dexamethasone (log*P* =1.77) as a model guest. Our specific interest lies in investigating the effect of derivatizing βCD with varying densities of a small, negatively charged moiety (carboxyls) and a large, neutral moiety (hydrazides) on the solubilization capacities and thermodynamic parameters of these host-guest interactions as well as the aggregative potential of the complexes (studied herein for the first time on a particle-by-particle basis by nanoparticle tracking analysis). CM/βCDs are of potential direct clinical interest given that they exhibit a high solubility in neutral and alkaline conditions but a reduced solubility in acidic conditions,[151] leading to interest in using CM/βCDs for site-specific drug delivery in the small intestine (i.e. slow release at the acidic conditions of the stomach and fast release at the more basic conditions in the intestine).[158] While Brauns and Muller used phase solubility analysis to report on the increase in digitoxin solubility imparted by a only single CM/βCD derivative (DS=0.26, compared to a full range of derivatizations explored in this work), Hzd/βCD is a CD derivative first reported in this study that holds significant potential as a functional unit in drug delivery vehicles given the relative orthogonality of hydrazide groups toward typical functional groups found *in vivo*;[159] furthermore, hydrazides can react rapidly (within seconds) with aldehyde groups and more slowly (within minutes) with ketone groups to form a hydrolytically-labile covalent bond under physiological conditions, making its potential use in the development of polymer-CD conjugates of particular interest. By grafting a Hzd/βCD derivative onto a polymer support and investigating its complexation behavior with dexamethasone, the effect of immobilizing a βCD moiety on its drug binding capacity can be demonstrated. Given the increasing frequency with which derivatized CDs are being incorporated in polymer-based systems,[157, 160] a detailed comparison of the binding capacity (stoichiometry, solubility enhancement, complexation efficiency), binding strength (association constant, binding enthalpy) and stability (complex aggregation) of a dexamethasone complex with free functionalized CDs relative to polymer-immobilized CDs provides critical insight to facilitate the rational development of controlled release devices.

2.2 Materials and methods

Materials

β-cyclodextrin (≥97% purity), adipic acid dihydrazide (ADH), N'-ethyl-N-(3-dimethylaminopropyl)-carbodiimide (EDC), N-hydroxysuccinimide (NHS), chloroacetic acid (≥ 99.0% purity), dexamethasone (HPLC grade, ≥98.0% purity), 8-anilino-1-naphthalenesulfonic acid ammonium salt (HPLC grade, ≥ 97.0% purity), dextran from *Leuconstroc spp* [M_r ~ 500,000] and sodium periodate (≥99.8% purity) were purchased from Sigma-Aldrich (Oakville, Ontario). Sodium hydroxide pellets were purchased from EMD Chemicals (Mississauga, Ontario), glacial acetic acid from Caledon Laboratory Chemicals (Georgetown, Ontario), ethylene glycol (99.8%) from Fischer Scientific (Ottawa, Ontario). All reagents were used without further purification. All HCl and NaOH solutions were prepared from Acculute standards, with all water used of Milli-Q grade.

Synthesis of βCD derivatives

CM/βCD

CM/βCD was prepared based on the method described by Rivera.[161] 5 g of βCD was dissolved in 42 mL of a 3 M solution of NaOH. 7.29 g of chloroacetic acid was added to the solution, and the mixture was stirred at room temperature until all components were dissolved. The solution was transferred to a water bath set at 70°C and the reaction was carried out for time intervals ranging from 10 min to 75 min, depending on the desired degree of functionalization of the derivative. The solution was cooled to room temperature and neutralized to pH 7.0 with glacial acetic acid. The reaction product was precipitated with methanol and collected through vacuum filtration to yield a syrupy product which was subsequently stirred in acetone overnight to fully precipitate. Following collection by vacuum filtration, the white powder was washed with acetone and dried in an oven at 60°C. To achieve a degree of substitution over 3, successive carboxymethylation steps were performed by repeating the procedure.[162] The average number of carboxymethyl groups on each βCD molecule was determined through potentiometric titration, performing a base-into-acid titration on 50 mg of the βCD derivative dissolved in 1 mM sodium chloride solution using 0.1M NaOH as the titrant and 10 minutes/unit pH as the addition rate (Mandel PC Titrator). (For raw data, see Appendix, Figs. 2A1-2A4) Samples are referenced in

the text as x CM/βCD, where x is the average number of hydroxyl groups on a single βCD ring converted to a carboxyl group.

Hzd/βCD

Hydrazide functionalized derivatives were synthesized from CM/βCD derivative precursors. Briefly, 5 g of a CM/βCD derivative was reacted with a quantity of ADH and EDC corresponding to a five times molar excess of the carboxymethyl content contained in the sample. The reactants were dissolved in deionized water and the pH of the solution was adjusted to 4.75 with 1 M HCl. The reaction was initiated with the addition of EDC and the pH was maintained at 4.75 by acid or base addition until it stabilized (approximately 4 hours total reaction time). The solution was neutralized to pH 7.0 with 1 M NaOH, after which water was removed from the product using a rotary evaporator at 60°C. The product exhibited a syrupy consistency and was precipitated with a large excess of acetone, followed by stirring in acetone overnight. A white powder was produced and collected through vacuum filtration. The degree of substitution of the hydrazide-functionalized product was determined through potentiometric titration as described in 2.2.1, with the average number of hydrazide groups per βCD molecule calculated by subtracting the number of unreacted carboxymethyl groups detected in the hydrazide-functionalized product from the number of carboxymethyl groups present in the initial carboxymethylated product. (For raw data, see Appendix, Figs. 2A1, 2A4-2A6). Samples are referenced in the text as y Hzd/βCD, where y is the average number of hydroxyl groups on a single βCD ring converted to a hydrazide group.

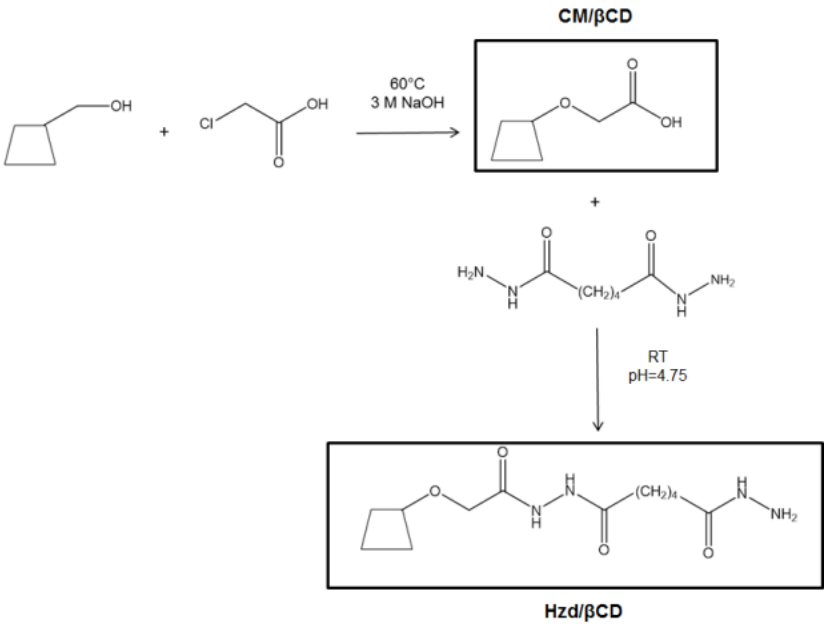

Fig. 2.1 Scheme illustrating the carboxymethylation of βCD and the addition of a hydrazide functionality to CM/βCD.

Synthesis of aldehyde-functionalized dextran (Dex-Aldehyde)

1.5 g of dextran (M_r = 500,000) was dissolved in 150mL of deionized water. The reaction was initiated with the addition of 5 mL of a 160 mg/mL solution of sodium periodate, which was added dropwise to the dextran solution. The reaction was allowed to proceed for two hours and was stopped with the addition of 0.4 mL of ethylene glycol and one hour of further stirring. The modified polymer was dialyzed against water for six cycles and isolated through lyophilization (3500 Da MWCO membrane, Spectrum Corporation). The degree of functionalization of the Dex-Aldehyde polymer was determined by quantifying the carboxylic acid groups generated by silver(I) oxide mediated oxidation of the aldehyde groups through potentiometric titration. Based on the method of Thomason and Kubler, 0.1 g of the Dex-Aldehyde polymer was dissolved in 10 mL of a 0.62 M NaOH solution. Following the addition of 0.3859 g of silver(I) oxide, the solution was stirred overnight.[163] 5 mL of the reaction solution was diluted with 45 mL of water and titrated with 0.1 N NaOH as the titrant and 10 minutes/unit pH as the addition rate (Mandel PC Titrator). Approximately ~6200 aldehyde groups were detected per chain of 500 kDa oxidized dextran. (For raw data, see Appendix, Fig. 2A7).

Synthesis of Dex-βCD

βCDs functionalized with 0.60 hydrazide groups were conjugated to the Dex-Aldehyde polymer via hydrazone linkages. Briefly, 0.6 g of Dex-Aldehyde was dissolved in 50 mL of water. 2 g of 0.6 Hzd/βCD was added to the polymer solution and the reaction was allowed to proceed for 24 hours. The reaction was dialyzed against water for six cycles (3500 Da MWCO membrane, Spectrum Corporation) and the product was isolated through lyophilization. The Dex-βCD polymer was treated with silver(I) oxide and the oxidized product was titrated with 0.1 N NaOH to detect residual (unreacted) aldehyde groups (Mandel PC Titrator). Approximately ~4200 aldheyde groups remained on the Dex-βCD polymer, indicating that ~2000 βCD moieties were grafted as pendant groups on each dextran chain. (For raw data, see Appendix, Figs. 2A7-2A8). Spectrofluorometric data generated from the host-guest interaction of βCD with 8-Anilino-1-naphthalenesulfonic acid ammonium salt (1,8-ANS) were used to validate the successful grafting of Hzd/βCD onto the dextran polymer support.[164] 1.5 wt% solutions of Dex-βCD (approximately 10 mM of βCD content) and Dex-Aldehyde were prepared in 10 mM phosphate buffered saline (PBS, pH=7.4) containing 3.4 mM of 1,8-ANS. Both polymer solutions were shaken at room temperature for 30 min prior to measurement. Steady-state fluorescence was measured using a Cary Eclipse fluorescence spectrophotometer (Varian) in a 1 cm^2 quartz cuvette at ambient temperature (excitation wavelength = 370 nm, emission range = 400-700 nm, excitation/emission bandwidths = 5 nm).

Phase solubility studies

Solubility studies were performed according to the methods of Higuchi and Connors.[165] Excess amounts of dexamethasone were added to CM/βCD, Hzd/βCD and Dex-βCD solutions prepared in 10 mM PBS at a range of different concentrations. The mixtures were shaken at room temperature for 3 days, after which the remaining undissolved drug was removed by passing the solutions through a 0.45 µm syringe filter (Pall Corp). Quantitative determinations of dexamethasone solubility were performed using a high-performance liquid chromatography (HPLC) system composed of a 2707 Autosampler, 2489 UV/Visible Detector and 1525 Binary HPLC Pump, all from Waters Corporation. Samples were analyzed on a reversed-phase Atlantis C18 column (100 mm x 4.6 mm, Waters Corporation) in triplicate. The mobile phase consisted

of 40% acetonitrile and 60% water. A flow rate of 1.0 mL/min resulted in a retention time of approximately 3.7 min. The absorbance was measured at 263 nm. Experiments were performed in triplicate, with errors expressed as the standard deviation of the replicates.

Continuous variation method (Job's method)

The stoichiometries of the βCD derivative inclusion complexes were determined by the continuous variation method.[166] Spectrofluorometric data generated from the host-guest interaction of βCD derivatives with 1,8-ANS were used to construct Job's plots. A constant total concentration of host and guest molecules was maintained at 9 mM, but with a different mole fraction of each component.[166] All solutions were freshly prepared using ultrapure deionized water (Millipore, Resistance >18 MΩ) and were shaken at room temperature for 30 min prior to measurement. Steady-state fluorescence was measured using a Cary Eclipse fluorescence spectrophotometer (Varian) using 10 nm excitation and emission bandwidths. Molecular geometries of 1,8-ANS and dexamethasone were determined computationally using Jmol 13.0 and Marvin View 6.2.0. Experiments were performed in triplicate, with errors expressed as the standard deviation of the replicates.

Isothermal titration calorimetry (ITC)

Calorimetric titrations were performed on a Nano ITC Low Volume system (TA Instruments–Waters LLC, Newcastle, DE, USA). The titration experiment consisted of 20 successive 2.5 µL injections of a βCD derivative into a reaction cell containing 170 µL of a dexamethasone solution (of the concentrations defined in Table 2.1) in water. Samples were prepared in 10 mM PBS and degassed prior to measurements. Experimental conditions used to study each βCD derivative are given in Table 2.1. All experiments were performed at room temperature under constant stirring at 350 rpm. The titration of βCD into dexamethasone resulted in heat signals that were processed by NanoAnalyze software (TA Instruments–Waters LLC, Newcastle, DE, USA). Data from the first injection was removed from the analysis, omitting errors originating from the diffusion of titrant into the calorimetric cell.[167] Dilution heat effects were subtracted from each run. Injection heat data were integrated and fitted to an independent, one-site binding model. The association constant (K_a) and the change in enthalpy (ΔH) were varied, while the stoichiometry of the interaction was set to 1 (as determined from the Job's plots analyses).[168]

These fitting constraints are predicted by the Wiseman isotherm for weak binding systems, which are characterized by a low "Wiseman c" value (product of the receptor concentration and the binding constant).[169] The reported errors represent the parameter values at ±95% confidence intervals of the curve fits.

Table 2.1 Experimental parameters used for each ITC titration

βCD Derivative	**Concentration of Titrant (βCD Derivative, mM)**	**Concentration of Cell (Dexamethasone, mM)**	**Injection Interval (s)**
βCD	5	0.1	200
1.7 CM/βCD	10	0.1	200
3.2 CM/βCD	10	0.1	200
5.5 CM/βCD	10	0.23	200
7.0 CM/βCD	10	0.23	200
1.0 Hzd/βCD	10	0.1	200
3.1 Hzd/βCD	10	0.23	200
5.1 Hzd/βCD	10	0.23	200
6.0 Hzd/βCD	30	0.23	300
Dex-βCD	30	0.23	200

Nanoparticle tracking analysis (NTA)

The size of βCD-drug complexes was analyzed using the NanoSight (NS) LM10 instrument (NanoSight, Amesbury, UK) in order to investigate the aggregation of βCD derivatives. Excess amounts of dexamethasone were added to 30 mM solutions of βCD derivatives prepared in 10 mM PBS; 15 mM of the unmodified βCD sample was used instead due to solubility restrictions. The mixtures were shaken at room temperature for 3 days, after which the remaining undissolved drug was removed by passing the solutions through a 0.45 μm syringe filter (Pall Corp.). Drug/βCD derivative suspensions were then analyzed by tracking the Brownian motion of particles with a laser illuminated microscope. Samples were flowed into the viewing unit using a syringe pump, ensuring continuous sample flow while monitoring a larger particle population. Particle movement was recorded over the course of 90 s and analyzed by nanoparticle tracking software (NTA version 2.2, NanoSight). Average particle sizes represent the number average size of all tracked particles, with the standard deviation of the mean reported as the error.

2.3 Results and Discussion

Synthesis of βCD derivatives with different numbers of carboxymethyl and hydrazide groups

Depending on the time over which the chloroacetic acid functionalization reaction was conducted, βCD derivatives with varying conversions of (mostly primary) alcohols to carboxymethyl (CM) groups could be produced. Fig. 2.2 shows the average number of CM groups per βCD molecule present as a function of reaction time (black diamond points) and reaction cycle (black square points). By tuning the reaction time, CDs with as few as 1.4 CM/βCD and as many as 2.6 CM/βCD could be synthesized in a single reaction cycle. Performing repeat reactions could drive the degree of functionalization even higher, up to a maximum of 7.0 CM/βCD over 5 reaction steps (likely corresponding to the 7 reactive primary alcohol groups available on each βCD molecule).

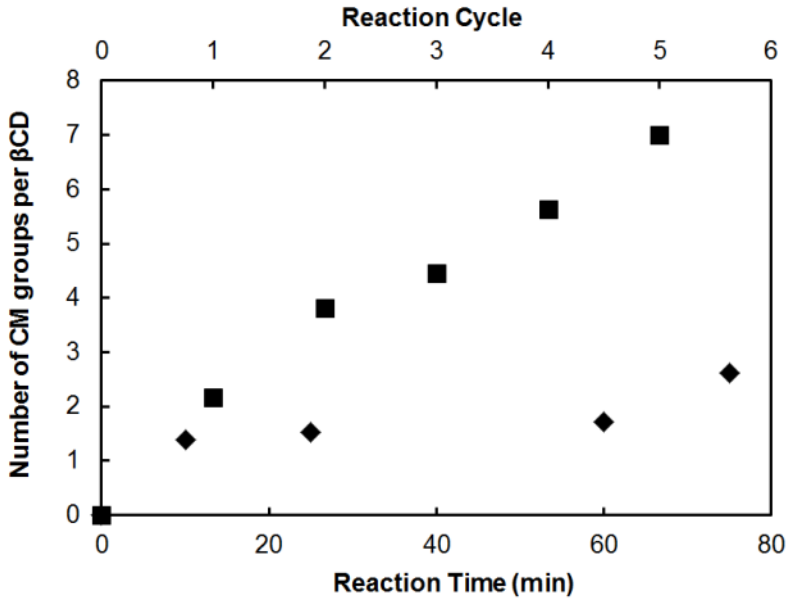

Fig. 2.2 Effect of varying the reaction time (black diamonds, bottom x-axis) and number of reaction cycles (75 min/cycle, black squares, top x-axis) on the number of carboxymethyl groups grafted to βCD.

Table 2.2 outlines the conjugation efficiency of hydrazide groups to CM/βCD precursor derivatives. The conversion yield of CM groups to Hzd groups is high for all of the Hzd/βCD derivatives synthesized, especially when the CM precursor possesses a higher degree of substitution. As such, the number of Hzd groups achievable per βCD molecule is roughly

equivalent to the number of –COOH groups, enabling comparisons between the two functionalized βCD derivatives.

Table 2.2 Efficiency of hydrazide conjugation to CM/βCD precursor derivatives

Number of CM groups/βCD	Number of Hzd groups/βCD	Graft Yield (%)
1.7	1.0	59
3.8	3.1	82
5.6	5.1	91
7.0	6.0	86

Synthesizing βCD derivatives with such varying degrees of substitutions allow for examination of the influence of the degree of functionalization on small molecule binding behavior.

Synthesis of Dex-βCD polymer

Comparison of the titrimetric analyses of the silver(I) oxide-oxidized Dex-βCD and Dex-Aldehyde samples suggested the presence of ~2000 βCD groups per polymer chain. Exposing equal concentrations of βCD-functionalized dextran and unreacted Dex-Aldehyde to 1,8-ANS resulted in a 10-fold increase in fluorescence intensity for the βCD-grafted polymer relative to the dextran polymer before βCD conjugation, confirming the effective conjugation and activity of Hzd/βCD groups on the dextran polymer (Fig.2.3).

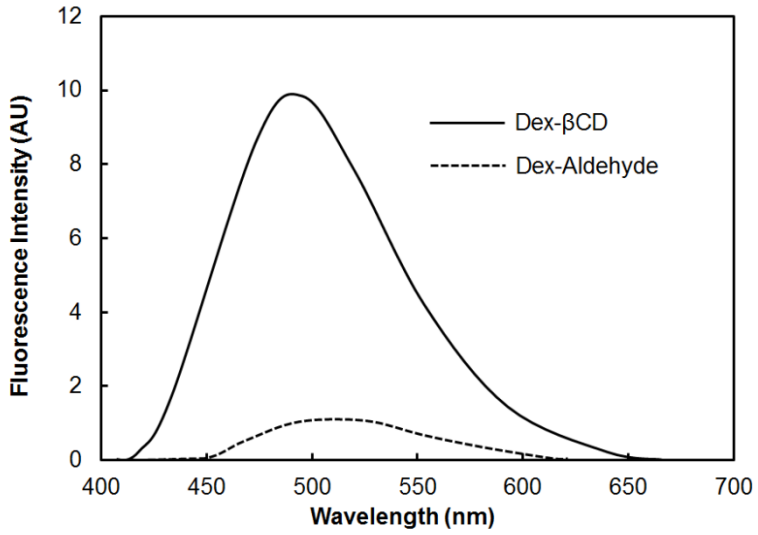

Fig. 2.3 Relative fluorescence spectra of Dex-βCD and dex-aldehyde polymer solutions at 1.5 wt% in a 3.4 mM solution of 1,8-ANS prepared in 10 mM PBS, pH 7.4; (βCD) 10 mM in the Dex-βCD solution.

Stoichiometry of βCD derivative inclusion complexes

We initially attempted to monitor βCD derivative-dexamethasone interactions directly using UV spectroscopy. Using this method, the UV absorption of samples containing a range of drug concentrations, with or without βCD, were measured, with any change in absorption observed upon the addition of βCD suggestive of complex formation.[170] However, given the limited solubility of dexamethasone in aqueous media, the absorbance values were too low to detect such spectral changes. Instead, Job's plots were constructed from spectrofluorometric data generated from the host-guest interaction of βCD derivatives with 1,8-ANS. 1,8-ANS has a similar molecular weight as dexamethasone (1,8-ANS: 316.4 g/mol; dexamethasone: 392.5 g/mol) as well as a similar Van der Waals volume (1,8-ANS: 252 $Å^3$; dexamethasone: 362 $Å^3$). Given the importance of size/shape matching in host-guest chemistry, the two compounds are likely to be subject to similar steric limitations encountered in βCD complexation.[36]

Figs. 2.4a-2.4i show the Job's plots of the interactions of all synthesized CM/βCD and Hzd/βCD derivatives with 1,8-ANS.

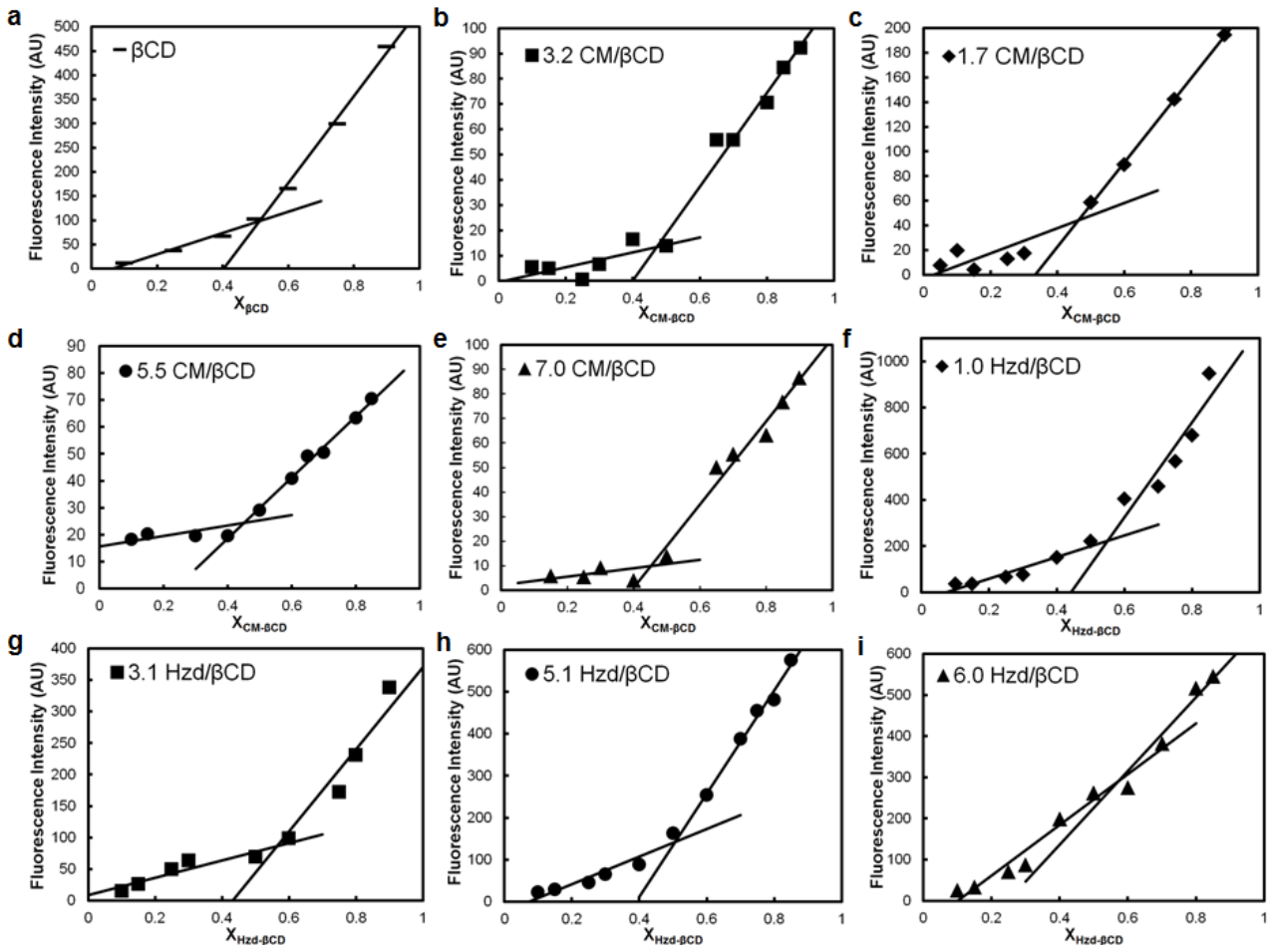

Fig. 2.4 Job's plots of CM/βCD and Hzd/βCD derivatives with 1,8-ANS in 10 mM PBS, pH 7.4. The total concentration of both components was maintained at 9 mM. Measurements were performed in triplicate, with errors expressed as the standard deviation of the replicates.

In the range of mole fractions that were examined, there were two linear regions in each plot, with the first slope corresponding to the case where βCD is the limiting reagent (lower mole fractions) and the second slope corresponding to the case where 1,8-ANS is the limiting reagent (higher mole fractions). As such, the intersection point represents a mole fraction corresponding to the stoichiometry of the complex.[171] In all of the plots, the two linear regions intersect at a βCD mole fraction of ~0.5, indicating a 1:1 binding stoichiometry for all of the complexes. This is consistent with previous studies on the complexation behavior of 1,8-ANS with native βCD and HPβCD, in which 1:1 binding stoichiometries were also observed.[164, 172] As such, functionalization of βCD groups does not significantly change the stoichoimetry of the binding interactions.

Phase solubility analysis

The phase solubility diagrams of dexamethasone in the presence of all synthesized CM/βCD and Hzd/βCD derivatives and the Dex-βCD polymer are shown in Figs. 2.5a and 2.5b, respectively. Note that native βCD was not included in the phase solubility analysis due to its limited water solubility; functionalization of βCD with as little as 1 CM or Hzd moiety per CD ring increased the water solubility of the βCD unit from ~15 mM (unmodified) to >100 mM.

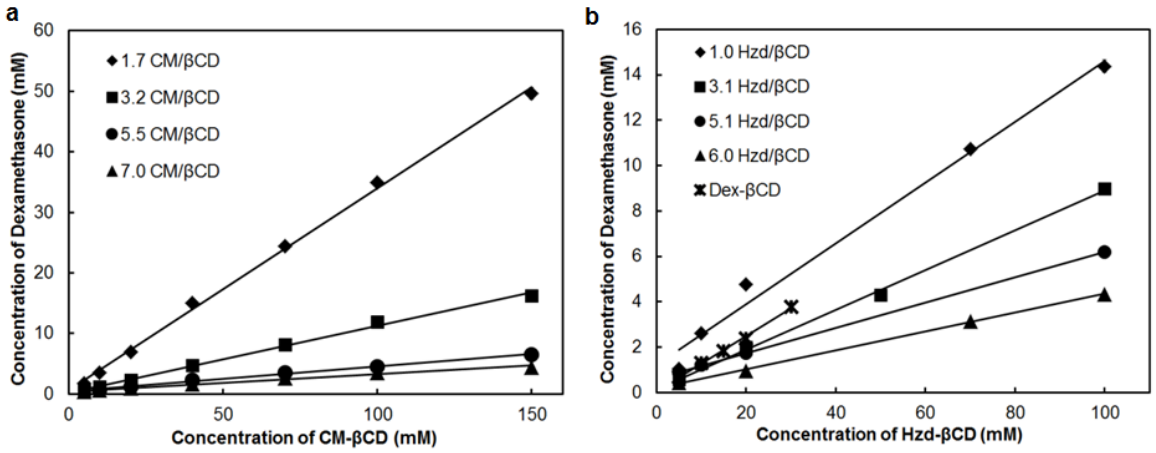

Fig. 2.5 Phase solubility diagrams of (a) CM/βCD, (b) Hzd/βCD derivatives and Dex-βCD (prepared by grafting 1.0 Hzd/βCD to dextran) with dexamethasone in 10 mM PBS, pH 7.4.

All of the phase-solubility profiles are of the A_L type and the slopes of the linear regions are all less than one, suggesting that the assumption of 1:1 drug/CD complexation is valid.[173] A more quantitative description of the complexation behavior can be achieved by considering the values of the apparent affinity constant, K_a, defined by Eq. 1:

$$K_a = \frac{\text{Slope}}{S_o(1-\text{Slope})} \qquad \text{(Eq. 1)}$$

K_a is calculated from the slope of the phase-solubility profile and S_o, the solubility of the drug in the absence of βCD (this value should be equivalent to S_{int}, the y-intercept of the linear region of the phase solubility plot). We have chosen to use S_o (0.08 mg/mL in PBS, measured at room temperature) in our calculations since the aggregation of drug molecules in a saturated solution can skew the measured S_{int} values away from the true S_o value.[174] Given the controversy around

the use of phase solubility analysis for determining the K_a of drugs with S_o <1 mg/mL (in which small solubility measurement uncertainties can lead to significant errors in the K_a calculation),[175] we have also calculated the complexation efficiency (CE), which has been proposed to be more accurate for comparing and contrasting complexation behaviors of βCDs.[46] Since the numerical value of CE is only dependent on the slope of the phase-solubility profile and is therefore independent of S_o and S_{int}, CE values are generally more consistent in comparison to calculated K_a values. CE is defined as the ratio of complexed CD to free CD as per Eq. 2:

$$CE = S_o \cdot K_{1:1} = \frac{\left[\frac{D}{CD}\right]}{[CD]} = \frac{Slope}{(1-Slope)} \quad \text{(Eq. 2)}$$

Table 3 gives the apparent affinity constants K_a and CE values for the synthesized CM/βCD and Hzd/βCD derivatives.

1.7 CM/βCD has the highest K_a value (2450±180 M^{-1}), similar to that of (2-Hydroxypropyl)-β-cyclodextrin, reported as 2193 M^{-1} from phase solubility analysis.[176]

Table 2.3 Apparent affinity constants of βCD derivative/dexamethasone inclusion complexes estimated from phase solubility diagrams. The reported errors represent the 95% confidence limits obtained from the regression analysis of the phase solubility data.

βCD Derivative	**K_a (M^{-1})**	**Complexation Efficiency (CE)**
1.7 CM/βCD	2450±180	0.50±0.04
3.2 CM/βCD	610±60	0.13±0.01
5.5 CM/βCD	210±40	0.04±0.01
7.0 CM/βCD	140±30	0.03±0.01
1.0 Hzd/βCD	760±220	0.16±0.04
3.1 Hzd/βCD	470±80	0.10±0.02
5.1 Hzd/βCD	290±40	0.06±0.01
6.0 Hzd/βCD	210±30	0.04±0.01
Dex-βCD	690±30	0.14±0.02

For both types of derivatives, the increase in the degree of functionalization reduces the stability constant associated with the βCD-dexamethasone complex. For example, the least functionalized CM derivative (1.7CM/βCD) has the highest K_a value (2450±180 M^{-1}) and CE value (0.50± 0.04) among all derivatives, while the least functionalized Hzd derivative (1.0Hzd/βCD) exhibits the second highest values of both K_a (760±220 M^{-1}) and CE (0.16± 0.04).

This result suggests that increasing the number of functional groups on the βCD ring limits the ability of dexamethasone to form an inclusion complex with βCD, likely by steric hindrance of dexamethasone approach and/or binding by the bulky ring substituents. However, electronic effects associated with the electron withdrawing carbonyl functionality adjacent to the main βCD ring in the derivatized CD compounds cannot be completely ruled out as contributing factors to this lower affinity. The presence of electron withdrawing groups on the βCD ring can negatively influence complexation with a guest molecule due to the reduction of electron density within the cavity; in contrast, a βCD cavity possessing an electron dense nature can promote positive enthalpic interactions with a potential guest molecule. With the exception of the lower functionalized derivatives (1.7 CM/βCD and 1.0 Hzd/βCD), the stability constants are similar for CM/βCD and Hzd/βCD derivatives functionalized to similar degrees despite the fact that the adipic acid hydrazide moiety has a molecular weight four times larger than that of the carboxymethyl group. As such, it is likely that some combination of steric and electronic effects contribute to binding affinity changes in these systems. Another potential interpretation of this result is that, above a certain threshold of near-cavity functionalization, the addition of the bulky hydrazide group does not significantly additionally increase the steric hindrance associated with dexamethasone binding.

It has previously been reported that βCDs derivatized with charged functionalities can enhance inclusion complex formation since electrostatic repulsion between functional groups can expand the hydrophobic cavity;[148] however, in this case, the solubilization capacity of CM/βCD is significantly decreased by functionalization. The solubilizing power of charged cyclodextrins has been reported to depend on the distance between the charged end group and the CD binding pocket, with enhanced complexation observed when the charge is located farther away from the cavity; this has been observed for example in sulfobutyl ether βCD derivatives (in particular, derivatives functionalized with 7 substituents) in which the length of the butyl ether spacer group promotes an augmented solubilization capacity relative to unmodified CDs.[177] We hypothesize that this effect is not observed for the higher functionalized CM/βCD derivatives studied since the charged substituents in the CM/βCD derivates are much closer to the cavity and are thus more likely to pose steric inhibition to drug binding to the cavity.

Of note, the Dex-βCD grafted polymer showed stability constants and CE values (K_a= 690±30, CE=0.14±0.02) within experimental error of the 1.0 Hzd/βCD derivative used to prepare the graft polymer (K_a=760±220, CE=0.16±0.04). These results strongly suggest that immobilizing a CD derivative does not change its complexation behavior with dexamethasone and further support our interpretation of steric considerations affecting drug binding only in terms of the steric bulk of substituents very close to the hydrophobic binding pocket.

Isothermal titration calorimetry (ITC)

Calorimetric measurements facilitate more accurate determination of the binding constants and the change in enthalpies associated with the dexamethasone-functionalized CD interactions. During complex formation, van der Waals interactions between solvent molecules and the CD substrates are replaced by more enthalpically favourable interactions between the guest and the CD cavity; however, the associated decrease in conformational freedom of both the host and the guest that results from complex formation typically makes binding entropically unfavorable.[148] Additional energetic considerations may arise from hydrophobic interactions between the host and guest enabling the release of water molecules contained in the CD cavity.[139] Consistent with the result of the phase solubility analyses, lower functionalized βCD derivatives form stronger inclusion complexes with dexamethasone (Table 2.4; see Appendix, Figs. 2A9 – 2A28 for raw and fitted data). This effect has previously been observed with other cyclodextrin derivatives possessing lower degrees of substitution; for example, randomly methylated βCDs and γCDs with a 0.6 degree of substitution exhibited higher solubilization capacity than their more highly functionalized counterparts.[178] In particular, binding efficiency is drastically reduced for higher functionalized CM/βCD derivatives, for which the K_a value associated with the 3.2CM/βCD complex is about half of the K_a value for the 1.7CM/βCD complex. ITC data also confirmed that Hzd derivatives prepared from each corresponding CM derivative had similar or slightly lower binding affinities, with hydrazide functionalizations with the highest conversions exhibiting the most similar binding constants.

Table 2.4 Thermodynamic parameters of βCD derivative/dexamethasone interactions obtained by ITC analysis. Errors are associated with 95% confidence intervals of the curve fits.

βCD Derivative	ΔH (kJ/mol)	K_a (M^{-1})
βCD	-25±1	6210±890
1.7 CM/βCD	-35±2	1940±310
3.2 CM/βCD	-27±3	850±250
5.5 CM/βCD	-18±3	670±180
7.0 CM/βCD	-22±3	540±140
1.0 Hzd/βCD	-28±3	1180±300
3.1 Hzd/βCD	N/A	850±300
5.1 Hzd/βCD	N/A	580±70
6.0 Hzd/βCD	N/A	260±140
Dex-βCD	-41±3	730±150

Calorimetric measurements made on the Dex-βCD polymer confirmed that immobilizing 1.0 Hzd/βCD did not affect the stability constant of the derivative, as both ITC derived K_a values were found to be statistically equivalent to those of the free, ungrafted βCD ($p > 0.05$, Table 2.4). Similar results were found by Nielsen et al. for βCD moieties grafted onto 70 kDa dextran chains using click chemistry, with analogous binding constants for grafted and non-grafted functional βCD moieties and slight decreases in stability constants observed for polymers functionalized with higher densities of βCD groups.[179]

ITC analyses also allowed for the direct comparison of native βCD complexation with that of the CM/βCD and Hzd/βCD derivatives, given the low concentrations (below the solubility limit of unmodified βCD in water) required for ITC analysis. Unmodified βCD formed an inclusion complex with dexamethasone with a K_a value over three times higher than even the lowest functionalized CM/βCD derivative, again confirming that the overall effect of both types of functionalization was a significant decrease in binding affinity for dexamethasone even at low degrees of substitution.

Changes in enthalpy were consistent across the different CM/βCD derivatives tested. However, due to low dexamethasone binding and thus the small amounts of heat generated by Hzd/βCD derivatives functionalized with 3 or more Hzd groups (see Appendix, Figs. 2A21-A26), it was difficult to obtain accurate approximations of the ΔH values from the multi-parameter fitting; as a result, these values are marked "N/A" in Table 2.4. This result is consistent with the large

negative enthalpy previously reported for CD host-guest inclusion complexation, while the entropic component can be either positive or negative depending on the primary driving force of the interaction.[138] Moreover, these ΔH values are similar to the change in enthalpy measured from the interaction of (2-hydroxypropyl)-βCD with the corticosteroid hydrocortisone (-20 kJ/mol)[148], confirming the validity of the technique for studying inclusion complex formation. The ΔH value derived from the binding isotherm of Dex-βCD and dexamethasone was -41±3 kJ/mol, again consistent with the result reported by Nielsen et al. for their click chemistry-grafted βCD-dextran polymer (30.8-32.6 kJ/mol). These results collectively suggest that that inclusion complex formation in the context of CM or Hzd functionalized βCD groups is primarily enthalpy driven[179] and that the binding affinity of the host-guest interaction decreases systematically with the degree of functionalization of the cyclodextrin.

Nanoparticle tracking analysis

CD-based aggregates have previously been analyzed using techniques such as osmometry, light scattering and electronic microscopy in CD/drug samples exhibiting an A_L type solubility profile such as the CM and Hzd βCD derivatives produced in this study.[149] This indicates that other mechanisms may be participating in drug solubilization, although it is typically understood that only a small proportion of CD molecules form aggregates in most cases.[138] To assay the capacity of CM and Hzd βCD derivatives to aggregate, we performed both dynamic light scattering and single nanoparticle tracking analysis to track the aggregate size and, in the case of nanoparticle tracking, concentration. Interestingly, CD aggregates were not detected when CM/βCD, Hzd/βCD, or Dex-βCD samples with any degree of functionalization were analyzed with dynamic light scattering (DLS) (data not shown), suggesting the potential utility of these solubilized cyclodextrins as delivery vehicles. However, since DLS is an ensemble technique and thus has limited capacity to detect small numbers of particularly small aggregates, nanoparticle tracking analysis (NTA) was also employed for the first time in the detection and sizing of CD aggregates. In NTA, the displacement of individual particles as a result of their Brownian motion is directly monitored using laser light scattered from each individual particle, permitting a direct calculation of the number-average size distribution in any sample not possible with DLS or other ensemble techniques that look at average properties. NTA, by counting individual particles, also enables direct measurements of particle concentrations or, in this case, the concentration of aggregates between samples prepared with the same initial (soluble) βCD

concentration, not possible with DLS or other conventional sizing techniques. Table 2.5 reports the mean particle sizes of aggregates and the concentration of aggregates found in βCD derivative samples saturated with dexamethasone, while Fig. 2.6 shows the particle size distributions for each βCD derivative alone or complexed with dexamethasone.

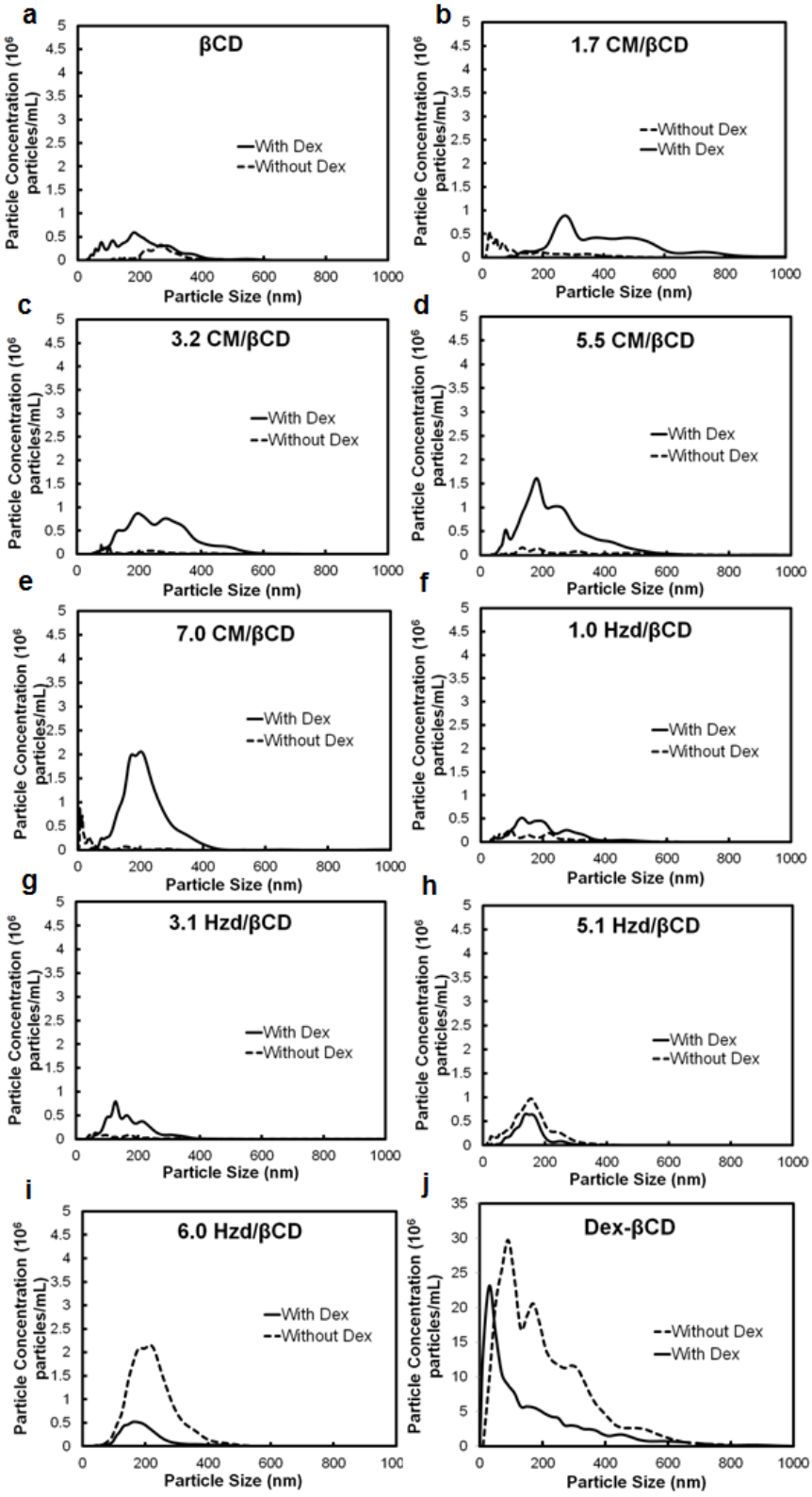

Fig. 2.6 Particle size distributions of CM/βCD, Hzd/βCD and Dex-βCD alone or complexed with dexamethasone in 10 mM PBS, pH 7.4 from nanoparticle tracking analysis.

Table 2.5 Particle sizes of CM/βCD and Hzd/βCD derivatives alone or complexed with dexamethasone. Measurements were made in 10 mM PBS, pH 7.4 and obtained by nanoparticle tracking analysis. Results are expressed as means ± standard deviations.

βCD Derivative	**With Dex**		**Without Dex**	
	Mean Particle Size (nm)	**Aggregate Concentration (10^6 particles/mL)**	**Mean Particle Size (nm)**	**Aggregate Concentration (10^6 particles/mL)**
βCD	213±101	114	212±78	39
1.7 CM/βCD	420±192	218	156±129	50
3.2 CM/βCD	272±105	207	191±154	16
5.5 CM/βCD	245±114	287	307±183	31
7.0 CM/βCD	220±95	301	87±118	24
1.0 Hzd/βCD	207±107	86	189±115	40
3.1 Hzd/βCD	175±69	85	146±85	14
5.1 Hzd/βCD	174±73	81	161±68	123
6.0 Hzd/βCD	203±88	75	224±71	346
Dex-βCD	172±174	150	206±140	315

The lowest functionalized CM/βCD derivative forms the largest aggregates when complexed with dexamethasone, with aggregate size slightly decreasing as the degree of functionalization of the βCD derivative increases. Indeed, for the CM/βCD derivatives, a correlation is observed between the CE values and the mean particle sizes of the aggregates formed following drug loading, in which a decrease in CE value is directly reflected by smaller aggregate sizes (Fig. 2.7, Two-way-ANOVA α=0.05, F=42.33, p=0.007). This effect is consistent with previous studies investigating the complexation of HPβCD with dextromethorphan, hydrocortisone, ibuprofen and ketoprofen.[180] We hypothesize that this trend may be related to the formation of effectively amphiphilic structures upon strong binding between a hydrophilic CD derivative with a hydrophobic drug; any part of the hydrophobic drug not contained directly within the binding pocket can behave as the hydrophobic part of an amphiphile that can drive hydrophobic self-assembly into aggregates. Specific to our model drug dexamethasone, ^{1}H NMR studies have indicated that the ring containing the ketone group in dexamethasone is more likely to be outside of CD while the other two rings are likely to be inside the cavity[181], providing a hydrophobic exposed tail that may drive self-assembly. This hypothesis is further supported by the significant increase in the total concentration of aggregates from extremely small (almost negligible) values in the absence of drug to significantly higher values upon addition of drug for each of CM-

functionalized derivative (Table 2.5), indicating an increased proclivity toward self-assembly following drug complexation.

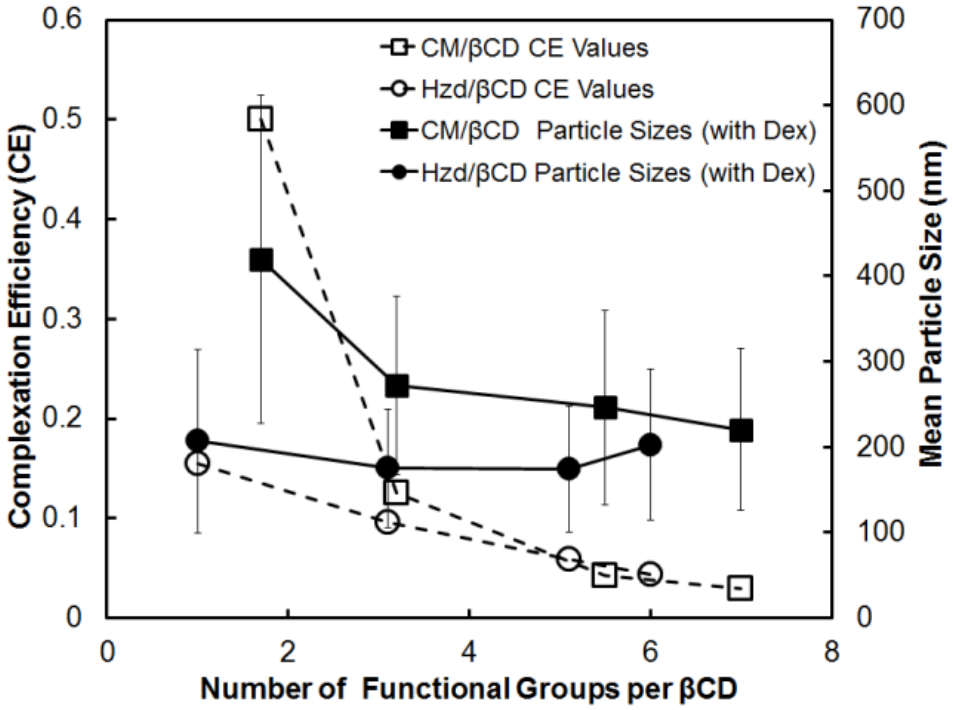

Fig. 2.7 Complexation efficiency (CE) values and mean particle sizes of CM/βCD and Hzd/βCD derivatives as a function of the number of CM or Hzd groups per βCD derivative.

In contrast, the Hzd/βCD derivatives showed no trend between the degree of functionalization, the aggregate particle size, and the complexation efficiency (Fig. 2.7), with aggregate size approximately independent of the number of hydrazide groups attached to βCD in the presence of the drug. Furthermore, the concentration of aggregates following drug binding to Hzd/βCD derivatives is significantly lower than that observed for CM/βCD derivatives, particularly at higher degrees of functionalization; indeed, in the case of Hzd/βCD, drug binding actually decreases the total aggregate concentration versus the non-complexed βCD derivative at higher degrees of Hzd functionalization, at which significant aggregation is observed in the non-drug loaded samples. We hypothesize this result is attributable to the bulkier nature of the hydrazide graft to the βCD core, effectively sterically "masking" of any part of the drug not contained directly inside the binding pocket of the βCD and thus resulting in weakly or non-amphiphilic structures less prone to self-assembly. Coupled with the biological orthogonality of Hzd groups in terms of reactivity with proteins and the similar binding constants between CM and Hzd βCD

derivatives with similar degrees of functionalization (Table 2.4), this result suggests that Hzd derivatives may have advantages over CM derivatives for use in delivery applications in terms of minimizing or avoiding complex aggregation upon drug binding.

It was not expected that the polymer grafted βCD moieties would display a tendency towards aggregative behavior since reducing the mobility of βCD molecules should limit self-association. Accordingly, NTA data shows that dexamethasone does not drive aggregate formation in Dex-βCD polymers; indeed, the size of the polymer species decreases upon addition of the drug (Fig. 2.6j). This result is consistent with the results of Fulop et al. for ester-conjugated βCD-dextran polymers with molecular weights ranging from 6 kDa to 70 kDa when complexed with hydrocortisone, with the increased hydrophobicity of the complexed polymers hypothesized to cause the individual chains to adopt a more condensed conformation.[182] However, dextran-βCD polymers synthesized with a range of other degrees of substitution and/or conjugation chemistries did form aggregates when complexed with hydrocortisone, albeit at a fraction of 10-30% and possessing limited stability.[182] On this basis, the hydrazone-functionalized βCD derivatives appear to offer a range of particularly attractive properties for performing βCD conjugations to polymers, including limiting the aggregation of the conjugate polymer, providing a simpler and more mild set of conjugation conditions relative to ester synthesis, and facilitating the formation of either hydrolysis-sensitive (in its native state) or hydrolysis-insensitive (in its reduced state, readily accomplished via mild reduction) linkages between the βCD groups and the polymer.[183]

Inclusion complex formation is influenced by van der Waals, hydrophobic and electrostatic interactions, as well as hydrogen bonding.[184] These forces can all significantly affect the stability of an inclusion complex, although the degree to which each force contributes to complexation is not fully understood.[185] Thus, derivatizing βCD in order to increase its solubility or facilitate CD grafting onto polymers must be strategically done in order to minimize the reduction in K_a values that can result when varying the substituent type and number while still minimizing or eliminating the aggregation of the βCD groups and/or the βCD-functionalized polymers. This is particularly critical when multi-functional βCDs are targeted with the aim of using the βCD as a cross-linking agent; phase solubility analysis indicates these derivatives have low binding constants for the target drug while NTA analysis suggests consistent aggregative behavior,

limiting the potential use of these multi-functional βCD entities as pharmaceutical excipients in, for example, hydrogel-based delivery vehicles in which the hydrogel is cross-linked with βCD groups. Given that the complexed Dex-βCD polymer can resist aggregation without compromising its drug binding capacity, it may hold greater potential as a delivery vehicle.

2.4 Conclusion

CM/βCD and Hzd/βCD derivatives exhibited similar complexation behaviors with dexamethasone including 1:1 stoichiometry, linear phase solubility profiles and consistent enthalpy changes. Increased functionalization was found to reduce the stability constants of the βCD derivative/dexamethasone complexes as well as the complexation efficiency (CE) of both βCD derivatives. When Hzd/βCD was grafted onto a polymer support, it displayed a CE value and a stability constant in a range similar to that of a free, monofunctionalized Hzd/βCD derivative, an affinity significantly higher than those of βCD units functionalized with multiple functional groups. A direct relationship was found between the CE values of the CM/βCD derivatives and the size of aggregates formed when complexed with dexamethasone; in contrast, Hzd/βCD aggregate size was independent of CE, with significantly lower aggregate sizes and concentrations observed relative to CM/βCD complexes at all degrees of functionalization. We hypothesize that this result relates to the improved blocking of hydrophobic drug residues outside the βCD cavity by the more bulky and highly polar hydrazide functionalized groups. Dex-βCD did not display a tendency towards aggregative behavior, indicating that inclusion complexation is likely the sole mechanism of drug solubilization associated with this system. Taken together, these findings can help in the design of CDs that can more effectively enhance the bioavailability of poorly soluble drugs or act as functional sites in polymeric drug delivery vehicles. Specifically, from this study, we can conclude (1) given the high solubility, drug binding constant, and aggregation stability noted for the polymer-grafted Dex-βCD derivative relative to the individual solubilized βCD units, polymer-bound βCD groups are attractive molecular carriers for hydrophobic drugs; (2) given the similar drug binding constants but significantly lower aggregation observed for Hzd/βCD derivatives relative to CM/βCD derivatives, Hzd/βCD may have utility as a robust solubilization agent for hydrophobic drugs.

Appendix

Appendix 2A. Supplementary data

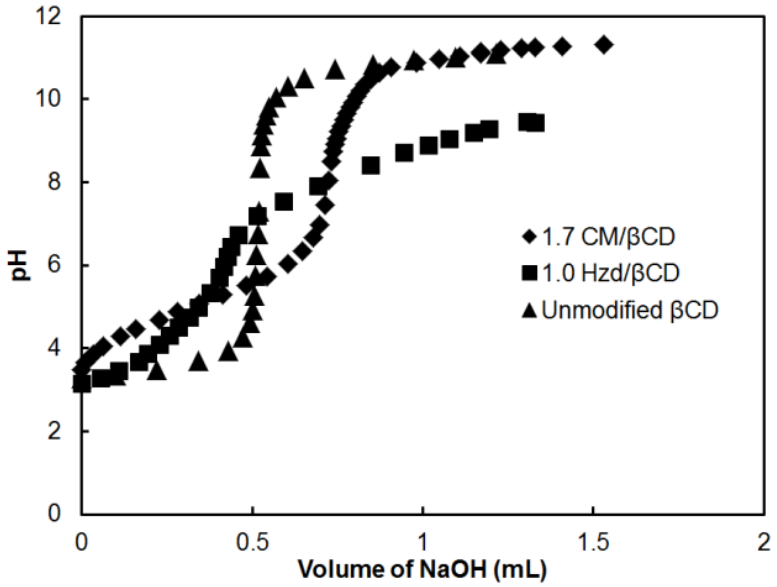

Fig. 2A1 Potentiometric titration curves of 1.7 CM/βCD and 1.0 Hzd/βCD. The 1.7 CM/βCD derivative was used as a precursor in the synthesis of the 1.0 Hzd/βCD derivative. The titration curve of an unmodified βCD sample is shown for comparison purposes.

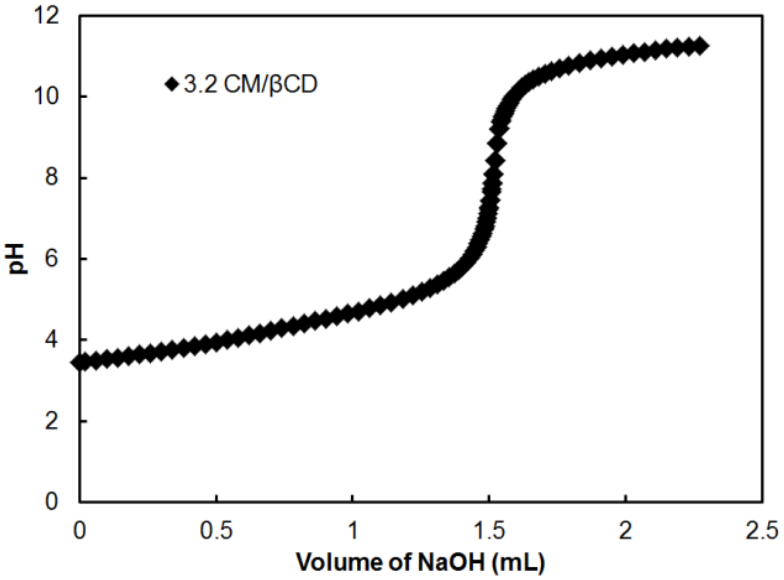

Fig. 2A2 Potentiometric titration curve of 3.2 CM/βCD.

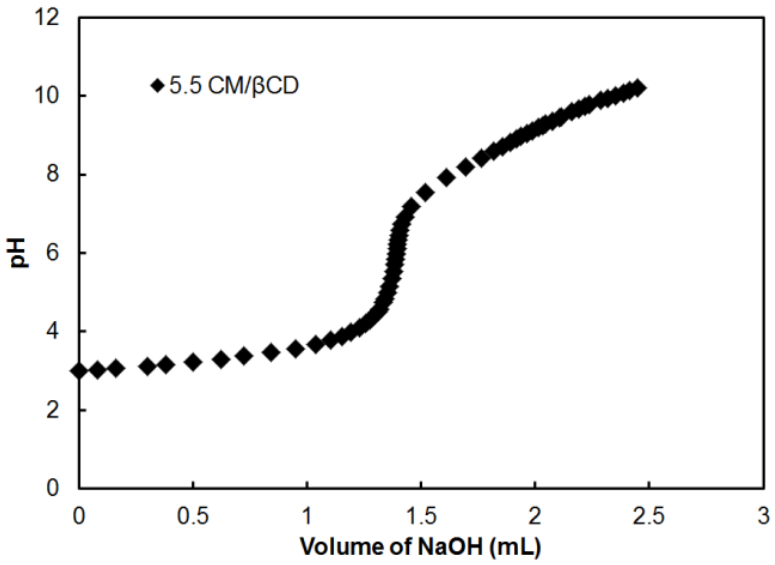

Fig. 2A3 Potentiometric titration curve of 5.5 CM/βCD.

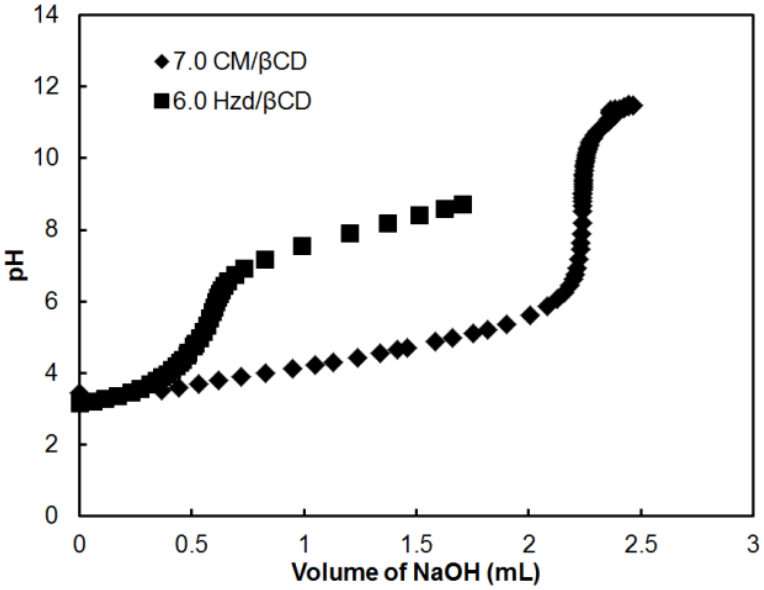

Fig. 2A4 Potentiometric titration curve of 7.0 CM/βCD and 6.0 Hzd/βCD. . The 7.0 CM/βCD derivative was used as a precursor in the synthesis of the 6.0 Hzd/βCD derivative.

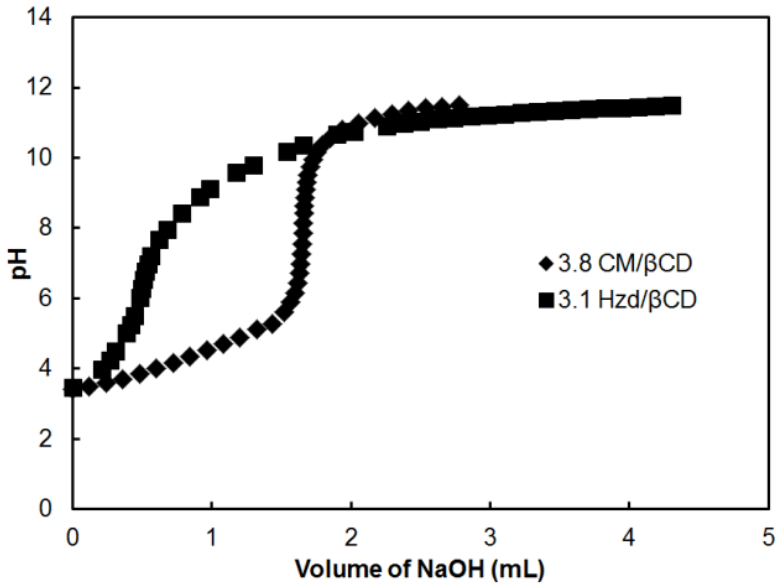

Fig. 2A5 Potentiometric titration curve of 3.1 Hzd/βCD. The 3.8 CM/βCD derivative was used as a precursor in the synthesis of the 3.1 Hzd/βCD derivative.

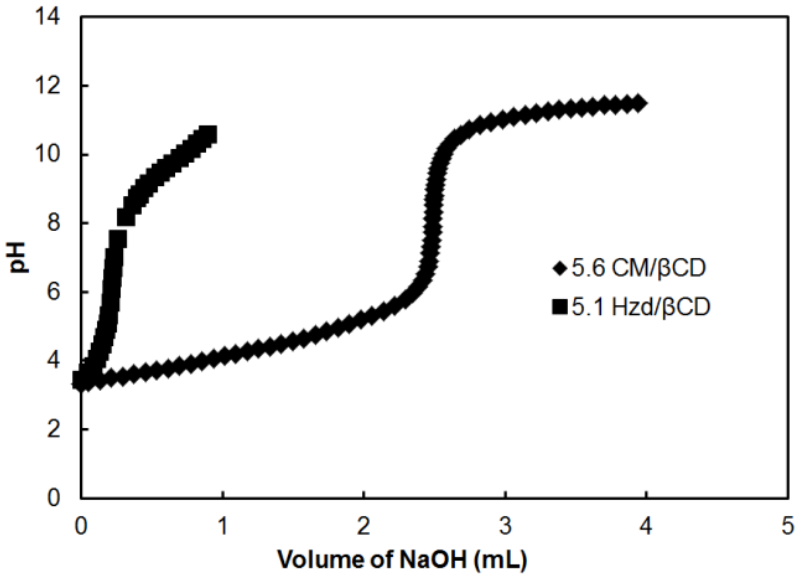

Fig. 2A6 Potentiometric titration curve of 5.1 Hzd/βCD. The 5.6 CM/βCD derivative was used as a precursor in the synthesis of the 5.1 Hzd/βCD derivative

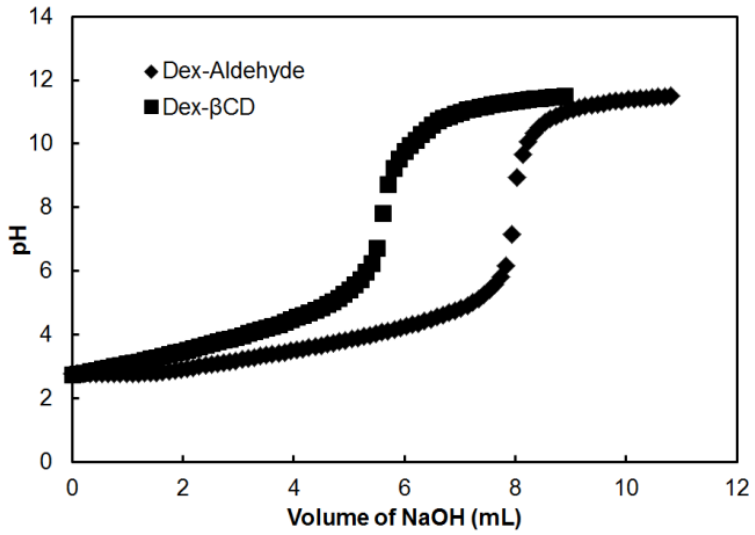

Fig. 2A7 Potentiometric titration curves of oxidized Dex-Aldehyde and Dex-βCD polymers following treatment with silver(I) oxide. βCDs functionalized with 0.60 hydrazide groups were conjugated to the Dex-Aldehyde polymer via hydrazone linkages.

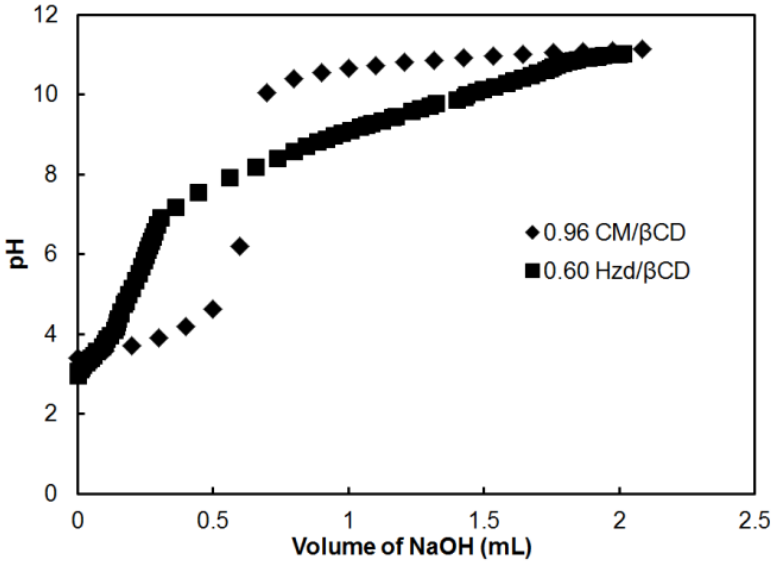

Fig. 2A8 Potentiometric titration curve of 0.60 Hzd/βCD. The 0.96 CM/βCD derivative was used as a precursor in the synthesis of the 0.60 Hzd/βCD derivative.

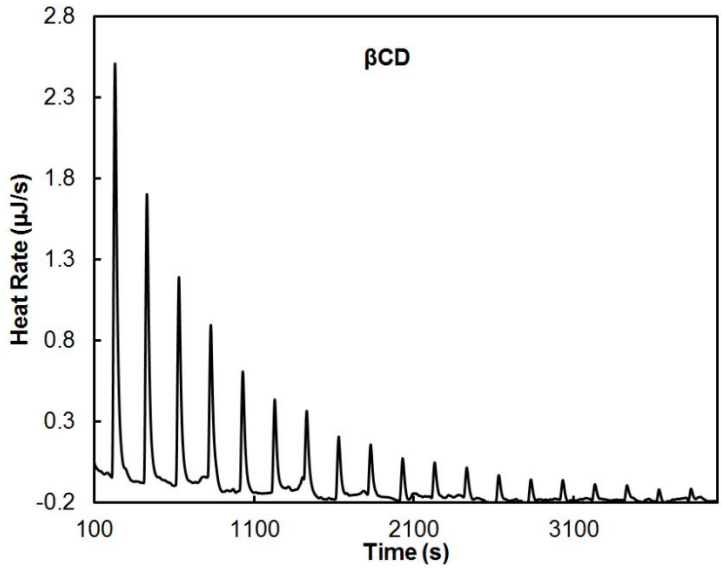

Fig. 2A9 ITC titration curve of βCD.

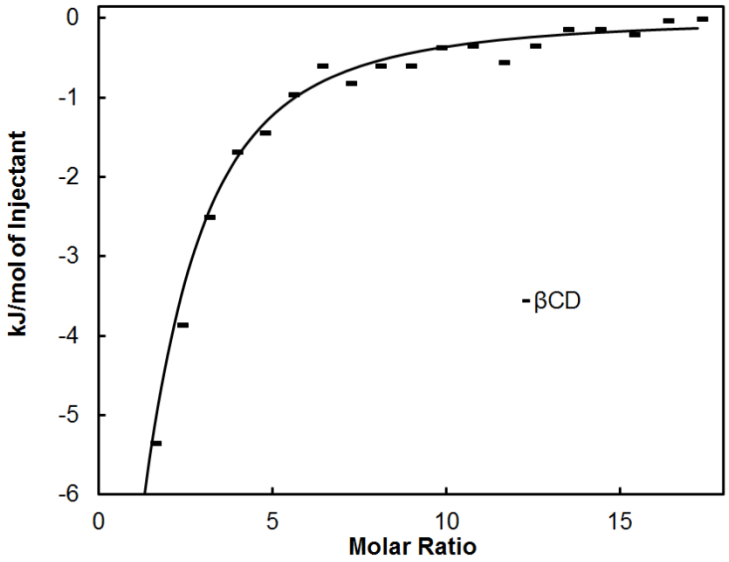

Fig. 2A10 ITC titration profile of βCD. The plot shows the corrected heat of reaction per mole of βCD injected as a function of the molar ratio of βCD to dexamethasone in the calorimeter cell, fitted to an independent, one-site binding model.

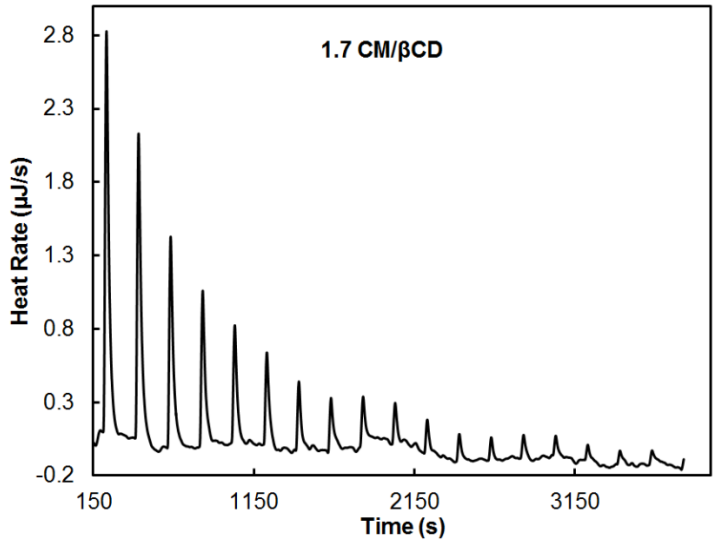

Fig. 2A11 ITC titration curve of 1.7 CM/βCD.

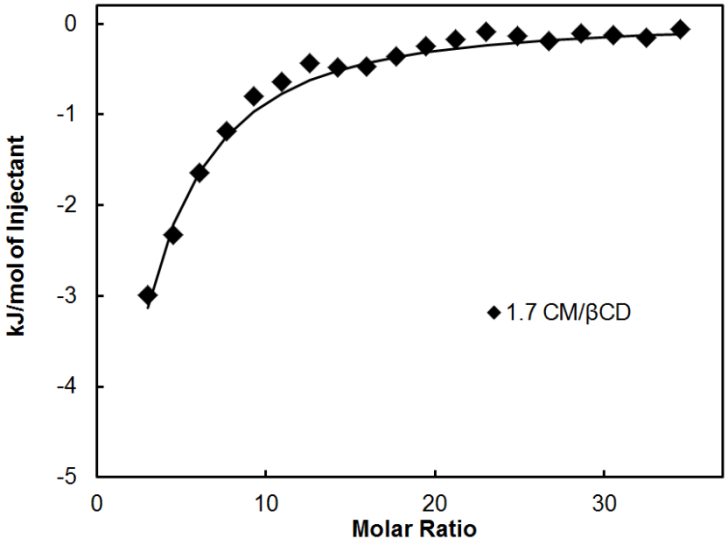

Fig. 2A12 ITC titration profile of 1.7 CM/βCD. The plot shows the corrected heat of reaction per mole of βCD derivative injected as a function of the molar ratio of βCD derivative to dexamethasone in the calorimeter cell, fitted to an independent, one-site binding model.

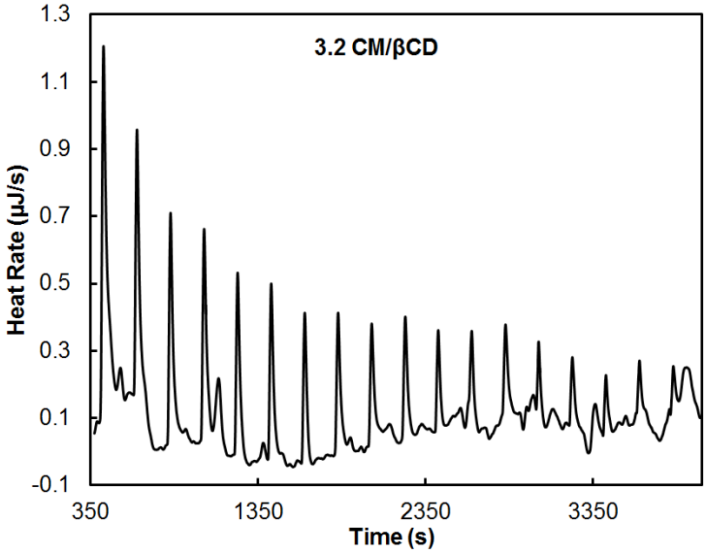

Fig. 2A13 ITC titration curve of 3.2 CM/βCD.

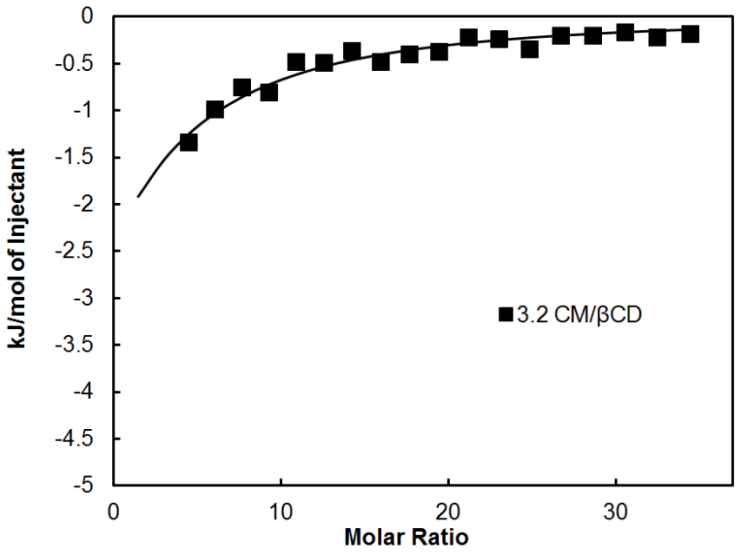

Fig. 2A14 ITC titration profile of 3.2 CM/βCD. The plot shows the corrected heat of reaction per mole of βCD derivative injected as a function of the molar ratio of βCD derivative to dexamethasone in the calorimeter cell, fitted to an independent, one-site binding model.

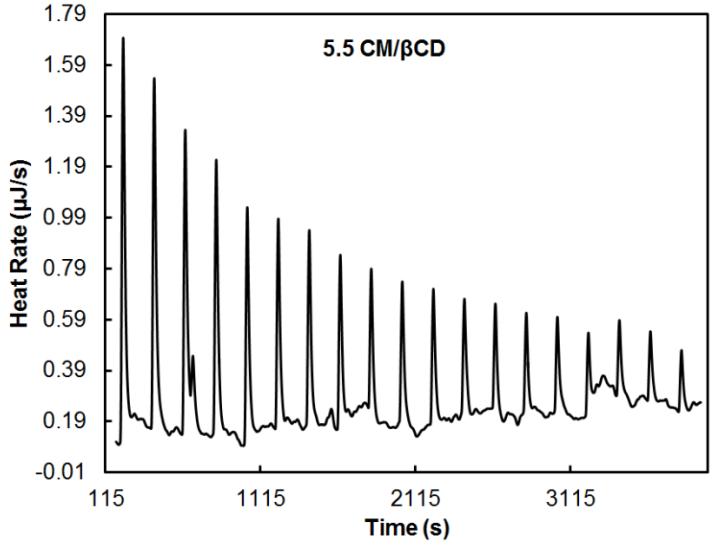

Fig. 2A15 ITC titration curve of 5.5 CM/βCD.

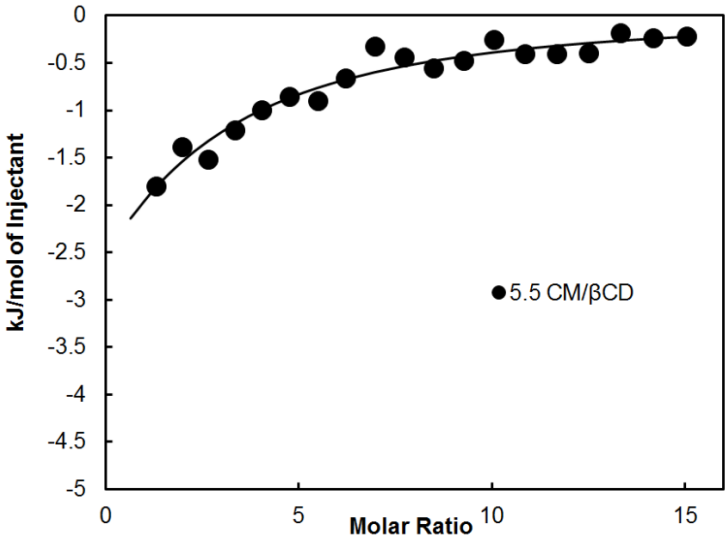

Fig. 2A16 ITC titration profile of 5.5 CM/βCD. The plot shows the corrected heat of reaction per mole of βCD derivative injected as a function of the molar ratio of βCD derivative to dexamethasone in the calorimeter cell, fitted to an independent, one-site binding model.

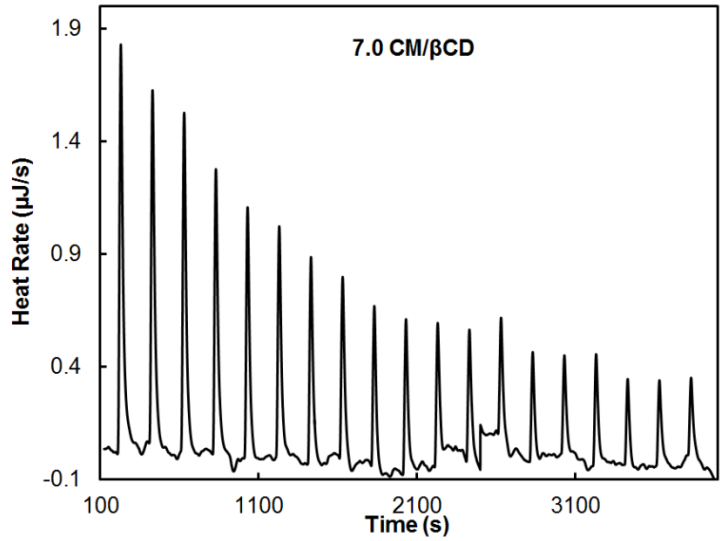

Fig. 2A17 ITC titration curve of 7.0 CM/βCD.

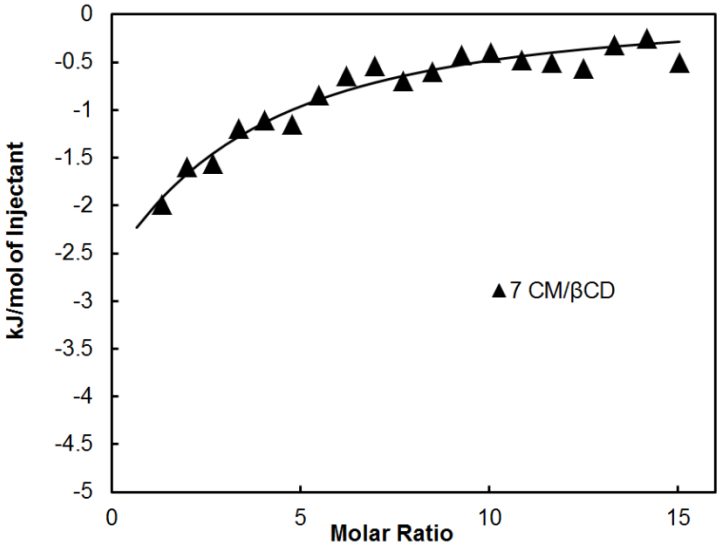

Fig. 2A18 ITC titration profile of 7.0 CM/βCD. The plot shows the corrected heat of reaction per mole of βCD derivative injected as a function of the molar ratio of βCD derivative to dexamethasone in the calorimeter cell, fitted to an independent, one-site binding model.

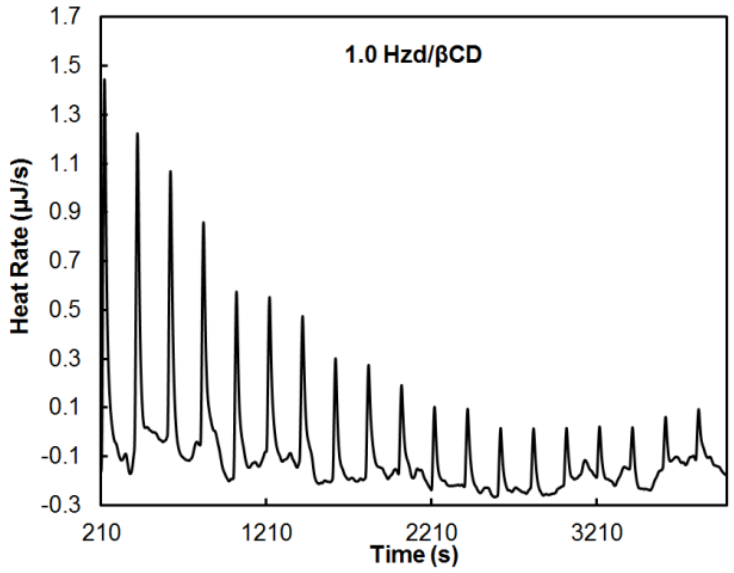

Fig. 2A19 ITC titration curve of 1.0 Hzd/βCD.

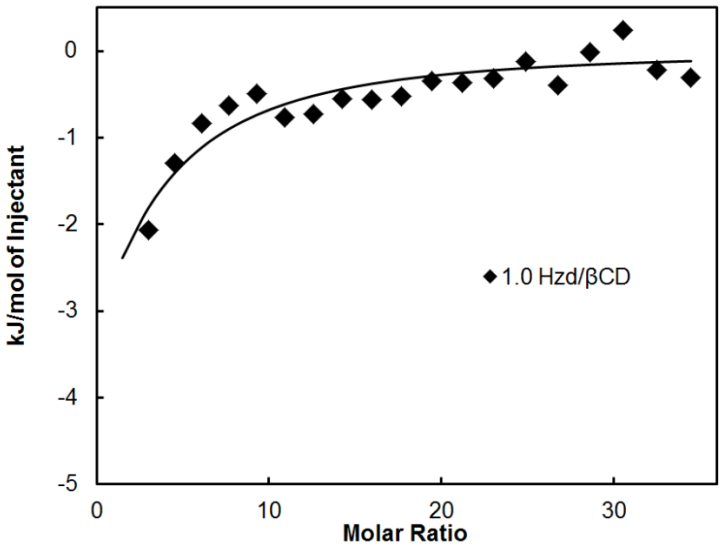

Fig. 2A20 ITC titration profile of 1.0 Hzd/βCD. The plot shows the corrected heat of reaction per mole of βCD derivative injected as a function of the molar ratio of βCD derivative to dexamethasone in the calorimeter cell, fitted to an independent, one-site binding model.

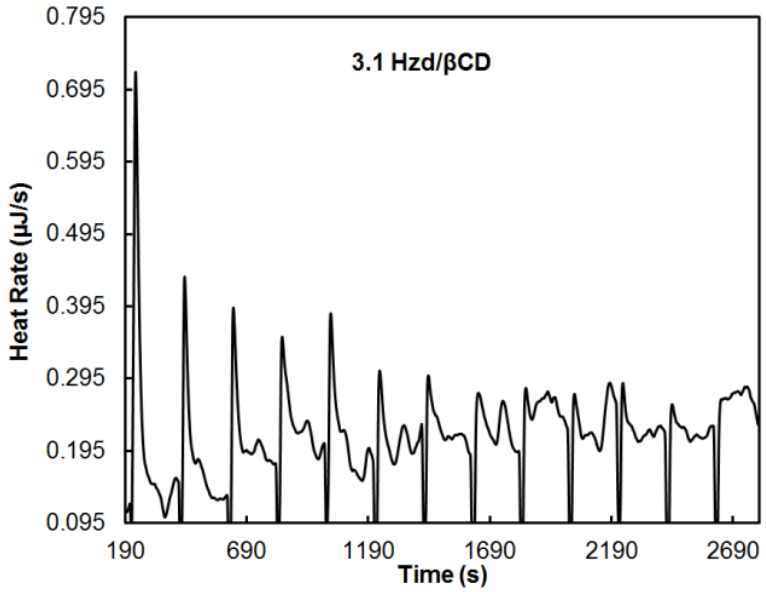

Fig. 2A21 ITC titration curve of 3.1 Hzd/βCD.

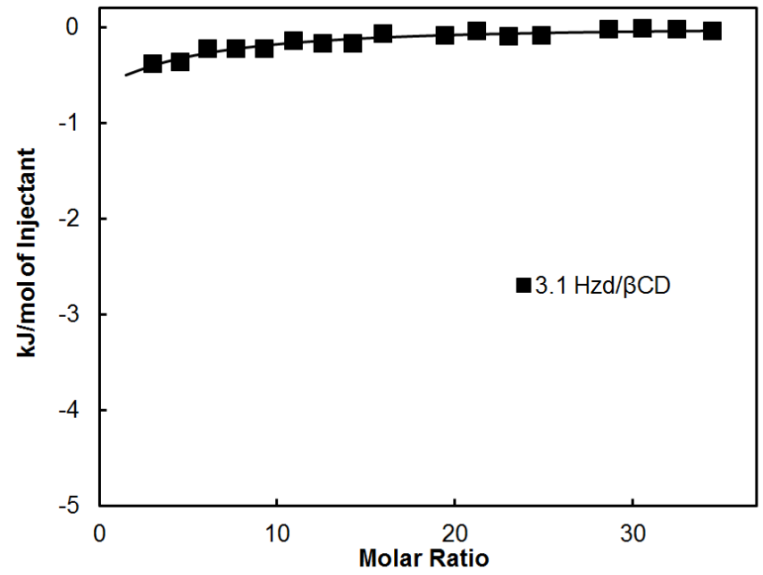

Fig. 2A22 ITC titration profile of 3.1 Hzd/βCD. The plot shows the corrected heat of reaction per mole of βCD derivative injected as a function of the molar ratio of βCD derivative to dexamethasone in the calorimeter cell, fitted to an independent, one-site binding model.

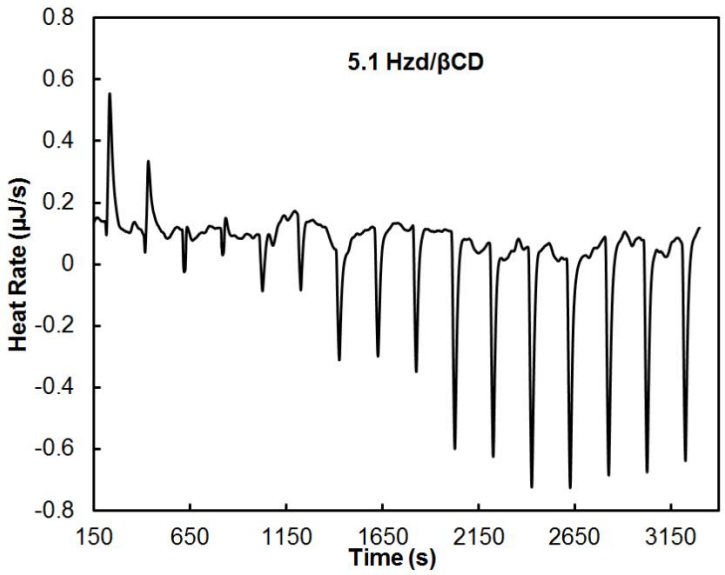

Fig. 2A23 ITC titration curve of 5.1 Hzd/βCD.

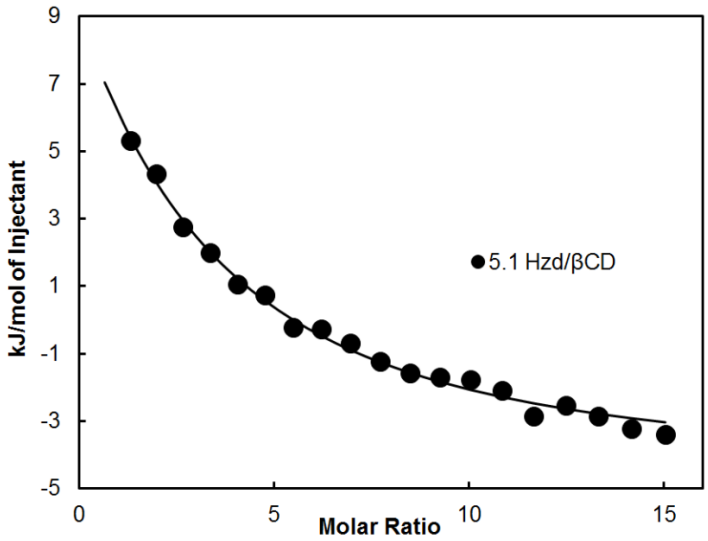

Fig. 2A24 ITC titration profile of 5.1 Hzd/βCD. The plot shows the corrected heat of reaction per mole of βCD derivative injected as a function of the molar ratio of βCD derivative to dexamethasone in the calorimeter cell, fitted to an independent, one-site binding model.

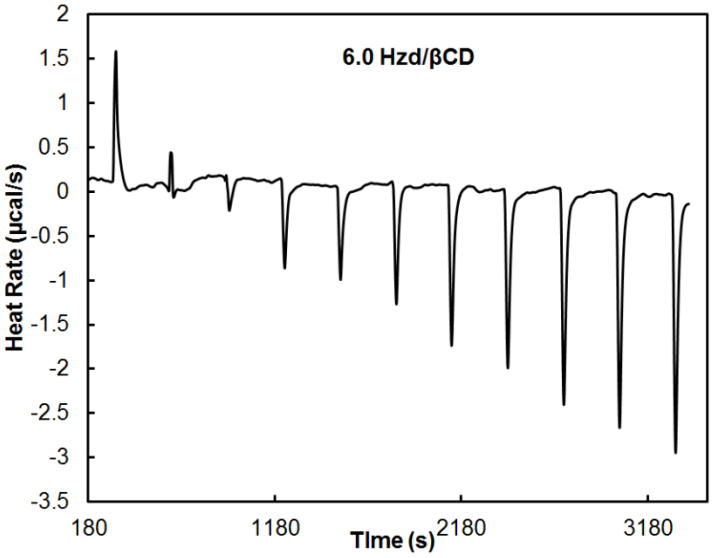

Fig. 2A25 ITC titration curve of 6.0 Hzd/βCD.

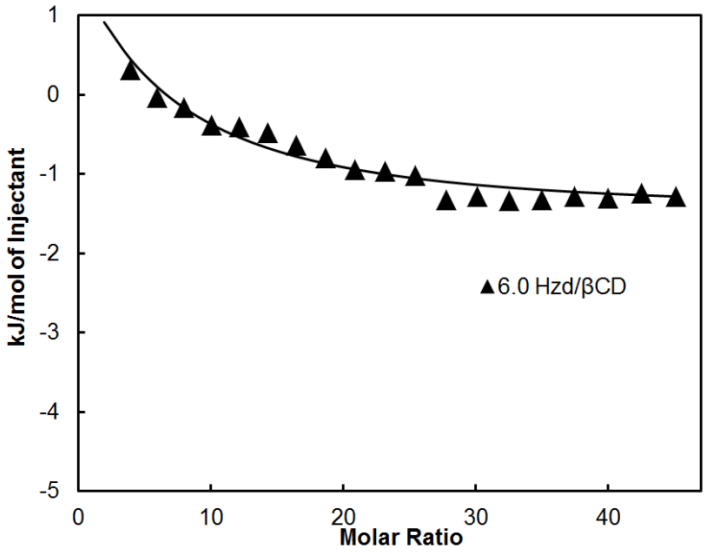

Fig. 2A26 ITC titration profile of 6.0 Hzd/βCD. The plot shows the corrected heat of reaction per mole of βCD derivative injected as a function of the molar ratio of βCD derivative to dexamethasone in the calorimeter cell, fitted to an independent, one-site binding model.

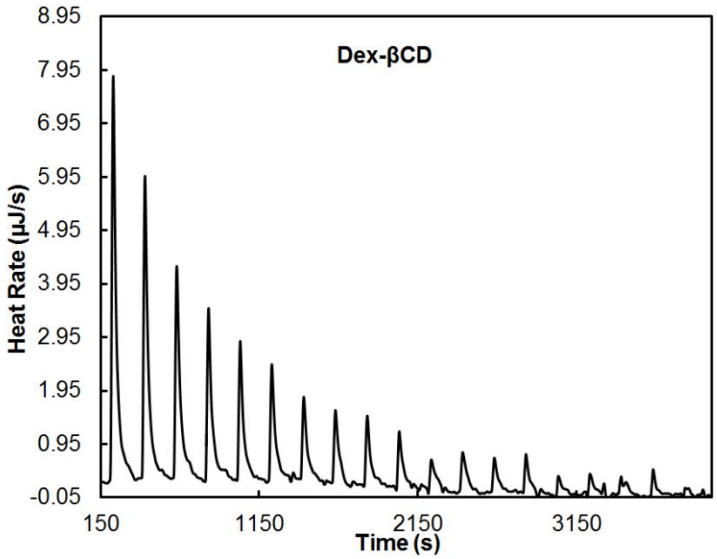

Fig. 2A27 ITC titration curve of 6.0 Hzd/βCD.

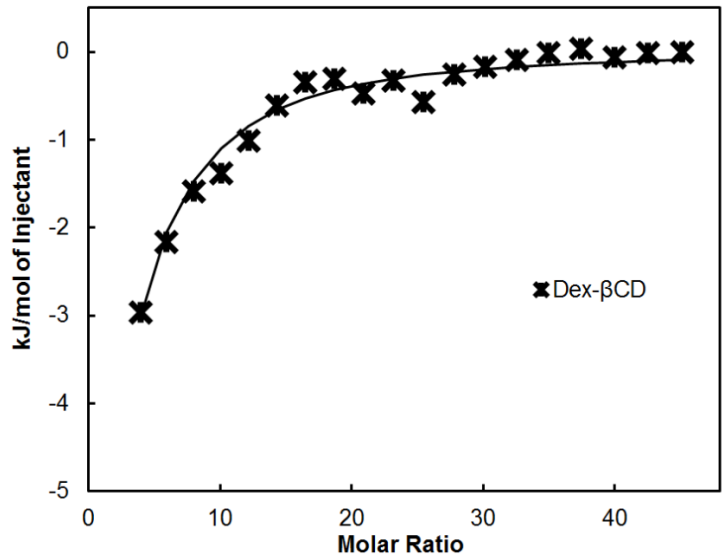

Fig. 2A28 ITC titration profile of Dex-βCD. The plot shows the corrected heat of reaction per mole of βCD derivative injected as a function of the molar ratio of βCD derivative to dexamethasone in the calorimeter cell, fitted to an independent, one-site binding model.

Chapter 3: Developing a printable hydrogel film as a platform for biomolecule immobilization

Preface

Chapters 3 and 4 are reproduced from the publication describing the development of a printable hydrogel microarray for a drug screening application. Chapter 3 describes the development and validation of a hydrogel printing protocol. The printable hydrogel is tested for its ability to immobilize a series of enzymes and facilitate the diffusion of small molecule substrates.

Rabia Mateen[1], M. Monsur Ali[2] and Todd Hoare* [1,3]

[1]School of Biomedical Engineering, McMaster University, Hamilton, Ontario L8S 4K1, Canada.

[2]Biointerfaces Institute, McMaster University, Hamilton, Ontario L8S 4L8, Canada.

[3]Department of Chemical Engineering, McMaster University, Hamilton, Ontario L8S 4L7, Canada.

Adapted from *Nature Communications* 9.1 (2018): 602.

Abstract

A printing protocol for the fabrication of hydrogel films was established and validated. The printed hydrogels were formulated from an injectable and *in situ* gelling system based on aldehyde-hydrazide chemistry. Chromatographic analysis and surface characterization techniques were employed in order to confirm the deposition of a hydrogel film on a nitrocellulose substrate. The printable hydrogel was tested for its ability to effectively entrap a series of enzymes while at the same time facilitating the diffusion of small molecule substrates.

3.1 Introduction

Hydrogel films are often incorporated in biomedical devices that mediate functions such as separations, wound healing, drug delivery and biosensing.[186] Several methods have been developed to fabricate hydrogel films on various substrates, including dip-coating[116], spray deposition[117], spin-coating[118] and drop-on demand printing[119]. Printing is particularly advantageous since it is amenable to dispensing small volumes (minimizing sample volumes for screening), can localize materials in specific patterns (enabling, for example, facile printing of multi-sample arrays on a substrate), and can be scaled to commercial production.[187,188, 189]

Applications that require the immobilization of enzymes can in particular benefit from the use of hydrogel films as both an encapsulating material and as a functional interface. Characteristics specific to hydrogels such as their high water content, porosity, and deformability can render these systems a more favourable environment for optimal enzyme function.[190] Moreover, the cross-linked structure can be modified such that the hydrogel can entrap compounds of various sizes ranging from ligands to enzymes to cells. Depositing a hydrogel film on a substrate can remove the diffusional restrictions often encountered in bulk hydrogels and thus improve the kinetics of enzyme-catalyzed reactions that occur within a hydrogel.[114]

The benefits of hydrogel films for enzyme immobilization have been widely demonstrated in the literature. For example, Zhu et al. developed a protocol to deposit a hydrogel layer onto a plastic substrate.[191] Lipase was entrapped in a poly (ethylene glycol) hydrogel matrix that was grafted onto a substrate via a light-induced surface-graft polymerization technique. The hydrogel layer was able to uniformly immobilize lipase and help support its operational stability over a number of cycles. Alternately, Yan et al. immobilized horseradish peroxidase in a poly (ethylene glycol)

hydrogel film that was patterned onto a glass substrate via photolithography and deposited through spin coating.[192] The patterned hydrogel film was able to detect the release of hydrogen peroxide from activated macrophages that were cultured on uncoated regions of the glass substrate. However, both these examples as well as most other examples of printable hydrogels are cross-linked via UV irradiation[193]. Since enzyme entrapment within a hydrogel mostly occurs during polymerization, the presence of UV irradiation or oxidizing initiators like ammonium persulfate may be detrimental to the stability of the enzyme.[191] As such, there is interest in developing covalently cross-linked hydrogels that are fabricated under more mild synthetic conditions.

Our lab has developed several *in situ*-gelling injectable, transparent, hydrogels based on aldehyde-hydrazide chemistry that rapidly form cross-links in the absence of external catalysts or UV irradiation. In particular, hydrazone cross-linked hydrogels based on poly(oligoethylene glycol methacrylate) (POEGMA) demonstrate good mechanical strength, low non-specific fouling, and stable encapsulation of biomolecules while also (by virtue of the rapid hydrazide-aldehyde cross-linking chemistry) remaining amenable to injection and/or latent *in situ* gelation.[106, 107] In this chapter, we establish a protocol to effectively print these hydrogels into films**,** characterize the deposited hydrogel layer, and evaluate the ability of the printed hydrogel to immobilize a series of enzymes on a nitrocellulose substrate.

3.2 Materials and Methods

Materials

Oligo(ethylene glycol) methyl ether methacrylate (OEGMA, M_n = 475 g/mol, Sigma Aldrich, 95%) and (diethylene glycol) methyl ether methacrylate ($M(EO)_2MA$, Sigma Aldrich, 98%) were purified on a column of basic aluminum oxide (Sigma Aldrich, type CG-20) to remove the inhibitors methyl ether hydroquinone (MEHQ) and butylated hydroxytoluene (BHT) respectively. N-(2,2-dimethoxyethyl)methacrylamide (DMEMAm) was synthesized as previously reported.[106]. Acrylic acid (AA, Sigma Aldrich, 99%), thioglycolic acid (TGA, Sigma Aldrich, 98%), 2,2-azobisisobutryic acid dimethyl ester (AIBMe, Wako Chemicals, 98.5%), adipic acid dihydrazide (ADH, Alfa Aesar, 98%), N'-ethyl-N-(3-dimethylaminopropyl)-carbodiimide (EDC, Carbosynth, Compton CA, commercial grade), sodium cyanoborohydride

($NaBH_3CN$, Sigma Aldrich, reagent grade), aminoacetaldehyde dimethyl acetal (Sigma Aldrich, 99%), 2,2,6,6-tetramethyl-1-piperidinyloxy (TEMPO, Sigma Aldrich, 98%), methacryloyl chloride (Sigma Aldrich, purum), fluorescein-5-isothiocyanate (5-FITC, Sigma Aldrich, 90%), rhodamine 123 (Sigma Aldrich, 85%) and bovine serum albumin (BSA, Sigma Aldrich, >96%) were all used as received. Hi-Flow plus cellulose ester membranes (EMD Millipore, HF12002XSS), glycerol (Sigma Aldrich, ≥99%), fluorescein (free acid) (Sigma Aldrich, 95%), alkaline phosphatase (AP, Roche, 20 U/μL), BCIP®/NBT-Purple Liquid Substrate System (Sigma Aldrich), urease from *Canavalia ensiformis*, Type III (Sigma Aldrich, 20 KU), phenol red solution (Sigma Aldrich, 0.5%), urea (Sigma Aldrich, ≥98%), recombinant β-lactamase TEM precursor from *Escherichia coli* (ProSpec, 700 U/mg), nitrocefin (Abcam, >95%) and sodium chloride (Sigma Aldrich, were all used as received. For all experiments, Milli-Q grade distilled deionized water (DIW) was used. Phosphate buffered saline (PBS) was diluted from a 10X liquid concentrate (Bioshop Canada Inc.).

Synthesis of poly(oligoethylene glycol methacrylate) polymers

Unfunctionalized poly(oligoethylene glycol methacrylate) (PO) was prepared by adding AIBMe (50 mg, 0.22 mmol), $OEGMA_{475}$ (0.90 g, 1.9 mmol), $M(EO)_2MA$ (3.1g, 16.5 mmol) and TGA (7.5 μL, 0.15 mmol) to a 50 mL Schlenk flask. 1,4-Dioxane (20 mL) was added, and the solution was purged with nitrogen for 30 minutes. The flask was sealed and submerged in a pre-heated oil bath at 75°C for 4 hours under magnetic stirring. After polymerization, the solvent was removed by rotary evaporation, and the poly($OEGMA_{475}$-co-$M(EO)_2MA$) polymer was purified by dialysis against DIW for 6 cycles (6 hours/cycle) and lyophilized to dryness. The polymer was dissolved in 10 mM PBS at 20 w/w% and stored at 4°C.

Aldehyde-functionalized poly(oligoethylene glycol methacrylate) (POA) was prepared similarly to the unfunctionalized PO polymer above except for the addition of DMEMAm (0.63 g, 3.61 mmol). Following solvent removal, the acetal groups of the DMEMAm residues were converted to aldehydes via hydrolysis by dissolving the copolymer in 100 mL of 0.25 M HCl and stirring for 24 hours. The polymer was purified by dialysis against DIW and lyophilized to dryness. POA was dissolved in 10 mM PBS at 20 w/w% and stored at 4°C. The number-average molecular weight was determined to be 14 kDa ($Đ$ = 2.03) from size exclusion chromatography.

The aldehyde content was determined to be 12 mol% using ^{1}H-NMR by comparing the integration of the proton signals of the methoxy (O-CH_3, 3H, δ = 3.3 ppm) and aldehyde (CHO, 1H, δ = 9.2 ppm) groups.

Hydrazide-functionalized poly(oligoethylene glycol methacrylate) (POH) was prepared by adding AIBMe (37 mg, 0.16 mmol), $OEGMA_{475}$ (0.90 g, 1.9 mmol), $M(EO)_2MA$ (3.1g, 16.5 mmol), AA (0.55 g, 7.6mmol), and TGA (7.5 μL, 0.15 mmol) to a 50 mL Schlenk flask. Polymerization proceeded similarly to that of PO and POA. Following solvent removal, the copolymer was dissolved in 100 mL DIW. ADH (4.33g, 24.8 mmol, 8.16 mol eq.) was added, and the pH of the solution was adjusted to 4.75. The reaction was initiated by the addition of EDC (1.93 g, 12.4 mmol, 3.80 mol eq.), after which the pH was maintained at 4.75 by the dropwise addition of 0.1 M HCl over 4 hours. The solution was left to stir overnight, dialyzed against DIW over 6 cycles (6 hours/cycle) and lyophilized to dryness. The polymer was dissolved in 10 mM PBS at 20 w/w% and stored at 4°C. The number-average molecular weight was determined to be 17 kDa ($Đ$ = 2.08) using size exclusion chromatography. The degree of hydrazide functionalization was determined to be 22 mol% by conductometric base-into-acid titration, comparing the carboxylic acid content before and after ADH conjugation (0.1 M NaOH titrant, 50 mg polymer in 50 mg of 1 mM NaCl titration solution, ManTech automatic titrator).

Polymer characterization

Size exclusion chromatography (SEC) was performed using a Waters 2695 separations module equipped with a Waters 2996 photodiode array detector, a Waters 2414 refractive index detector, a Waters 2475 multi λ fluorescence detector and four Polymer Labs PLgel individual pore size columns maintained at 40 °C, using a 5 μm bead size and pore sizes of 100, 500, 103 and 105 Å. THF was used as the eluent at a flow rate of 1.0 mL min^{-1}, and poly(methyl methacrylate) standards were used for calibration. ^{1}H-NMR was performed using a Bruker AVANCE 600 MHz spectrometer using deuterated chloroform as the solvent.

Fluorescent labelling of polymers and bovine serum albumin (BSA)

Fluorescein isothiocyanate (FITC) was conjugated to POH (FITC-POH) by reacting 1 g of POH was reacted with 5 mg of FITC in water at pH=8, stirring overnight at room temperature (2 mol% hydrazide groups labeled). Rhodamine 123 was conjugated to POA (Rhodamine-POA) via reductive amination, reacting 1 g of POA with 5 mg of Rhodamine 123 in water for 12 hours and then reducing the resulting Schiff base with sodium cyanoborohydride (8.25 mg, 10-fold molar excess to the rhodamine) to create a stable conjugate. Both labeled polymers were dialyzed against DIW for 6 cycles (6 hours/cycle) in the dark, lyophilized to dryness, dissolved in 10 mM PBS at 10% w/w, and stored at 4°C in the dark.

FITC-BSA was prepared by dissolving 50 mg of BSA and 1 mg of FITC in 100 mL of aqueous carbonate buffer at pH = 9.0. The reaction was carried out for 12 hours under magnetic stirring. The FITC-labelled protein was purified by dialyzing against DIW for 6 cycles (6 hours/cycle) and then lyophilized. FITC-BSA was stored at 4°C in the dark.

Hydrogel printing

A nitrocellulose microzone plate was fabricated by printing hydrophobic wax barriers onto a nitrocellulose membrane (EMD Millipore) using a Xerox ColorQube 8570N solid wax printer and a 96 well-plate template (3 mm diameter wells, ~9 mm inter-well distance). The wax-printed paper was placed into an oven at 120 °C for 2 minutes to melt the wax through the paper. Polymer inks comprised of 6 w/w% aldehyde-functionalized poly(oligoethylene glycol methacrylate) (POA) or hydrazide-functionalized poly(oligoethylene glycol methacrylate) (POH) (see Supplementary Methods for details on synthesis and characterization) were printed in 10 mM PBS containing 5 w/w% glycerol as a humectant and viscosity modifier; the resulting viscosities of the POA and POH inks were 3.27 mPa·s and 4.85 mPa·s respectively. A BioJet HR™ non-contact solenoid dispenser was used to print the inks on the paper microzones. The two reagent lines were charged with POA and POH, the dispenser valve was programmed to stay open for 6 ms, and the frequency was set to 100 Hz. The hydrogel film was fabricated by dispensing 2 µL POA onto the microzone, immediately followed by 2 µL POH. The samples were dried and stored at room temperature.

Enzyme entrapment studies

POH ink solutions containing one of the tested model enzymes were prepared with enzyme concentrations listed in Table 3.1. Entrapped protein samples were printed as previously described, followed by washing with 10 mM PBS at 300 rpm on an IKA MS3 Basic Shaker for 10 minutes. The relevant substrate solutions for each enzyme were then pipetted onto the washed samples using the solutions and volumes listed in Table 3.2 to assess enzyme activity. Images of the resulting colorimetric read-out were taken with an IPhone 5C camera. Image analysis to determine colorimetric intensity was performed using Fiji, an open-source program based on ImageJ. The converted substrate colour was extracted using the Color Deconvolution plugin. Extracted images were inverted and converted to 8 bit grayscale images. The intensity of each sample was measured and presented as a ratio of the corresponding control image (a sample printed with the same concentration of enzyme but not washed to remove any non-adsorbed enzyme).

Table 3.1 Enzyme concentrations in hydrazide-functionalized poly(oligoethylene glycol methacrylate (POH) inks

Enzyme	**Concentration in POH Ink ($U\ \mu L^{-1}$)**
Alkaline phosphatase (AP)	0.5
Urease	0.2
β-lactamase (β-Lac)	0.02

Table 3.2 Substrates and added volumes used for each enzyme studied in this work

Enzyme	**Substrate**	**Volume of Substrate Added (μL)**
Alkaline phosphatase (AP)	BCIP®/NBT-Purple Liquid Substrate System	10
Urease	0.5 mM acetic acid, 5 mM urea, 0.005% phenol red	20
β-lactamase (β-Lac)	500 μM nitrocefin (19.4 μM DMSO stocks diluted in 10 mM PBS)	10

Characterization of printed hydrogels

ATR-FTIR was performed on printed polymer samples following extensive washing with 10 mM PBS using a Vertex 70 FTIR Diamond ATR (Bruker). XPS spectra were recorded with a Physical Electronics (PHI) Quantera II spectrometer using a monochromatic Al K-α X-ray source (1486.7 eV) at 50 W (15 kV). Survey (280 eV pass energy), high-resolution carbon (26 eV pass energy) and high-resolution nitrogen (55 eV pass energy) XPS scans were obtained using a 45° take-off angle. Data analysis was performed using PHI MultiPak software. Peak assignments were made according to the values reported in the NIST XPS Database. The surface morphology of both printed and non-printed surfaces was evaluated by scanning electron microscopy (SEM) (FEI-Magellan XHR) using secondary electron image (SEI) mode with voltages of 2.0 kV (1000x magnification).

Printed polymer chromatography

Rhodamine-POA or FITC-POH were printed alone, with PO (unfunctionalized poly(oligoethylene glycol methacrylate)) or with the corresponding, unlabelled reactive polymer. Paper samples were cut into 0.5x4.5 cm strips, and chromatography was subsequently performed by placing the end of each strip in 50 μL of a 70:30 methanol:water solvent mixture. The samples were imaged through the fluorescein and rhodamine channels of the ChemiDoc™ MP System (BioRad). Image processing was performed in Image Lab™ software (BioRad).

Protein adsorption

Printed POA/POH hydrogels were soaked in 10 mM PBS for 12 hours, after which the hydrated samples were submerged in a 100 μg mL^{-1} solution of FITC-BSA and gently shaken for 2 hours. The samples were imaged through the fluorescein channel of the ChemiDoc™ MP System (BioRad). Image processing was performed using Image Lab™ software (BioRad).

Fluorescein and FITC-BSA entrapment

POH ink solutions were co-dissolved with 10 μM fluorescein or 0.05 mg mL^{-1} FITC-BSA. Samples printed with fluorescein were washed in 0.1 M NaOH + 0.1% Tween 20, while samples printed with FITC-BSA were washed in 10 mM PBS and shaken at 300 rpm on an IKA MS3 Basic Shaker for 30 minutes.; each rinse solution was selected to maximize the solubility of the

fluorescently-labeled probe and thus maximize the potential for washing the probe away from the surface if it was not effectively immobilized. Afterwards, both samples were imaged through the fluorescein channel of the ChemiDoc™ MP System (BioRad). Image processing was performed in Image Lab™ software (BioRad). FITC-BSA printed samples were also imaged with a Nikon Eclipse LV100ND optical microscope equipped with an Andor Zyla sCMOS camera at 20x magnification through the fluorescein channel to assess the distribution of FITC-BSA on the printed hydrogel surface.

Chromatographic experiments confirming immobilization of encapsulated fluorophores upon gel printing were additionally performed by printing the relevant POA or POH solutions on a nitrocellulose paper substrate as described above, cutting the printed paper into 0.5x4.5 cm strips, and performing chromatography by dipping the end of the strip in 50 µL of a 50:50 methanol:water solvent. The samples were imaged through the fluorescein channel of the ChemiDoc™ MP System (BioRad). Image processing was performed using Image Lab™ software (BioRad).

The distribution of Rhodamine-POA and FITC-BSA within the printed gel layer was assessed using confocal fluorescence microscopy (CLSM, Nikon). Confocal z-stack images (3D view) were collected by scanning the printed gel samples at 2 µm intervals to a depth of 80 µm (326 x 326 µm area probed). Excitation/emission wavelengths of 488/525 nm (FITC-BSA) and 561/595nm (Rhodamine-POA) were used to acquire the images.

Enzyme leaching study

1 µM β-lactamase was printed in the PO-based hydrogel, followed by washing of the printed samples in 10 mM PBS for varying amounts of time. β-lactamase activity was assessed in the wash solutions by adding nitrocefin to a final concentration of 200 µM and tracking the hydrolysis of nitrocefin by monitoring solution absorbance at 492 nm via UV-vis spectrophotometry (Infinite M1000 spectrophotometer, Tecan). The resulting absorbance readings were reported as a ratio relative to the control (the absorbance of buffer itself at 492 nm, without any substrate added). Subsequently, the residual activity of the printed samples washed over 5 h was measured via image acquisition and analysis as described for the entrapment

studies, with the results presented as a ratio of the corresponding control image (a printed hydrogel sample not washed to remove any non-adsorbed enzyme).

3.3 Results and Discussion

Printing a hydrogel film

A drop-on-demand syringe solenoid printer was used to sequentially print hydrazide (POH) and aldehyde (POA) functionalized poly(oligoethylene glycol methacrylate) (PO) precursor polymers, previously shown to rapidly gel upon mixing via hydrazone bond formation[106], on a nitrocellulose substrate (Fig.3.1a and Appendix Fig.3A1 for ^{1}H NMR spectra of polymers). Polymer inks were prepared at 6 w/w% in 10 mM PBS, with glycerol added at 5 w/w% to both adjust the viscosity to enhance printability[194] and act as a humectant to avoid nozzle clogging during printing.[194] Gelation was validated by examining whether polymers remained immobilized at their printed positions when exposed to a methanol-water chromatographic separation process. Fluorescently labeled POH (FITC-POH) or POA (Rhodamine-POA) polymers were printed alone, with an unfunctionalized PO polymer (incapable of covalent cross-linking with POH or POA), or with the corresponding unlabelled reactive polymer precursors (POA or POH respectively) (Fig.3.1b). When FITC-POH or Rhodamine-POA was printed alone (Fig.3.1b, Panels i and iv) or with unfunctionalized PO polymer (Fig.3.1b, Panels ii and v), the fluorescent precursor could transport up the nitrocellulose strip, indicating poor immobilization; conversely, when the reactive POA and POH polymers were sequentially printed in either sequence (Fig.3.1b, Panels iii and vi), the labeled polymer remained localized at the printed site, suggesting effective gelation. ATR-FTIR further confirmed successful deposition of the polymer inks at the paper surface (Appendix Fig.3A2).

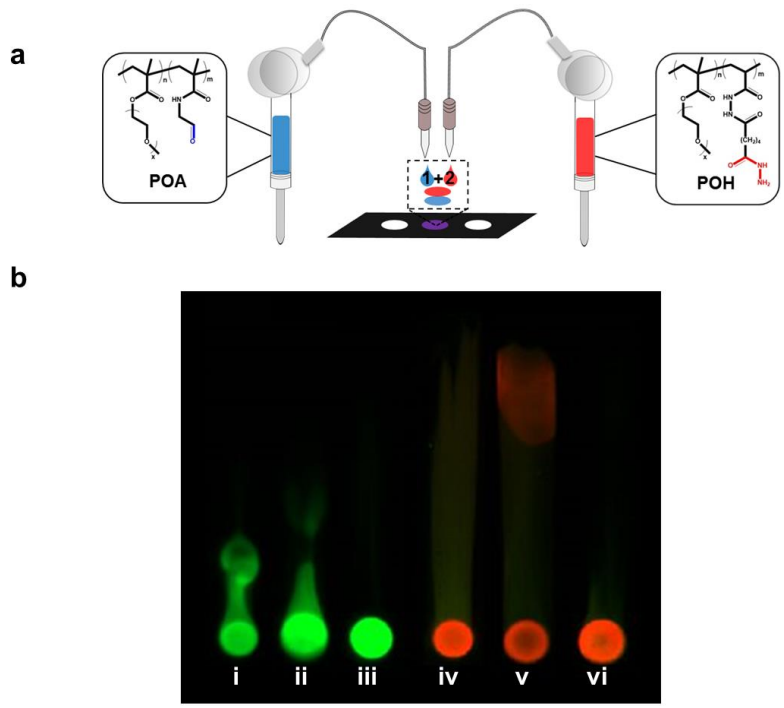

Fig. 3.1 Illustration of polymer printing method and validation of polymer cross-linking via chromatographic analysis (a) Schematic of aldehyde-functionalized poly(oligoethylene glycol methacrylate) (POA) and hydrazide-functionalized poly(oligoethylene glycol methacrylate) (POH) polymers sequentially printed onto a nitrocellulose paper substrate using a solenoid-controlled drop-on-demand printing system; **(b)** Chromatographic separation of printed polymers on nitrocellulose strips in 70:30 methanol:water: i. Fluorescein isothiocyanate-labeled hydrazide-functionalized poly(oligoethylene glycol methacrylate) (FITC-POH) alone; ii. FITC-POH printed on top of unfunctionalized poly(oligoethylene glycol methacrylate) (PO) (PO+FITC-POH); iii. FITC-POH printed on top of aldehyde-functionalized poly(oligoethylene glycol methacrylate) (POA) (POA+FITC-POH); iv. Rhodamine-labeled aldehyde-functionalized poly(oligoethylene glycol methacrylate) (Rhodamine-POA) alone; v. Rhodamine-POA printed on top of PO (PO+Rhodamine-POA); vi. Rhodamine-POA printed on top of POH (POH+Rhodamine-POA)

Printed samples were subsequently analyzed to investigate the chemical, morphological and interfacial changes made to the nitrocellulose substrate following hydrogel deposition. X-ray photoelectron spectroscopy (XPS) measurements on samples sequentially printed with POA and POH indicated a peak in the high-resolution nitrogen spectrum at 401.7 eV that corresponds to the –C=N functional group characteristic of a hydrazone bond (Fig.3.2a and Appendix Fig.3A3). SEM images of vigorously washed gel-printed nitrocellulose strips indicate that the rough and bulbous morphology of unmodified nitrocellulose remains unchanged when (unreactive) PO and

POH are sequentially printed, consistent with these polymers being removed from the substrate during the washing step (Fig.3.2b, panels i and ii); conversely, printing the (reactive) POA+POH pair results in significant smoothing of the substrate consistent with the formation of an interfacial gel layer (Fig. 3.2b, panel iii). The printed hydrogel also significantly suppresses non-specific protein adsorption to the nitrocellulose substrate (Fig.3.2c), a notable benefit for optimizing the sensitivity of any bioassay. This degree of protein repellency is consistent with our previous work on sequential dip-coating of POA/POH on cellulose paper[116]; however, the printing method used here is both significantly faster (seconds as opposed to hours[116]) and enables the localized gel printing essential for creating microarrays. This method allows for a covalently cross-linked hydrogel to be printed in the absence of UV photopolymerization to facilitate gelation[195], avoiding the need for a secondary processing step as well as eliminating the potential for enzyme denaturation sometimes observed due to the radical species generated during polymerization.[196]

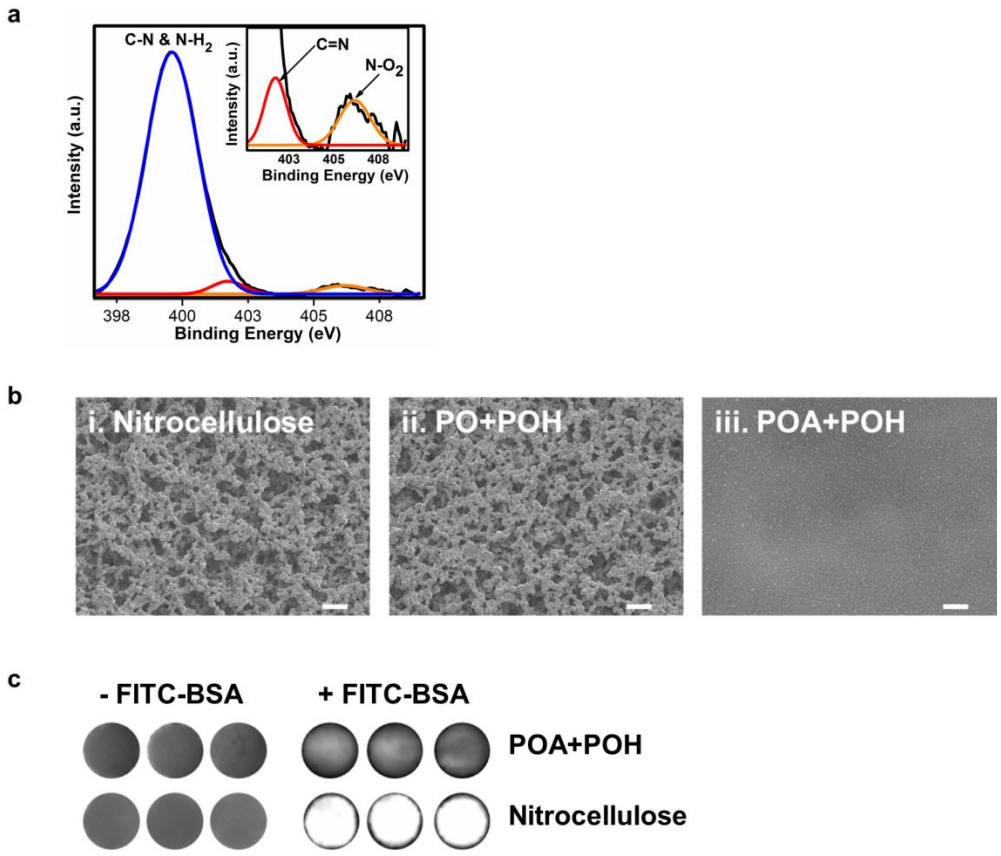

Fig.3.2 The chemical, morphological and interfacial changes made to the nitrocellulose substrate following hydrogel deposition (a) High-resolution XPS spectra of printed hydrogel (POA+POH) on a nitrocellulose substrate collected in the N 1s region. The peak at 401.7 eV corresponds to the –C=N group characteristic of a hydrazone bond, confirming gel formation; **(b)** SEM images of i. bare nitrocellulose, ii. an uncross-linked polymer assembly (PO+POH) printed on nitrocellulose, and iii. a printed hydrogel (POA+POH) on nitrocellulose following vigorous washing of the samples in 10 mM PBS. Scale bars, 10 µM; **(c)** Fluorescence scans of bare nitrocellulose and printed hydrogel (POA+POH) samples before and after incubation in 100 µg mL^{-1} FITC-BSA show a significant reduction in non-specific protein adsorption following the printing of the hydrogel on the substrate.

Entrapping biomolecules in the printed hydrogel

The printed hydrogel can entrap molecules of varying sizes and effectively immobilize them on the nitrocellulose surface. POH ink solutions were prepared with dissolved fluorescein (332 Da) or FITC-BSA (66.5 kDa) and subsequently layer-by-layer printed with POA. Both fluorescein

(POA+(POH+F)) and BSA (POA+(POH+BSA)) remained entrapped in the cross-linked polymer assembly after the samples were washed vigorously, while the POH+F or POH+BSA ink printed alone or with an unreactive (PO) polymer resulted in almost complete washing of immobilized agent from the surface (Fig.3.3a). Printed samples subjected to chromatographic separation similarly showed minimal transport of the fluorescent dopants from the gel-printed samples but rapid transport when the dopants were printed alone or with an unreactive PO polymer (Fig.3.3b).

Fluorescence microscopy images of printed FITC-BSA confirmed the uniform distribution of the protein on the nitrocellulose surface when entrapped in the hydrogel film (Fig. 3.3c), while confocal microscopy images of FITC-BSA encapsulated inside a hydrogel prepared with Rhodamine-POA confirm that the printed protein is distributed evenly throughout both the cross-section and the depth of the printed hydrogel microzones (Fig.3.3d).

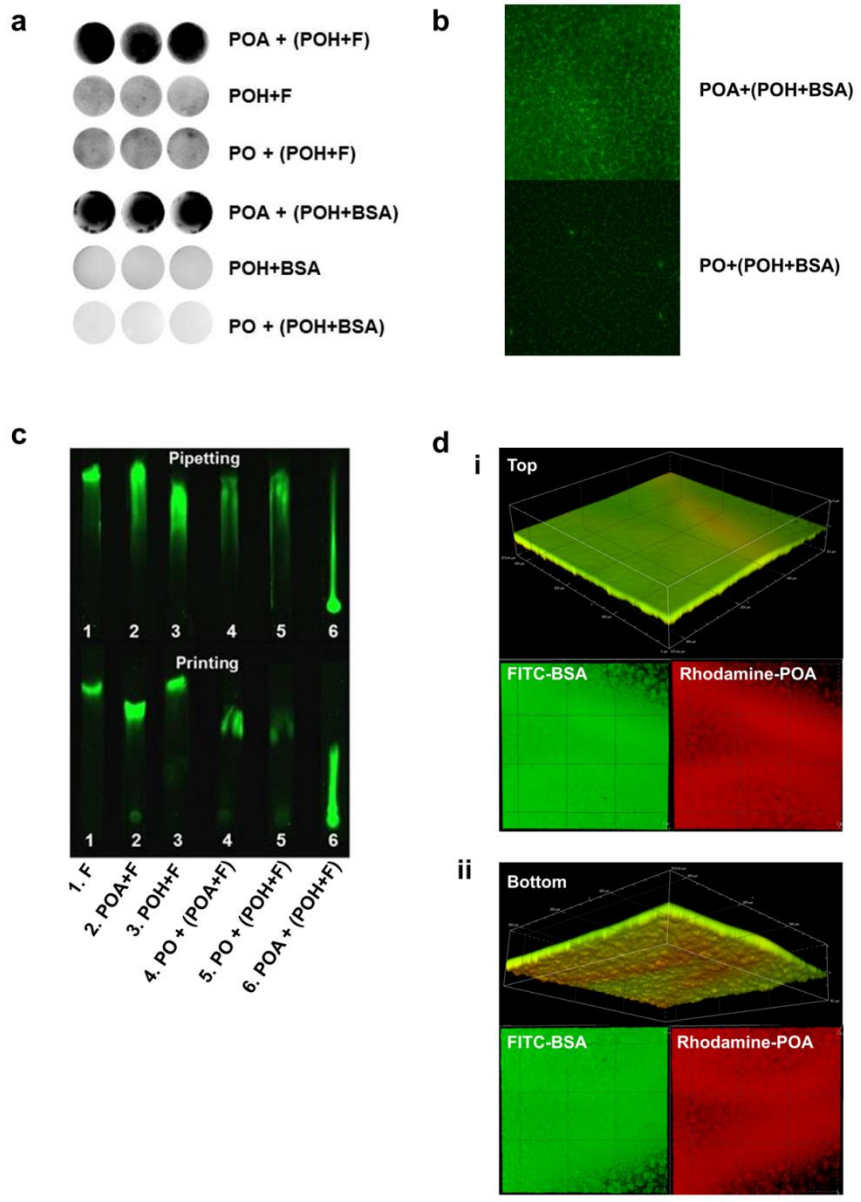

Fig.3.3 Printed hydrogels can immobilize molecules of varying sizes a) Retention of fluorescein (F, ~332 Da) printed in hydrogel (POA+(POH+F)) following washing in 0.1 M NaOH + 0.1% Tween 20 and fluorescein isothiocyanate-labeled bovine serum albumin (FITC-BSA, ~66 kDa) printed in hydrogel (POA+(POH+BSA)) following washing in 10 mM PBS for 30 minutes. The high retained fluorescence signal confirms the efficacy of gel inks for protein immobilization. The three adjacent images in each series are replicates, confirming the reproducibility of the result; **(b)** FITC-BSA printed in a gelling ink (POA+POH) and a non-gelling ink (PO+POH) imaged by fluorescence microscopy following washing in 10 mM PBS for 30 minutes (20x magnification); **(c)** Chromatography of polymers inks mixed with fluorescein (F). In the pipetting experiment, polymer inks were mixed with fluorescein and the corresponding reactive or unreactive polymer and directly pipetted onto a nitrocellulose paper substrate. In the printing experiment, reactive polymer inks (aldehyde-functionalized and

hydrazide-functionalized poly(oligoethylene glycol methacrylate) (POA and POH, respectively) were mixed with fluorescein (F) and printed onto a nitrocellulose substrate, followed immediately by printing of the corresponding reactive polymer or an unreactive polymer (poly(oligoethylene glycol methacrylate) (PO). Chromatography was performed in a 50:50 methanol:water mixture. Lane 6 shows that the pipetted or printed polymer assembly (POA+POH) successfully immobilizes a large fraction of the fluorescein (with the portion eluting consistent with controlled release from a hydrogel), while all other samples tested result in transport of essentially all of the printed fluorescein up the strip, indicating a lack of effective encapsulation. Lane 1: fluorescein (F) only; Lane 2: aldehyde-functionalized poly(oligoethylene glycol methacrylate) mixed with fluorescein (POA+F); Lane 3: hydrazide-functionalized poly(oligoethylene glycol methacrylate) mixed with fluorescein (POH+F); Lane 4: (POA+F) printed on top of or pipetted with poly(oligoethylene glycol methacrylate) (PO+(POA+F)); Lane 5: (POH+F) printed on top of or pipetted with PO (PO+(POH+F)); Lane 6: (POH+F) printed on top of or pipetted with POA (POA+(POH+F)); **(d)** Confocal microscopy of printed hydrogel microzones. FITC (fluorescein isothiocyanate) channel (green), rhodamine channel (red), and overlaid fluorescence images confirm the co-localization of fluorescein isothiocyanate-labeled bovine serum albumin (FITC-BSA) within the gel phase as well as the relatively uniform distribution of FITC-BSA within the printed gel. The printed hydrogel was prepared by printing rhodamine-labeled aldehyde-functionalized poly(oligoethylene glycol methacrylate) (Rhodamine-POA) as the base polymer on a nitrocellulose substrate followed by hydrazide-functionalized poly(oligoethylene glycol methacrylate) (POH) ink (unlabeled) containing 0.005 mg mL^{-1} of FITC-BSA. Images represent the top (a) and bottom (80 μm depth) (b) of the 326 x 326 μm cross-sectional slice.

Subsequently, alkaline phosphatase (AP), urease (Ur), and β-lactamase (β-Lac) were printed alone (E) or in POA or POH ink (POA+E or POH+E) on top of either untreated nitrocellulose or nitrocellulose pre-printed with POA or (unfunctionalized) PO. All tested enzymes were effectively immobilized and stabilized in the printed hydrogel (POA+(POH+E)), with >90% activity maintained for AP and β-Lac and >85% activity maintained for urease relative to enzymes printed in the same manner but not rinsed prior to activity testing (Fig. 3.4a-c). In comparison, co-printing enzymes with POH alone, POA alone, or in combination with unfunctionalized PO showed only limited benefits in terms of immobilizing and stabilizing the enzymes. Note that although nitrocellulose has a high capacity for protein retention[197], printed enzyme did not remain associated with unmodified nitrocellulose after washing; as such, the observation of residual enzyme activity after washing confirms effective enzyme entrapment. High entrapment efficiencies were also confirmed via washing experiments in which enzyme activity was assayed in sequential wash solutions; minimal activity losses are observed after the first 10 minute wash cycle (which removes poorly entrapped near-surface enzyme), and the

printed hydrogel retains >90% of its original activity following five hours of washing (Fig.3.5). Furthermore, full substrate conversion occured within 15 minutes for each entrapped enzyme, demonstrating that the printed hydrogel possesses a combination of sufficiently high porosity and low diffusional path length to allow for efficient diffusion of substrate molecules to the enzyme active sites and rapid read-out of enzyme activity.

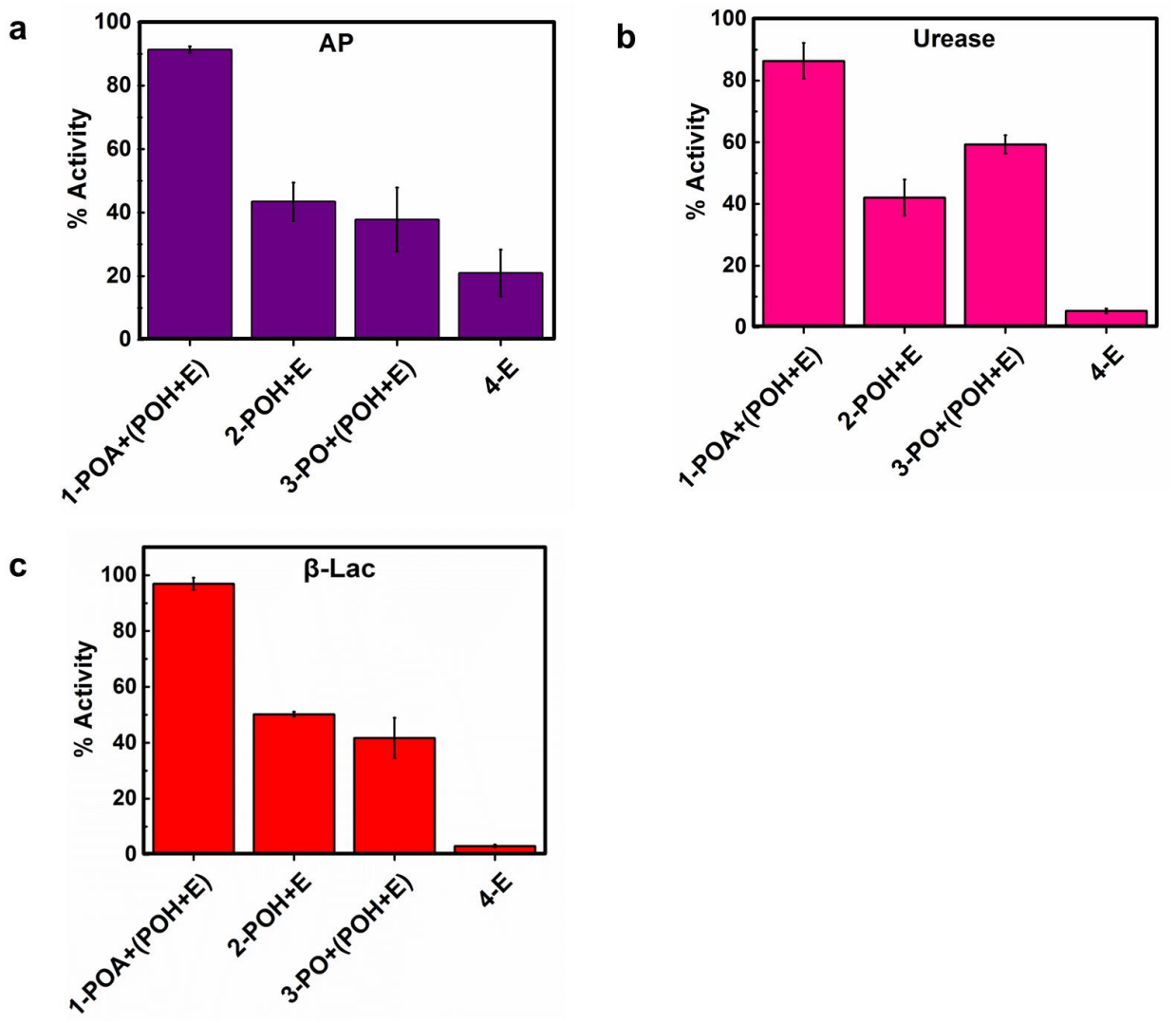

Fig.3.4 Immobilization of enzymes in printed hydrogel Residual activity of enzymes (E) following washing of samples in 10 mM PBS for 10 min, normalized relative to the corresponding unwashed control. **(a)** Alkaline phosphatase (~69 kDa). **(b)** Urease (~546 kDa). **(c)** β-lactamase (~29 kDa). Values are represented as mean ± SD ($n = 3$)

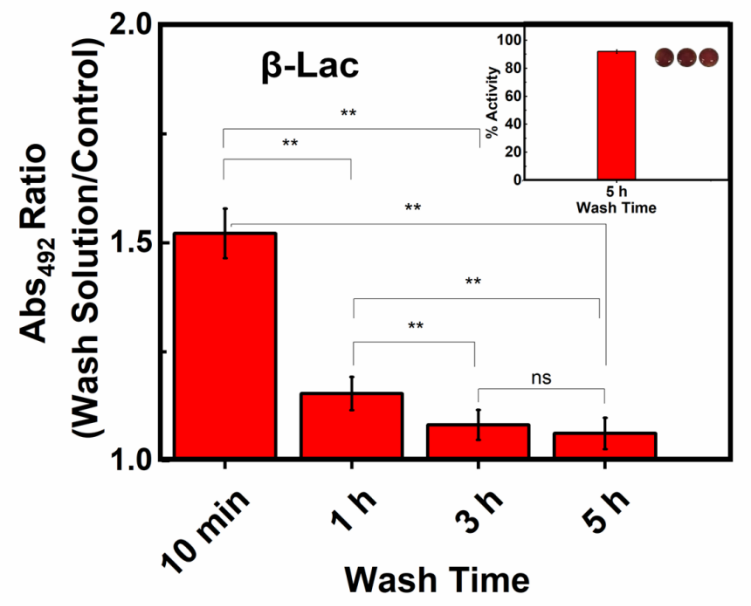

Fig.3.5 Printing β-lactamase in hydrogel minimizes enzyme leaching Printed samples were washed in 10 mM PBS for varying amounts of time. β-lactamase activity was then assessed in the wash solutions using UV-vis spectrophotometry to track the hydrolysis of nitrocefin by monitoring solution absorbance at 492 nm. The resulting absorbance readings are reported as a ratio of the control (i.e. the absorbance of buffer itself at 492 nm); as such an absorbance ratio of one indicates zero leached enzyme activity in the wash solution. Residual activity of samples washed for 5 h relative to the corresponding unwashed control is presented in the inset graph, confirming that minimal quantities of enzyme are leached from the printed hydrogel. Data are presented as means ± standard deviations (n=3); NS, not significant. ** $p<0.001$ by Student's *t*-test.

The printing method described herein offers distinct advantages in the context of enzyme immobilization for a wide range of applications. Covalent conjugation often reduces enzyme activity, while physical adsorption or entrapment of enzymes often results in enzyme desorption and/or denaturation (via charge or hydrophobic interactions) over time. The mixing-induced gelation chemistry used also makes printing much simpler and more reproducible than equilibrium gelation systems like sol-gels, which could otherwise in theory be used in a similar context.

The molar ratio of aldehyde to hydrazide functionalities on the reactive PO polymers used in the fabrication of this hydrogel film was chosen such that there was a stoichiometric excess of hydrazide groups in the overall gel given the potential concerns with residual aldehydes in the context of this application. First, residual aldehydes in the hydrogel can potentially react with encapsulated enzymes via a reversible Schiff base reaction with protein-associated amine

moieties. Schiff base formation between aldehydes and amine groups may in fact be encouraged by a cooperativity phenomenon attributed to the polymer-based immobilization of enzymes, potentially leading to additional (albeit highly labile) cross-link points within the hydrogel network to further limit the penetration of external proteins into the hydrogel film. Moreover, while excess aldehydes may ultimately promote protein denaturation, low aldehyde contents may instead help to preserve enzyme activity by stabilizing an active enzyme conformation via reversible imine bonds while at the same time promoting enzyme entrapment within the hydrogel[198]. Second, over time, self-condensation of aldehydes via acid or base catalyzed aldol condensation can be observed in some polymeric systems[199]. In the context of the PO-based hydrogel film, the presence of ethylene oxide side chains on the PO polymer backbone would likely pose steric constraints that can limit such self-reactions under neutral conditions. Although we did not observe negative implications of residual aldehyde reactivity in this particular hydrogel film system, the substitution of aldehydes with ketone functionalities that are significantly less reactive than aldehydes is an option, although hydrazone bond formation would occur on a slower time-scale[200]. While the polymer pairs chosen in this work did gel rapidly in the bulk, rapid gelation may not be necessary for printing hydrogel films given that drying (and thus concentration of the polymer precursors) is observed between printing steps; in fact, increasing the time for diffusion of sequentially printed layers may help to produce a hydrogel film with a more homogenous morphology.

The printable PO-based hydrogel demonstrates several characteristics that render this material a suitable interface for biosensing applications, including the ability to resist the non-specific adsorption of proteins, entrap molecules and enzymes of varying sizes, and allow for the efficient diffusion of small molecules. The printing protocol described in this chapter can be used to fabricate interfaces for sensing devices such as lateral-flow assays, paper-based microfluidic chips and microarray-based assays.

3.4 Conclusion

In summary, we have established a protocol for printing an interfacial hydrogel film. Chromatographic analysis and surface characterization methods corroborate the deposition of a covalently cross-linked hydrogel layer onto the nitrocellulose substrate. This represents the first description of a method to print a covalently cross-linked hydrogel in the absence of

ultraviolet (UV) photopolymerization to initiate gelation. The printed hydrogel was able to immobilize biomolecules and enzymes of varying sizes and facilitate the efficient transport of small molecule substrates, demonstrating its potential as a platform for biosensing applications.

Appendix

Appendix 3A. Supplementary data

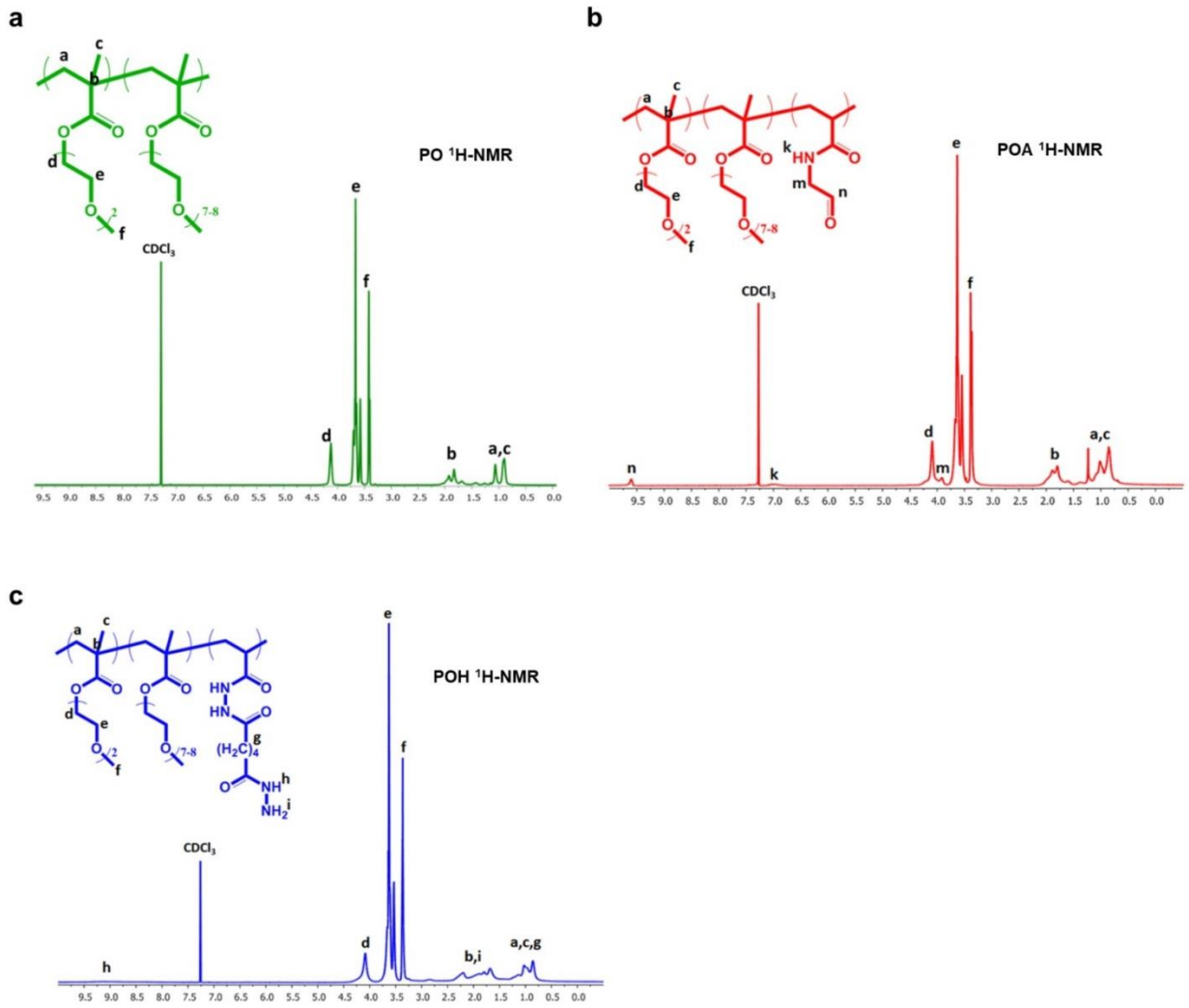

Fig.3A1 ^{1}H-NMR spectra of polymers (a) Unfunctionalized poly(oligoethylene glycol methacrylate) (PO) (b) Aldehyde-functionalized poly(oligoethylene glycol methacrylate) (POA) (c) Hydrazide-functionalized poly(oligoethylene glycol methacrylate) (POH). Chemical shifts are reported relative to residual deuterated solvent peaks. Peak assignments are given on each spectrum based on the anticipated chemical structure of each polymer.

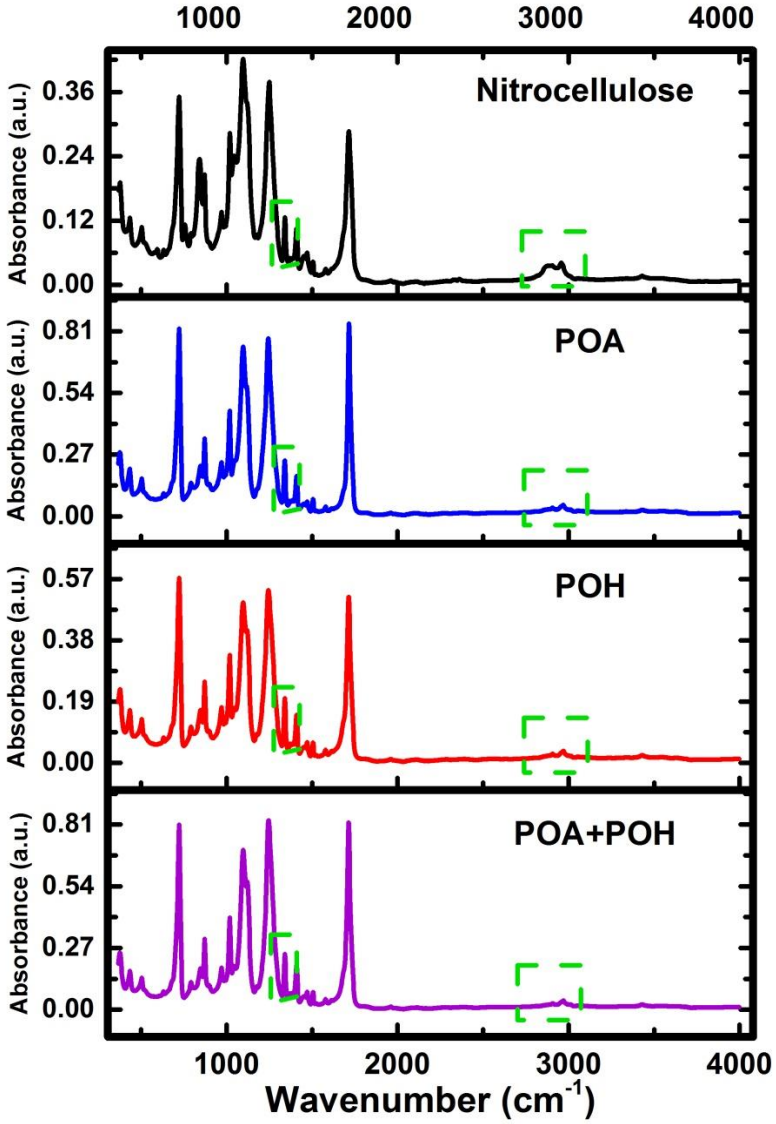

Fig.3A2 ATR-FTIR absorbance spectra of printed polymers In the nitrocellulose spectrum, the peak at 1340 cm^{-1} corresponds to the nitro group ($-NO_2$) stretch while the peak at 2960 cm^{-1} corresponds to the -CH group stretch in the cellulose backbone (peak absorbance is measured in absorbance units (a.u.)). In the printed aldehyde-functionalized and hydrazide-functionalized poly(oligoethylene glycol methacrylate) (POA and POH, respectively) spectra, the peak at 1715 cm^{-1} corresponds to the ester group (-C=O) stretch from the poly(oligoethylene glycol methacrylate) (PO) polymer side chain. Hydrazide and aldehyde groups also both appear in the range of the ester signals and are convoluted with these ester peaks; however, the C=O signal is primarily associated with the PO polymers rather than the nitrocellulose. The decrease in intensity of both the nitro group and the cellulose -CH stretch peak relative to the carbonyl peak in the printed polymers suggests that the polymers were successfully printed onto the nitrocellulose paper surface.

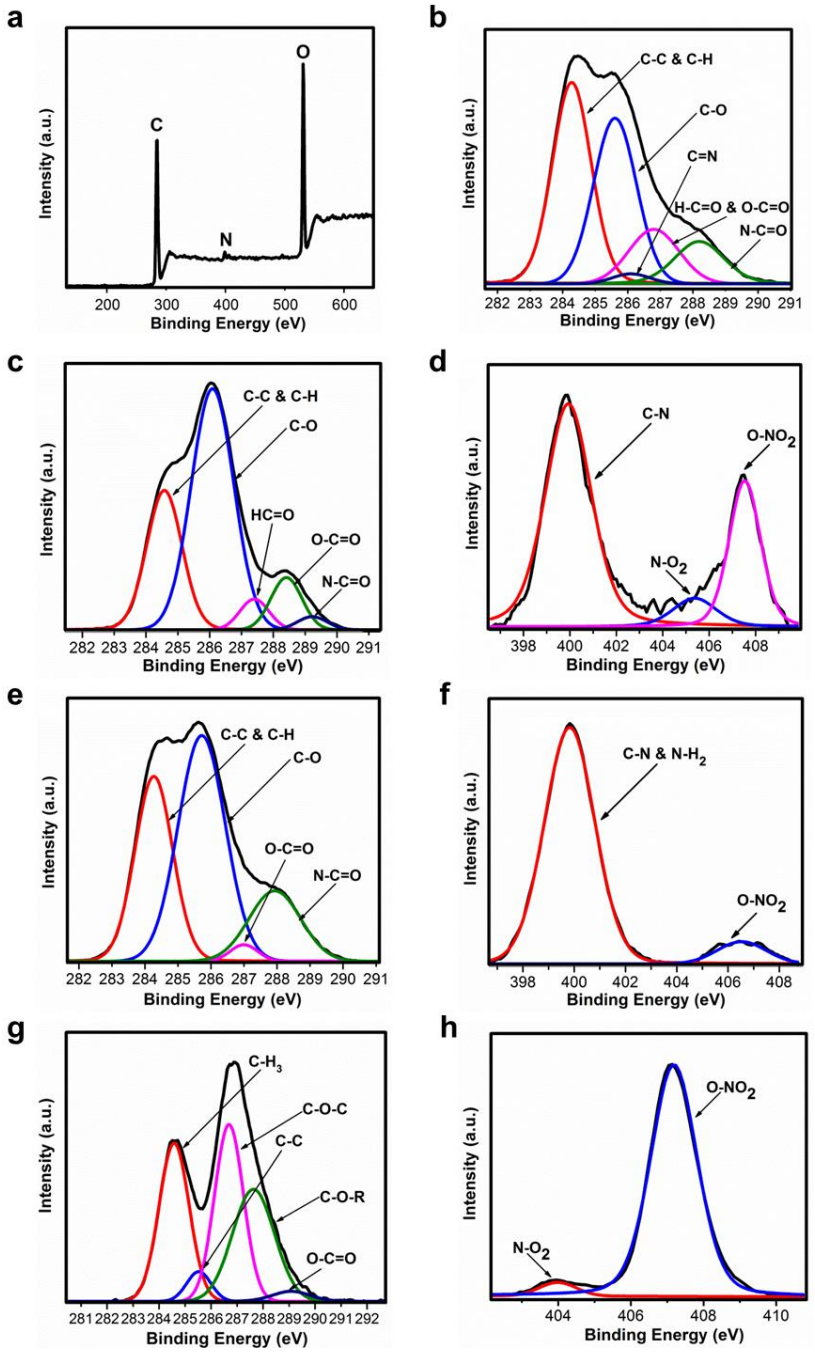

Fig.3A3 High-resolution XPS spectra of printed polymers (a) Survey scan of POA+POH printed on a nitrocellulose substrate. (b) Spectrum of POA+POH printed hydrogel samples collected in the C 1s region. The peak at 286.1 eV corresponds to the –C=N group found in the hydrazone bond. (c) Spectrum of POA collected in the C 1s region. (d) Spectrum of POA collected in N 1s region. (e) Spectrum of POH collected in C 1s region. (f) Spectrum of POH collected in N 1s region. (g) Spectrum of nitrocellulose collected in C 1s region. (h) Spectrum of nitrocellulose collected in N 1s region.

Chapter 4: A printable hydrogel microarray for drug screening avoids false positives associated with promiscuous aggregating inhibitors

Preface

Chapters 3 and 4 are reproduced from the initial publication describing the development of a printable hydrogel microarray for a drug screening application. Chapter 4 describes the application of the printable hydrogel as a biosensing interface. The printable hydrogel is tested for its ability to stabilize a series of enzymes against protease-induced and time-dependent denaturation. The hydrogel platform is used to fabricate a microarray-based assay for the screening of β-lactamase inhibitors. The assay was able to reduce the sample volume requirements that are necessitated by traditional solution-based screens and was able to discriminate between true inhibitors and a class of non-specific inhibitors referred to as promiscuous aggregating inhibitors.

Rabia Mateen[1], M. Monsur Ali[2] and Todd Hoare* [1,3]

[1]School of Biomedical Engineering, McMaster University, Hamilton, Ontario L8S 4K1, Canada.

[2]Biointerfaces Institute, McMaster University, Hamilton, Ontario L8S 4L8, Canada.

[3]Department of Chemical Engineering, McMaster University, Hamilton, Ontario L8S 4L7, Canada.

Adapted from *Nature Communications* 9.1 (2018): 602.

Abstract

A significant problem in high-throughput drug screening is the disproportionate number of false-hits associated with drug candidates that form colloidal aggregates. Such molecules, referred to as promiscuous inhibitors, non-specifically inhibit multiple enzymes and are thus not useful as potential drugs. Herein, we report a printable hydrogel-based drug screening platform capable of non-ambiguously differentiating true enzyme inhibitors from promiscuous aggregating inhibitors, critical for accelerating the drug discovery process. The printed hydrogels can both immobilize as well as support the activity of entrapped enzymes against drying or treatment with a protease or chemical denaturant. Furthermore, the printed hydrogel can be applied in a high-throughput microarray-based screening platform (consistent with current practice) to rapidly (<25 minutes) and inexpensively identify only clinically promising lead compounds with true inhibitory potential as well as accurately quantify the dose-response relationships of those inhibitors, all while using 95% less sample than required for a solution assay.

4.1 Introduction

High-throughput screening approaches for identifying lead compounds have been widely and successfully used to accelerate the drug discovery process.[201] Optimizing drug lead identification is particularly important when it comes to pressing clinical issues such as antibiotic resistance due to the β-lactamase-mediated degradation of β-lactam antibiotics,[202] motivating intensive drug discovery activities in identifying new β-lactamase inhibitors that can reclaim antibiotics that have previously been rendered ineffective.[203] Current techniques for high-throughput drug screens for this and other drug discovery goals are limited by two key factors. First, the typical microplate assays used require significant sample volumes and are thus relatively costly to run, particularly when screening higher value and/or synthetically demanding compounds.[204]. Replacing microplates with microarrays in which target proteins are immobilized on a substrate (and thus interactions occur only interfacially) would significantly reduce the required assay volumes while preserving or even enhancing assay sensitivity and specificity relative to solution-based methods.[136, 205] However, while a range of protein immobilization methods including enzyme cross-linking,[206] physical adsorption[207] or covalent attachment[208] to a support, or physical entrapment in a polymer network[209], silica based sol-gel,[210] or metal organic framework[211] have been explored, all suffer from drawbacks in terms of

their reproducibility and capacity for stably immobilizing target proteins, limiting their utility in drug screening.[212]

Second, current screening methods suffer from many false-positive hits,[213]with compounds that behave non-specifically (i.e. promiscuously) often incorrectly identified as promising drug candidates during screening; subsequent secondary screening of these false positives results in time and money invested in lead compound candidates that are not truly functional inhibitors.[214] Such promiscuous inhibition is typically linked to the tendency for some compounds to self-associate and form colloidal aggregates that sterically, rather than biologically, inhibit binding to active sites of a range of structurally and functionally unrelated enzymes.[61] The inhibitory interaction typically occurs due to protein adsorption onto the surface of aggregates,[60] which sequesters enzymes away from their substrates while also often resulting in partial protein denaturation.[215] Significant effort has been invested in examining the nature of these aggregates and determining methods to identify compounds demonstrating aggregative potential,[59, 216, 217] with only limited success. Because the formation of aggregates can occur over minor changes in concentration, it is difficult to predict potential aggregators strictly based on physical properties.[218] Computational models have been designed to predict the presence of these compounds in pharmaceutical libraries, but have been shown to regularly generate both false positive and false negative results.[218] Furthermore, the addition of a non-ionic detergent can disrupt some colloidal aggregates,[219] but cannot fully prevent aggregation and has been shown to interfere with other assay components,[220] creating challenges with reliable quantification.

In the context of these challenges, hydrogel-based enzyme immobilization platforms offer particular promise. The high water binding capacity of hydrogels can preserve enzyme hydration over a broad range of storage/application conditions,[221, 222, 223] promote high enzyme mobility and flexibility,[224] and maintain physiologically-mimetic conditions for optimal enzyme catalyzed reactions.[76] In addition, the tunable porosity of hydrogels can enable selective transport of substrates to and from the entrapped enzyme via size selectivity,[225] offering potential to sterically block a drug aggregate from reaching the enzyme binding site and thus minimize (or even eliminate) issues associated with promiscuous inhibition. Interfacial hydrogel films are particularly attractive since they can minimize the kinetic/diffusional drawbacks associated with bulk hydrogels in biosensing applications, promoting fast assay speeds[127] while maintaining the

benefits of size selectivity.[123] Several methods have been developed to fabricate hydrogel films on various substrates, including dip-coating,[116] spray deposition,[117] spin-coating[118] and drop-on demand printing.[119] Printing is particularly advantageous since it is amenable to dispensing small volumes (minimizing sample volumes for screening), can localize materials in specific patterns (enabling, for example, facile printing of multi-sample arrays on a substrate), and can be scaled to commercial production.[187, 188, 189]

Herein, we report the fabrication of a printable hydrogel microarray that can both immobilize and stabilize a wide range of enzymes on a cellulose-based substrate and demonstrate the utility of these printed gels in a high-throughput drug screening application that can discriminate between actual and promiscuous inhibitors of β-lactamase. We demonstrate that our printable enzyme immobilizing/stabilizing hydrogel microarrays can enable both quantitative predictions of the IC50 values of real inhibitors as well as discriminate true inhibitors from promiscuous aggregating inhibitors within a high-throughput assay format, potentially impactful for more rapidly and inexpensively identifying clinically promising leads.

4.2 Materials and Methods

Materials and methods describing hydrogel printing and enzyme entrapment are outlined in Chapter 3.

Materials

Urea (Sigma Aldrich, ≥98%), recombinant β-lactamase TEM precursor from *Escherichia coli* (ProSpec, 700 U/mg), nitrocefin (Abcam, >95%), proteinase K (ThermoFisher, 20 mg/mL), tazobactam sodium salt (Abcam, >99%), sulbactam sodium salt (Santa Cruz Biotechnology), clavulanic acid potassium salt with cellulose, 1:1 w/w (Santa Cruz Biotechnology), rottlerin (Abcam, >95%), bisindolylmaleimide IX (BIS IX, Abcam, >98%) 3′,3″,5′,5″-tetraiodophenolphthalein (TIPT, Santa Cruz Biotechnology, >95%), 1,4-dithiothreitol (Sigma Aldrich, ≥97%), TRIS hydrochloride (Sigma Aldrich, >99%), sodium chloride (Sigma Aldrich, ≥99%) and Slide-A-Lyzer™ MINI Dialysis Devices (0.1 mL, 3.5 kDa MWCO, ThermoFisher) were all used as received. For all experiments, Milli-Q grade distilled deionized water (DIW)

was used. Phosphate buffered saline (PBS) was diluted from a 10X liquid concentrate (Bioshop Canada Inc.).

Protease protection studies

10 μL of a 2 mg mL^{-1} proteinase K solution (prepared in 10 mM PBS and 1 mM $CaCl_2$) was pipetted on the printed enzyme samples both with and without hydrogel encapsulation. The samples were incubated in a closed container for 2 hours at room temperature, after which substrate solutions were pipetted on the treated samples at the volumes listed in Supplementary Table 2. Image acquisition and analysis was performed as described for the entrapment studies. The intensity of each sample was measured and presented as a ratio of the corresponding control image (the same hydrogel/enzyme combination not treated with protease).

Long-term stability studies

Printed enzyme samples were stored in a closed, dark container at room temperature for varying periods of time. Image acquisition and analysis was performed as described previously for the entrapment and proteinase K degradation studies. The intensity of each sample was measured and presented as a ratio of the corresponding control image (freshly printed using the same hydrogel/enzyme combination).

Denaturation study

For the printed hydrogel denaturation study, 10 μL of urea denaturation buffer (8 M urea, 5 mM dithiothreitol, 50 mM Tris-Cl (pH=7.5), 150 mM NaCl) was pipetted onto samples of 1 μM β-lactamase entrapped in the printed hydrogel. The samples were incubated in a closed container for 30 min. at room temperature and then washed with DIW. Image acquisition and analysis was performed as described for the entrapment studies. The intensity of each sample was measured and presented as a ratio of the corresponding control image (samples treated with 10 mM PBS). For the solution denaturation study, 1 μM β-lactamase was prepared in 100 μL of urea denaturation buffer and incubated for 30 min. at room temperature, after which nitrocefin was added to a final concentration of 200 μM. β-lactamase activity was then assessed via UV-vis spectrophotometry, tracking the hydrolysis of nitrocefin (Infinite M1000 spectrophotometer, Tecan) by monitoring solution absorbance at 492 nm. For the solution refolding study, 1 μM β-

lactamase samples prepared in urea denaturation buffer were dialyzed against 10 mM PBS using a 3.5 kDa MWCO dialysis device (ThermoFisher) for 20 cycles (20 min/cycle). β-lactamase activity was then re-assessed via UV-vis spectrophotometry as described above.

Optimizing the β-lactamase concentration in a printed hydrogel-based screening assay

β-lactamase concentrations ranging from 0 to 25 nM were printed in the PO-based hydrogel as described previously. Each microzone was treated with 100 μM tazobactam (5 μL) or water (5 μL) for 20 min., followed by the addition of 500 μM nitrocefin (5 μL). Images of the microzones were taken with a Canon DSLR camera (operated in manual focus mode without flash) 25 min. after substrate addition and analyzed via image analysis as previously described.

Solution-based β-lactamase assay

True inhibitor (tazobactam, sulbactam and clavulanic acid) solutions were prepared in DIW and promiscuous inhibitor (rottlerin, BIS IX and TIPT) solutions were diluted in DIW from 10 mM DMSO stock solutions. The assay mixture contained 25 nM β-lactamase and a range of inhibitor concentrations relevant to the IC50 of the true inhibitors and the apparent IC50 of the aggregating promiscuous inhibitors in 100 μL of 10 mM PBS buffer. β-lactamase and inhibitor were pre-incubated for 10 minutes, after which nitrocefin was added to a final concentration of 200 μM. β-lactamase activity was then assessed via UV-vis spectrophotometry by tracking the hydrolysis of nitrocefin by monitoring solution absorbance at 492 nm (Infinite M1000 spectrophotometer, Tecan).

Printed hydrogel-based β-lactamase assay

POH ink solution was prepared with a final concentration of 50 nM β-lactamase and used to print hydrogel spots on a 96-well paper microzone plate as described previously. 5 μL of tazobactam, sulbactam and clavulanic acid solutions (at starting concentrations of 100 μM) were added to each microzone using a Tecan Freedom Evo 200 liquid handling robot (Tecan, Switzerland). The inhibitor was incubated with the printed β-lactamase for 20 minutes, after which the assay was initiated with the addition of 5 μL of nitrocefin (500 μM) to each microzone. A similar protocol was used to test the promiscuous inhibitors rottlerin, BIS IX and TIPT, again using starting concentrations of 100 μM. Images were taken with a Canon DSLR camera (operated in

manual focus mode without flash) after 25 minutes. The wax printed background was filtered out using GIMP software (Version 2.8.16). Image analysis was performed using Fiji, with the converted substrate colour extracted using the Color Deconvolution plugin. Extracted images were inverted and converted to 8 bit grayscale images. The intensity of each sample was measured and presented as a ratio of the control image (i.e. a microzone not treated with inhibitor). Calculation of IC50 values was carried out in OriginPro by plotting the calculated percentage inhibition against the added inhibitor concentration. Curve fitting was performed with the dose-response function (OriginLab Corporation, Northampton, MA U.S.A.).

Promiscuous aggregating inhibitor size measurement

Dynamic light scattering measurements were performed using a Zetasizer Nano ZS instrument (Malvern). The intensity of backscattered light was measured at a 173° angle. Data collection and analysis were performed using the Dispersion Technology Software (version 6.0) from Malvern. Samples of Rottlerin, BIS IX and TIPT at 100 μM concentrations were analyzed in a plastic cuvette with a 10 mm path length. Prior to measurement, samples were equilibrated for 120 s at 23°C. For each sample, 10 runs were performed with three repetitions. The intensity size distribution, Z-average diameter and polydispersity index was collected for each sample. Note that no significant signal was acquired from DLS measurements on the true inhibitors, confirming their solution state.

4.3 Results and Discussion

Stabilizing enzymes in the printed hydrogel

In Chapter 3, the ability of the printed hydrogel to immobilize small molecules and enzymes was demonstrated. In addition to immobilization, the printed hydrogel layer has benefits in terms of protecting encapsulated enzymes from proteolytic degradation (via size exclusion), chaotropic agent interference (via competitive hydrogen bonding) as well as minimizing activity losses upon dry storage (via moisture retention). The printed hydrogel prevented proteolytic deactivation of all tested enzymes by proteinase K, with each enzyme retaining >80% of its pre-treatment activity (Fig.4.1); in contrast, urease and β-Lac printed directly on the nitrocellulose substrate without the hydrogel retained <10% of their activity over the same treatment time. While the steric barrier presented by the hydrogel is likely the main reason for this result, the ability of the

PO-based hydrogel to resist non-specific protein adsorption may also be beneficial to reduce the probability of proteinase K binding close to the enzyme. In comparison, co-printing enzymes with POH alone or in combination with unfunctionalized PO also showed only limited benefits in terms of stabilizing both urease and β-Lac against deactivation. AP was a slight outlier in this regard, retaining ~40% of its activity when printed alone and >80% of its activity when printed with POH even in the absence of gel formation (Fig.4.1a); this is consistent with the noted high stability of AP relative to other enzymes.[226] However, even with AP, each hydrogel-printed enzyme exhibited better activity retention than any other printed sample tested. Printed hydrogels showed similar efficacy in resisting chaotropic agent-induced denaturation, with hydrogel-printed β-Lac retaining >95% activity following urea challenge compared to only <20% activity retention in solution (Fig.4.2).

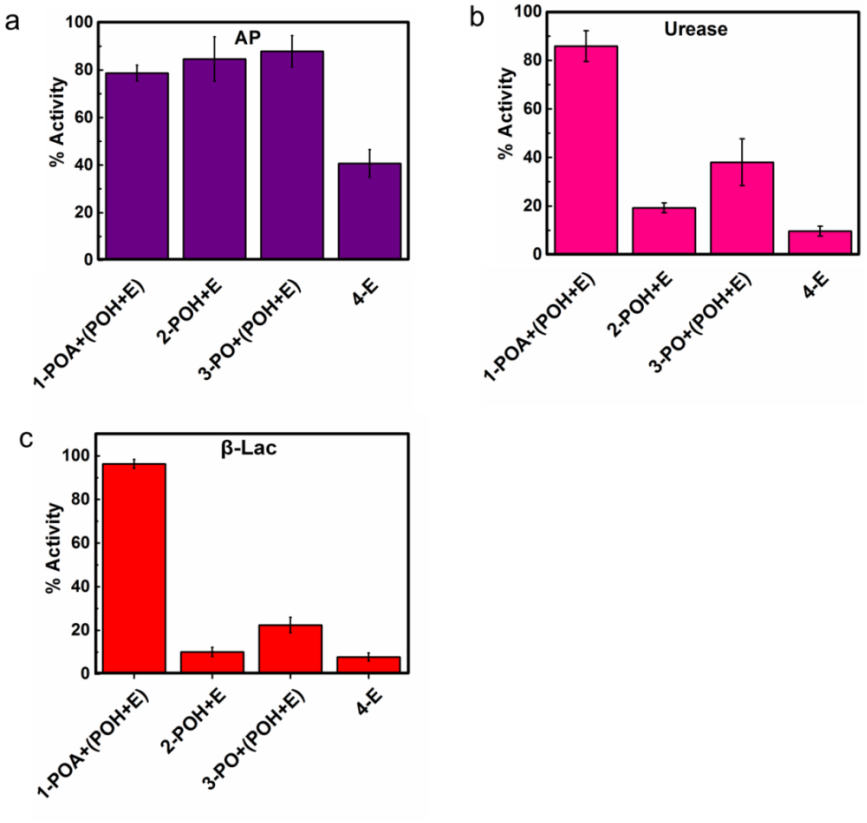

Fig.4.1 Printed hydrogels can protect enzymes against proteolytic degradation Remaining activity of enzymes (E) was quantified after 2 hours of protease treatment with proteinase K (a protease that hydrolyzes peptide bonds with broad specificity) and normalized relative to the initial activity of a freshly printed sample. The hydrogel protects the enzymes against proteolytic degradation by proteinase K. **(a)** alkaline phosphatase; **(b)** urease; **(c)** β-lactamase. Data are presented as means ± standard deviations (n=3)

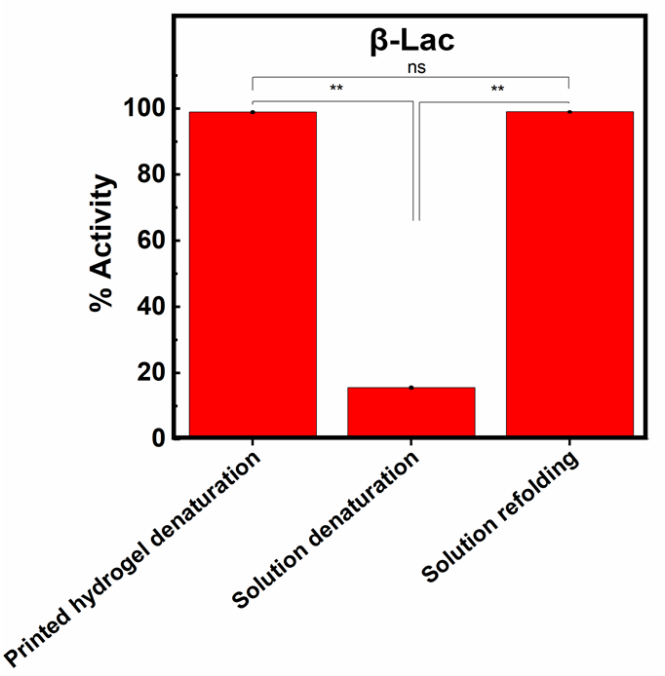

Fig.4.2 Printed hydrogel protects β-lactamase against denaturation The remaining activity of β-lactamase printed in a hydrogel or in solution was quantified after 30 min. of treatment with urea denaturation buffer (a chaotropic agent) and normalized to the activity of the control incubated in 10 mM PBS. The solution refolding activity was measured by dialyzing a solution of β-lactamase prepared in urea denaturation buffer against 10 mM PBS in order to promote protein refolding and then re-testing the enzymatic activity; the full recovery of enzyme activity following dialysis confirms that urea was the driving force for the solution denaturation, as such denaturation is known to be reversible. Data are presented as means ± standard deviations (n=3); NS, not significant. ** $p<0.001$ by Student's *t*-test.

The printed hydrogels are also capable of stabilizing enzymes for long-term storage under (dry) ambient conditions. The hydrogel-entrapped enzymes retained ~100% activity after at least three months of storage for AP, urease, and β-Lac (Fig.4.3); in contrast, direct printed enzymes lost >70% of their activity within one week for urease and β-Lac and within one month for AP. While similar efficacy in enzyme stabilization has previously been reported with dried carbohydrate films[227], such films dissolve when placed back in an aqueous environment, leading to rapid leaching of the enzyme from the substrate. In contrast, the printed hydrogel maintains a confined environment for the enzyme under aqueous conditions, maintaining immobilization while also driving local hydration to promote enzyme activity. Taken together, these results demonstrate that the printed hydrogel has the capacity to protect entrapped enzymes against both

degradative agents and time-dependent denaturation, facilitating effective storage and distribution of bioassays developed based on this platform.

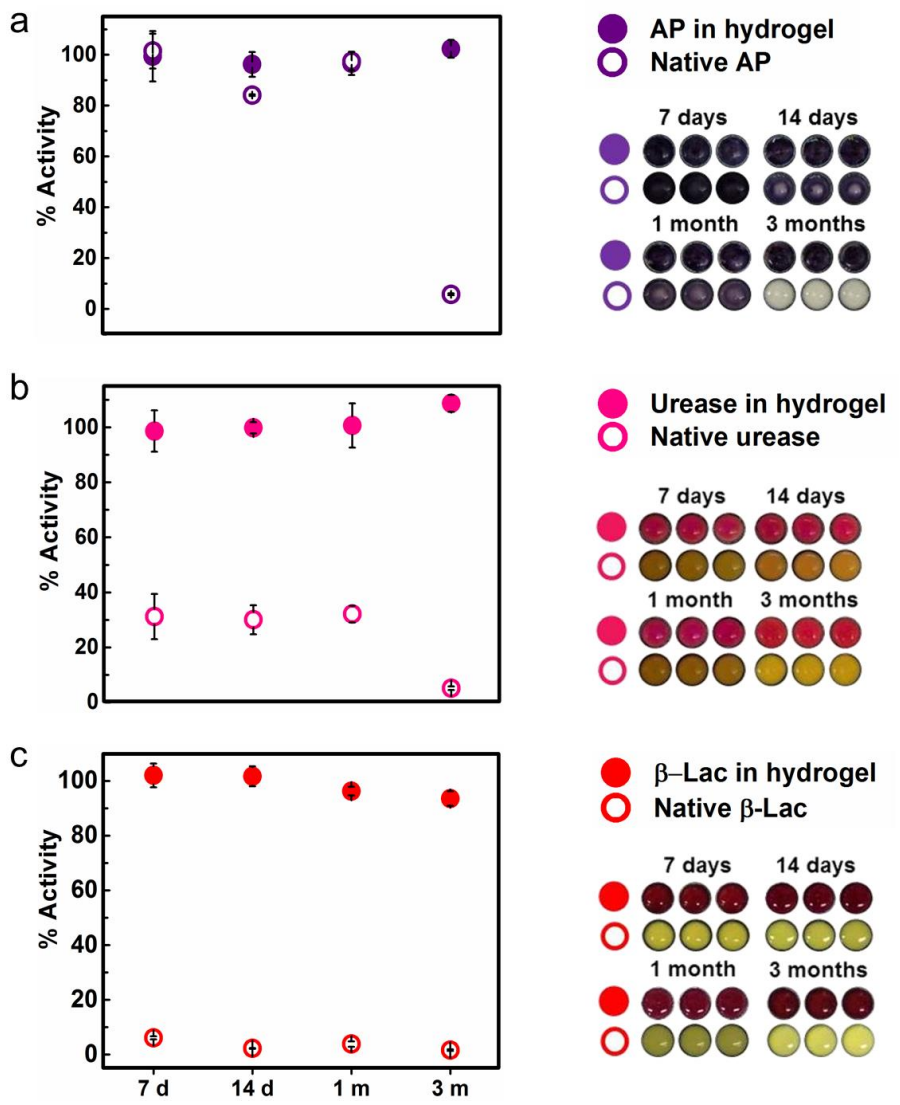

Fig.4.3 Printed hydrogels can protect enzymes from time-dependent denaturation
Remaining activity of enzymes (E) was quantified following dry storage at room temperature for varying periods of time and normalized relative to the initial activity of a freshly printed sample. The hydrogel supports enzyme stabilization for long-term storage. **(a)** alkaline phosphatase; **(b)** urease; **(c)** β-lactamase. Data are presented as means ± standard deviations (n=3)

Fabricating a hydrogel-based β-lactamase microarray

To demonstrate the potential of printable hydrogel-enzyme films for practical biosensing, TEM-1β-lactamase was printed in a POA/POH hydrogel array onto the microzones of a 96-well nitrocellulose wax-printed template, creating a microplate mimic adaptable to current high-throughput screening protocols. Inhibitor solutions and nitrocefin (a colorimetric β-lactamase substrate) were subsequently deposited on the microzones at different concentrations using a high-throughput dispensing robot. The resulting colorimetric readout of β-lactamase activity was quantified via image analysis.

First, well-established true inhibitors of β-lactamase (tazobactam, sulbactam, and clavulanic acid) were screened to compare IC_{50} values measured via the printed hydrogel assay with solution values determined from a conventional microplate assay. Using the printed hydrogel assay, IC_{50} values of 0.07 μM, 4.1 μM and 0.15 μM were calculated for tazobactam, sulbactam and clavulanic acid respectively (Fig.4.4, Table 4.1); these values compare favorably to the measured solution-based assay IC_{50} values (Fig.4.4, Table 4.1) as well as literature IC_{50} values (Table 4.1) for these same inhibitors. The excellent quantitative correlation between these results suggests that the printed hydrogel-based assay can determine dose-response relationships of β-lactamase inhibitors with high accuracy. Furthermore, IC_{50} measurements using the printed hydrogel-based assay require only 5% of the total sample volume used for the solution assay, a significant benefit in screening high value potential inhibitors (i.e. only 1/20 of the drug candidate mass is required to screen the same drug concentrations). Note also that the potential of the printed hydrogel to stabilize each enzyme enabled 100% activity inhibition at high inhibitor concentrations in each case; in contrast, the increased potential for partial enzyme denaturation in solution over the timescale of the assay led to lower maximum inhibitions in each solution-based assay performed. Lower enzyme concentrations could also be printed to improve the sensitivity of the assay for low K_i inhibitors, with detectable colour differences noted between inhibited and non-inhibited printed enzymes at as low as 5 nM enzyme concentrations (Appendix Fig.4A1).

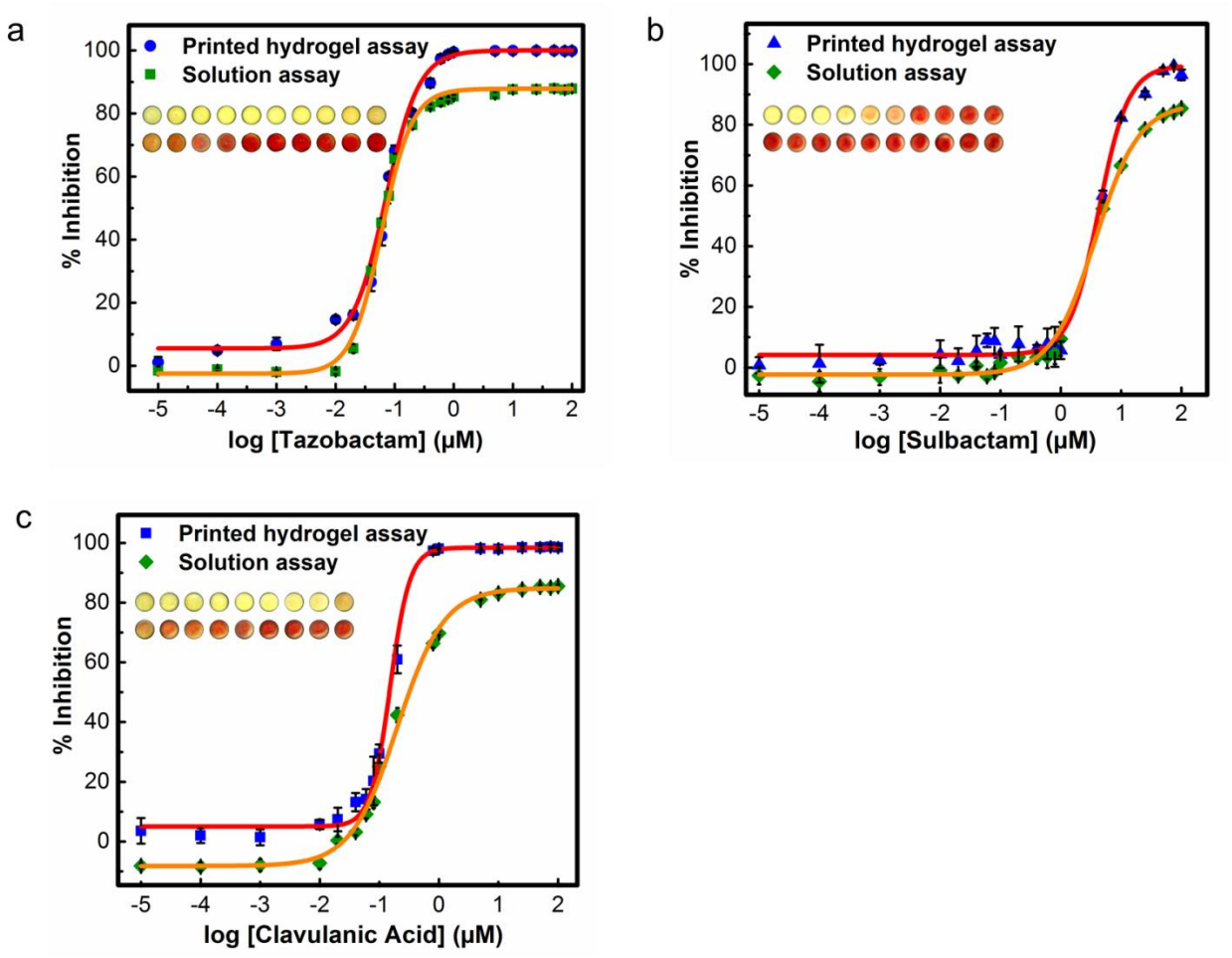

Fig.4.4 A printed hydrogel-based β-lactamase drug screening assay The printed hydrogel-based β-lactamase screening assay can determine dose-response relationships of classic β-lactamase inhibitors. Comparison of solution versus printed hydrogel-based inhibition curves for true β-lactamase inhibitors: **(a)** tazobactam; **(b)** sulbactam; **(c)** clavulanic acid. Data are presented as means ± standard deviations (n=3)

Table 4.1 Comparison of IC_{50} values of classic β-lactamase inhibitors IC_{50} values of tazobactatm, sulbactam and clavulanic acid measured by the printed hydrogel assay relative to the conventional solution assay and reported literature values. Values are represented as mean ± standard deviation (n=3)

β-Lactamase Inhibitor	**IC_{50} (μM)**		
	Printed hydrogel assay	**Solution assay**	**Literature[225]**
Tazobactam	0.07 ± 0.01	0.06 ± 0.01	0.04
Sulbactam	4.1 ± 0.2	4.0 ± 0.3	6.1
Clavulanic acid	0.15 ± 0.01	0.19 ± 0.01	0.09

Next, to assess the capacity of the printed hydrogels to differentiate between specific and non-specific inhibition, the confirmed promiscuous (aggregating) inhibitors rottlerin[216] and BIS IX[216] (both kinase inhibitors) and tetraiodophenolphthalein (TIPT)[60] were tested against TEM-1 β-lactamase both in solution (modeling a conventional microplate assay) and using a printed hydrogel array. In each case, the aggregating compounds inhibited β-lactamase in the solution-based assay (a false positive hit) but were correctly observed to induce no specific inhibition of β-lactamase in the hydrogel-based assay (Fig.4.5). Comparing the aggregate diameter range of ~154-365 nm (Appendix Fig.4A2, Table 4A1) to the ~2 nm characteristic correlation length (i.e. average pore size) of PO hydrogels of this type[229], this performance benefit is likely linked to aggregates not being able to diffuse into the hydrogel and thus being unable to sterically inhibit the enzyme as they can in solution. In this way, the size selectivity of the printed hydrogel layer excludes the promiscuous inhibitors from accessing the entrapped enzyme and thus avoids the false positive hits observed in solution assays (Fig.4.6).

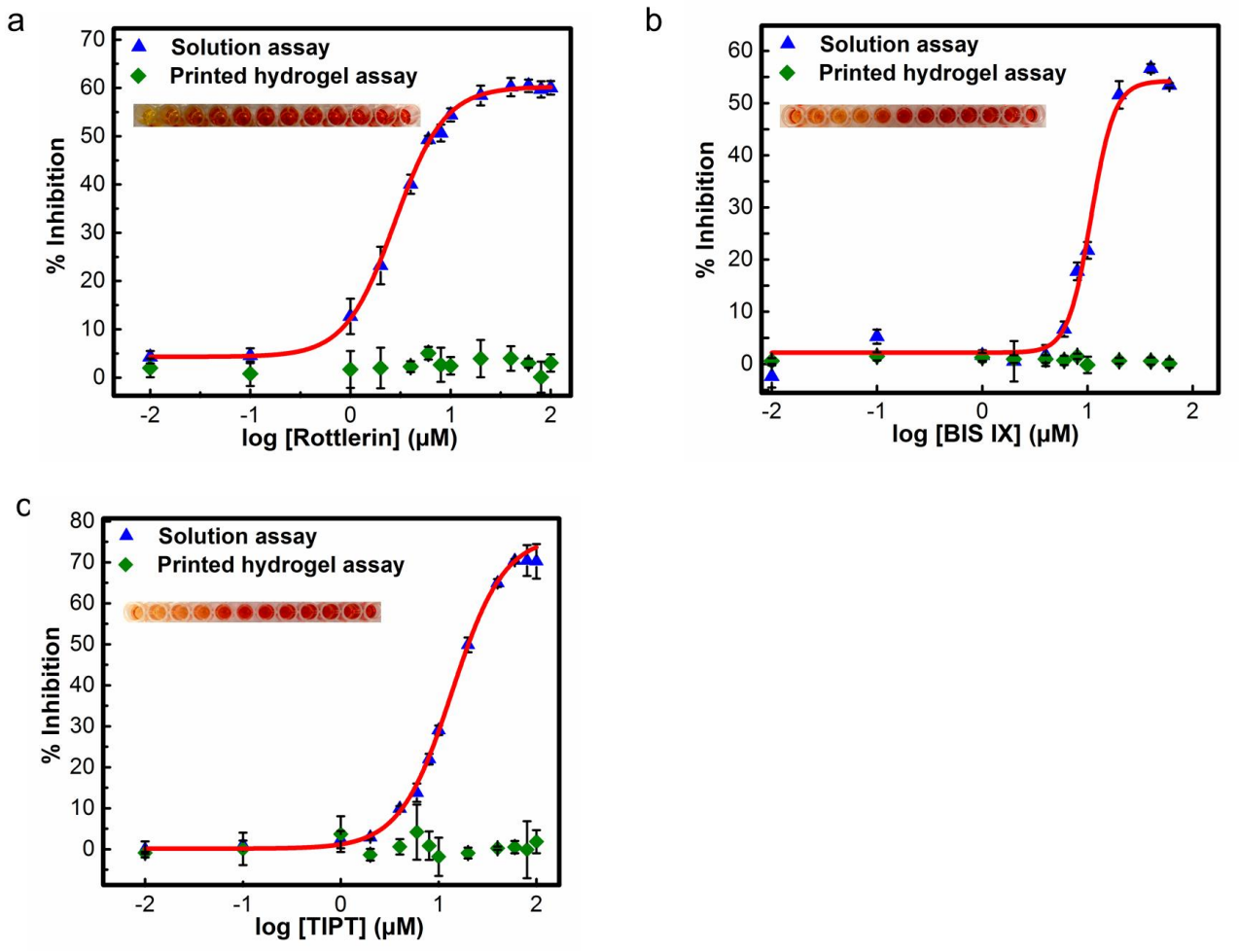

Fig. 4.5 A printed hydrogel-based β-lactamase drug screening assay The printed hydrogel-based β-lactamase screening assay can discriminate between true and promiscuous aggregating inhibitors. Comparison of solution versus printed hydrogel-based inhibition curves for known promiscuous inhibitors of β-lactamase: **(a)** rottlerin; **(b)** BIS IX; **(c)** TIPT. Data are presented as means ± standard deviations (n=3)

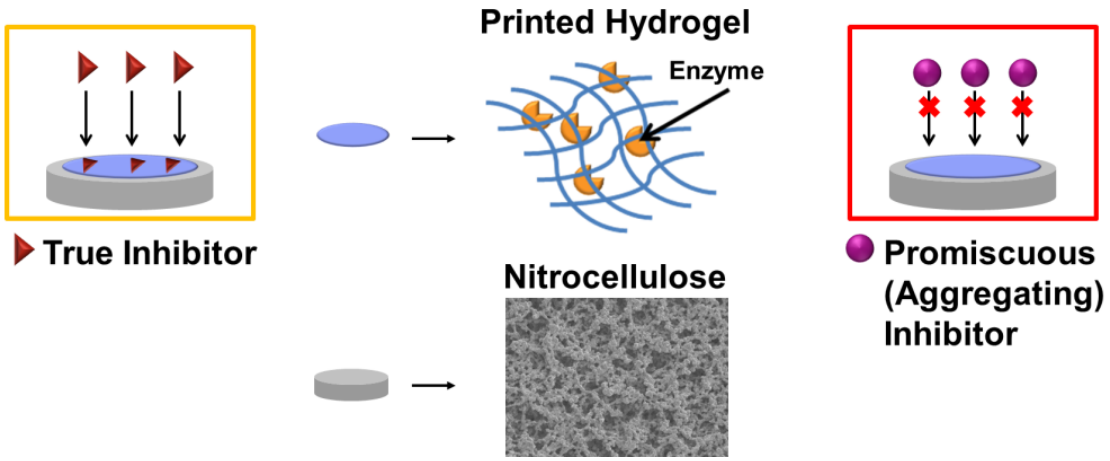

Fig. 4.6 Printed hydrogel-based β-lactamase drug screening assay Schematic illustrating how the size selectivity of the printed hydrogel layer excludes the colloid-forming drug (promiscuous aggregating inhibitor) from accessing the encapsulated enzyme but can permit the diffusion of a soluble drug (true inhibitor) to generate a positive signal for true inhibitors only.

The printed hydrogel screening assay reported herein addresses the key limitations associated with current microplate assay platforms for drug discovery by significantly reducing reagent volumes, eliminating costs associated with microtiter plates, and improving assay sensitivity. Sensitivity improvements are gained both in terms of avoiding false hits associated with the aggregation of inhibitor candidates as well as the removal of errors associated with the non-specific adsorption of enzymes on the surface of polystyrene or polypropylene-based microplates (reported to introduce significant measurement errors for enzymes present in the nanomolar concentration range[230]), the latter leveraging the high protein repellency of PO-based hydrogels.[116] It should be emphasized that these sensitivity improvements were achieved without causing significant increases in screening time, with the full assay (from start to finish) completed within 25 minutes using only 5% of the total sample volume required for a solution-based assay.

The demonstrated ability of the hydrogel platform to discriminate true inhibitors from promiscuous aggregating inhibitors is highly significant given that promiscuous inhibitors are arguably the most widespread artefact encountered in high-throughput screening. Up to 95% of the active compound hits identified in a typical library consisting of ~70,000 small molecules have been attributed to aggregate-based inhibition.[231] Colloidal aggregates also have a broadly

detrimental impact in other pharmaceutical screening contexts, and previously explored techniques to avoid or compensate for such aggregation may denature the enzyme (e.g. detergent-based assays[217]), can alternatively bind to and thus sequester any de-aggregated small molecules (e.g. bovine serum albumin pre-treatments),[219] or cannot be readily transferred to a high-throughput context (e.g. NMR-based assays of self-aggregation).[232] In contrast, the hydrogel-based screening assay demonstrates minimal interference, the ability to be adapted directly to current high-throughput pharmaceutical screening practices, and exploits a fundamental property of all aggregate-based inhibitors (i.e. size) to exclude their effects on the assay results, strongly suggesting the assay's potential to consistently eliminate false positive hits.

4.4 Conclusion

We have demonstrated a printable hydrogel platform that allows for the immobilization, protection, and long-term stabilization of a diverse set of enzymes. Using β-lactamase inhibitors as a model, a low-volume hydrogel-based microarray assay based on this printed gel platform was shown to both accurately measure IC_{50} values of well-established β-lactamase inhibitors and prevent the occurrence of false positive hits by promiscuous, non-specific inhibitors that function via aggregation instead of a specific binding interaction. Combining the functionality of the assay with the facile printing of multi-sample substrates amenable to use in current high throughput screening formats, this approach offers potential to significantly improve the resolution of drug lead optimization testing and thus streamline the drug discovery process. The ease of fabrication, potential for long-term stabilization of labile biomolecules both in solution and in dry storage, and the versatile functionality of this platform make this approach promising not only for drug discovery but also in a range of other sensing and analytical applications.

Appendix

Appendix 4A. Supplementary data

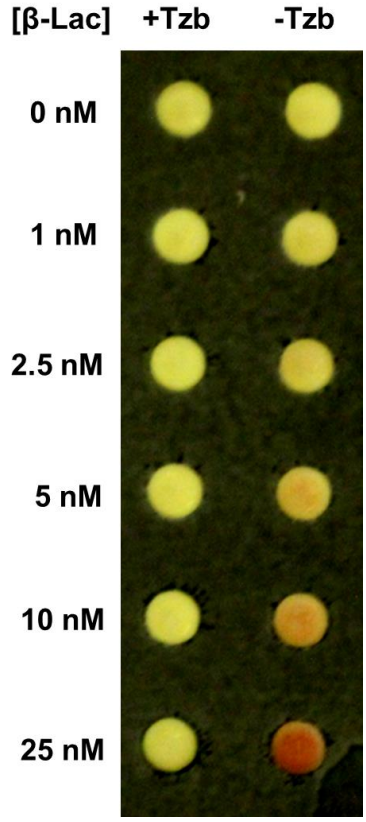

Fig.4A1 Detection limit of β-lactamase drug screening assay A range of β-lactamase concentrations was encapsulated via printing in the POA+POH hydrogel, with the colorimetric readouts compared with and without tazobactam (a known inhibitor of β-lactamase, 100 μM concentration added). Significant and detectable colour differences were observed using enzyme concentrations as low as 5 nM, providing additional flexibility for the assay in detecting low K_i inhibitors.

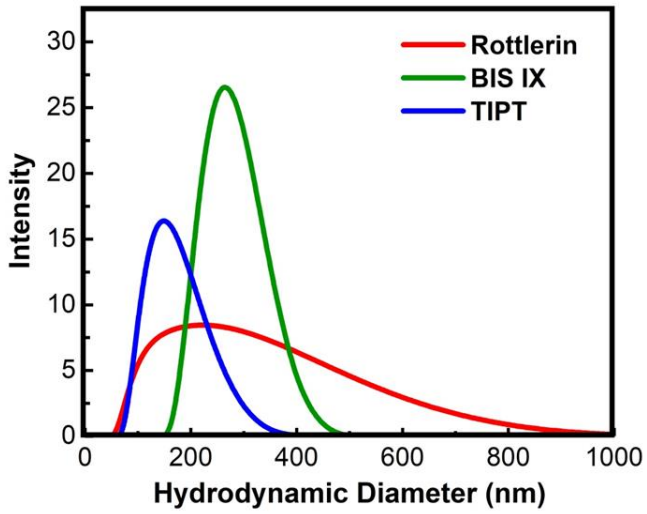

Fig.4A2 Particle size distribution of aggregating inhibitors Intensity distributions of 100 μM solutions of rottlerin, bisindolylmaleimide IX (BIS IX) and tetraiodophenolphthalein (TIPT) were measured using dynamic light scattering (DLS). Each of these known promiscuous inhibitors shows clear evidence of aggregate formation on the order of 50-800 nm particle sizes, the full size range of which would be sterically excluded from diffusing into the printed hydrogel mesh.

Table 4A1 Size and polydispersity of aggregating inhibitors The aggregate size was measured in 100 μM solutions of rottlerin, bisindolylmaleimide IX (BIS IX) and tetraiodophenolphthalein (TIPT) using dynamic light scattering (DLS).

Inhibitor	Size (nm)	Polydispersity
Rottlerin	188 ± 1	0.24 ± 0.01
BIS IX	365 ± 9	0.36 ± 0.02
TIPT	154 ± 1	0.16 ± 0.02

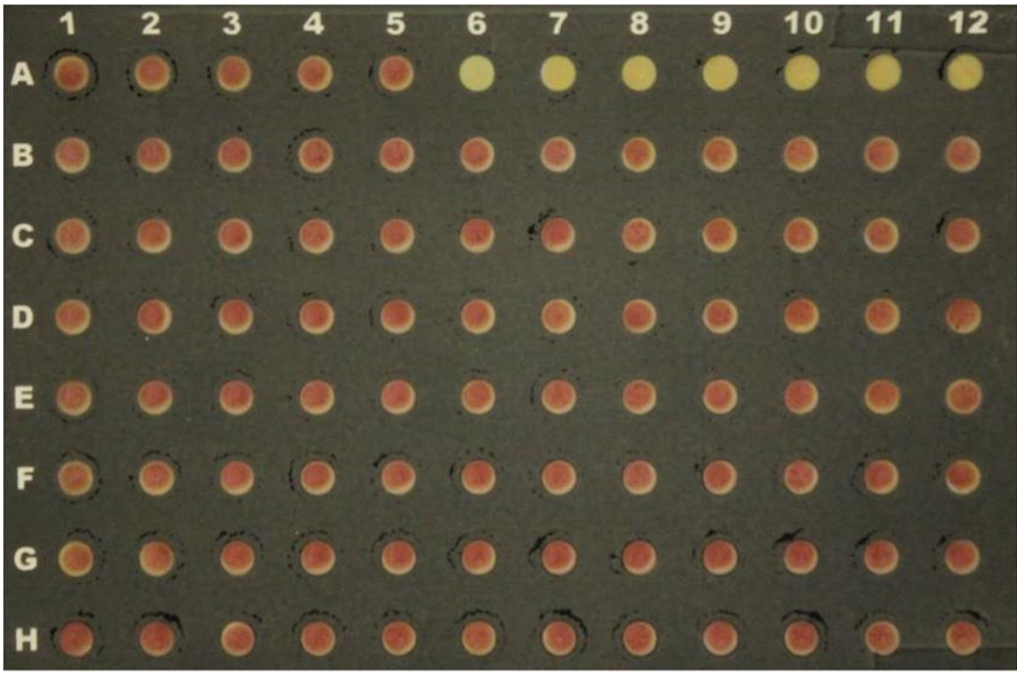

Fig.4A3 A printable hydrogel microarray for drug screening Hydrogel spots entrapping β-lactamase were printed on microzones initially defined by wax-printing a 96-well pattern on nitrocellulose. The microplate has the same dimensions as a traditional 96-well microplate; smaller microplate mimics (e.g. 384 well formats) could similarly be printed if desired, as the resolution of the printing process is sufficient for such fabrication. The assay is performed by a liquid handling robot that dispenses inhibitor solutions and the enzymatic substrate onto the microzones

Chapter 5: Developing a printable hydrogel microarray for DNA hybridization detection

Preface

Chapter 5 describes the application of the printable hydrogel-based microarray in a hybridization assay. A long, concatemeric DNA molecule was used as an immobilized sensing material for the detection of a small fluorophore-labeled oligonucleotide. The properties of the printable hydrogel were investigated for their ability to successfully entrap and immobilize a DNA molecule on a paper-based substrate.

Abstract

In this chapter, we establish the principles of a DNA hybridization microarray assay based on the poly(oligoethylene glycol methacrylate) (PO) printable hydrogel platform. Rolling circle amplification (RCA) product, a long single-stranded DNA molecule consisting of tandemly repeated sequences, is used as the sensing material in the assay. The PO-based hydrogel platform demonstrates the capacity to immobilize and reproducibly deposit RCA product onto a nitrocellulose substrate. Hybridization is performed with a fluorescein labelled DNA probe. Several hydrogel configurations and assay conditions are tested for their ability to promote effective DNA hybridization and reduce background noise associated with non-specific interactions of the DNA probe with the hydrogel system. Modifications to the hydrogel platform are suggested in order to improve the low signal-to-background ratios generated in the assays.

5.1 Introduction

The development of rapid and sensitive nucleic acid detection technologies remains a critical challenge in both clinical and academic research. Applications of DNA hybridization-based sensors include disease diagnosis, gene expression analysis, and forensic and genetic identification[233, 234, 235]. The DNA microarray is the most prominent example of this nucleic acid sensing technology[236]. The device consists of a large collection of DNA "spots" immobilized on a solid surface that can probe for the presence of specific nucleic acid sequences[237], with current assay methods operating under a simple detection strategy that exploits the phenomenon of DNA hybridization or the reannealing of two complementary single strands of DNA[238]. DNA microarray technology has become an invaluable tool in molecular biology, facilitating large scale investigations that have revealed mechanistic insights into cellular processes.[239] More specifically, DNA microarrays allow for analyses to be performed in a miniaturized, parallel, and high throughput manner, making complex tasks like searching for single base pair variations in a DNA sequence within an entire genome an achievable undertaking[240].

Although DNA microarrays are a well-established diagnostic and sensing platform, there remain unresolved drawbacks associated with the conventional 2-dimensional system including slow diffusion kinetics[241], the requirement of covalent attachment of DNA[242], the absence of

protection against degradative agents[243], low sensitivity[244], and a non-uniform distribution of the assay signal (particularly fluorescence)[245]. Hydrogel-based microarrays can address these disadvantages[246]. The hydrogel interface allows the DNA sensing material to be strongly physically immobilized on the substrate, avoiding the need for synthetically-challenging covalent immobilization while providing significantly improved stability relative to simple physical adsorption. In addition, the hydrogel can maintain a hydrated microenvironment that can support rapid diffusional transport (and thus accelerate hybridization kinetics) and sterically protect the entrapped DNA from possible degradation incurred by nucleases[247]. Another advantage of hydrogels is that they are three-dimensional matrices that can immobilize substantially more DNA per unit area, up to 100 times more product than microarrays deposited on a two-dimensional glass support[248]. The 3D hydrogel matrix provides a solution for maximizing the total number of DNA sensors and thus the fluorescence signal generated upon hybridization with a labeled DNA probe[249] while also avoiding steric restrictions that occur upon the assembly of a high density of DNA spots on a planar microarray that reduce the accessibility of hybridization sites on the immobilized DNA. Since a hydrogel can uniformly load the DNA sensing material within the three-dimensional matrix, the probe is unlikely to encounter diffusional restrictions and an evenly distributed fluorescence signal can be generated upon hybridization within the hydrogel microenvironment.[250]

Hydrogel-based interfaces have been widely investigated in DNA microarray development. For example, Le Goff et al. fabricated a DNA hydrogel microarray by covalently immobilizing aminated oligonucleotides in a poly(dimethylacrylamide) hydrogel deposited on a shrinkable polystyrene based substrate[251]. High signal increases were observed when samples containing low target analyte concentrations were applied to the microarray, demonstrating that the hydrogel network can facilitate enhanced diffusion of target DNA probe. Soto et al. developed a DNA microarray constructed with a sugar polyacrylate-based hydrogel film cast onto an aldehyde functionalized glass slides.[252] An acrylated galactopyranoside monomer was polymerized with *N*-(3-aminopropyl)methacrylamide and cross-linked via N,N'-methylenebisacrylamide into a hydrogel film, after which the amine-terminated oligonucleotides were covalently attached to the amine functionalized carbohydrate network via bis(sulfosuccinimidyl)suberate, an amine-to-amine homobifunctional cross-linker. Target DNA was able to diffuse through the hydrogel film and successfully hybridize with the immobilized

oligonucleotides. However, neither these examples nor other reported hydrogel-based microarrays offer the combined advantages of being fabricable using facile methods while also exhibiting enhanced hybridization kinetics, low background signal and high assay sensitivity[253, 254, 255].

The printable hydrogel microarray platform described in Chapters 3 and 4 demonstrated the capacity of *in situ*-gelling hydrogels to immobilize and stabilize enzymes, offering distinct advantages in a drug screening application. Building on that promise, in this Chapter, we investigate this hydrogel platform in the context of DNA hybridization detection. In addition to exhibiting the advantages conferred by hydrogel-based microarrays, the printable hydrogel platform should increase the specificity of this assay by reducing the likelihood of non-specific adsorption/absorption interactions. The poly(oligoethylene glycol methacrylate) (PO) based hydrogel is designed to demonstrate the characteristic protein and cell-repulsive behaviours exhibited by poly(oligoethylene glycol) (PEG)[106], which has been shown to specifically resist the non-specific adsorption of oligonucleotides in a previous demonstration of a PEG hydrogel-based DNA microarray.[256] In place of short oligonucleotide sequences, rolling circle amplification (RCA) product will be used as the sensing material in this microarray platform. RCA products are very long single-stranded DNA molecules generated from an isothermal amplification process[257] that are concatemeric (i.e. they consist of a specific sequence repeated many times in tandem)[258]. The concatemeric nature of the RCA product increases the likelihood of hybridization events and thus eliminates the need for signal amplification—a critical bottleneck for employing DNA microarrays in diagnostic applications[259].

5.2 Materials and Methods

Materials

Oligo(ethylene glycol) methyl ether methacrylate (OEGMA, M_n = 475 g/mol, Sigma Aldrich, 95%) and (diethylene glycol) methyl ether methacrylate ($M(EO)_2MA$, Sigma Aldrich, 98%) were purified on a column of basic aluminum oxide (Sigma Aldrich, type CG-20) to remove the inhibitors methyl ether hydroquinone (MEHQ) and butylated hydroxytoluene (BHT) respectively. N-(2,2-dimethoxyethyl)methacrylamide (DMEMAm) was synthesized as previously reported[106]. Acrylic acid (AA, Sigma Aldrich, 99%), N,N-dimethylaminoethyl

methacrylate (DMAEMA, Sigma Aldrich, 98%), thioglycolic acid (TGA, Sigma Aldrich, 98%), 2,2-azobisisobutryic acid dimethyl ester (AIBMe, Wako Chemicals, 98.5%), adipic acid dihydrazide (ADH, Alfa Aesar, 98%), N'-ethyl-N-(3-dimethylaminopropyl)-carbodiimide (EDC, Carbosynth, Compton CA, commercial grade), aminoacetaldehyde dimethyl acetal (Sigma Aldrich, 99%), 2,2,6,6-tetramethyl-1-piperidinyloxy (TEMPO, Sigma Aldrich, 98%), methacryloyl chloride (Sigma Aldrich, purum), glycerol (Sigma Aldrich, ≥99%), streptavidin coated microspheres (1.4 w/v%, Polysciences, Inc.), biotin-4-fluorescein (ThermoFisher, 96%), and Hi-Flow plus cellulose ester membranes (EMD Millipore, HF12002XSS) were all used as received. All DNA oligonucleotides were obtained from Integrated DNA Technologies (IDT) and purified by standard 10% denaturing (8 M urea) polyacrylamide gel electrophoresis (dPAGE) or high-performance liquid chromatography (HPLC). Ulysis™ Alexa Fluor™ 647 Nucleic Acid Labeling Kit, T4 polynucleotide kinase (PNK), T4 DNA ligase, ATP solution, dNTP mix, phi29 DNA polymerase (ϕ29DP), Denhardt's Solution (50x), UltraPure™ Salmon Sperm DNA Solution and SYBR Gold (10,000x concentrated stock in DMSO) were all purchased from ThermoFisher Scientific. For all experiments, Milli-Q grade distilled deionized water (DIW) was used. Phosphate buffered saline (PBS) and saline-sodium citrate (SSC) were diluted from a 10x liquid concentrate and 20x liquid concentrate, respectively (Bioshop Canada Inc.).

Preparation of circular DNA template

Circular DNA template (CDT, Table 5.1) was synthesized through template-assisted ligation using T4 DNA ligase. To introduce a 5' phosphate to the linear precursor of the circular DNA template (LDT, Table 5.1), a total of 500 pmol LDT was first mixed with 30 U PNK, 2.5 mM ATP, and 20 µL of 10x PNK buffer in a total volume of 200 µL. The mixture was then incubated at 37°C for 20 min, followed by heating at 90°C for 5 min. The 200 µL reaction mixture was subsequently divided into 50 µL aliquots. Into each aliquot, 250 pmol of DNA template primer (TP, Table 5.1) was added, heated at 90°C for 5 min, cooled down, and left at room temperature for 20 min. Following, 80 µL of 5x T4 DNA ligase buffer and 10 U T4 DNA ligase were added to each aliquot. The reaction mixture (total 400 µL) was incubated under ambient conditions for 2 h, followed by heating at 90°C for 5 min to deactivate the ligase. The

ligated circular DNA product was concentrated by standard ethanol precipitation and purified by 10% dPAGE.

Table 5.1 Sequences of DNA oligonucleotides used to synthesize RCA and detect DNA hybridization

Name of DNA oligonucleotide	Sequence (5`-3`)
Linear precursor of circular DNA template (CDT) LDT (60 nt)	GAT CGT AGA CAA GAT GAT ACA GCA TTG AAG TCG AGG GTG TAT GAT GTG GTA AAG TAA GTG
DNA template primer TP (24 nt)	TT GTC TAC GAT CCA CTT ACT TT AC
DNA probes DP1 (FAM labeled at 5` end) DP2 (FAM labeled at 5` end; 18-atom hexa-ethyleneglycol labeled at 3` end)	AAAGTAAGTGGATCGTAGAC AAAGTAAGTGGATCGTAGAC

RCA reaction

The RCA reaction was carried out with 11.25 pmol of CDT (Table 5.1) and 10 pmol of TP (Table 5.1) in autoclaved deionized water (100 μL total volume). The mixture was heated at 90 °C for 1 min and then cooled to room temperature. 10 μL of 10x ϕ29 polymerase buffer, 5 μL of 10 mM dNTP mix, and 10 U of ϕ29 polymerase were added to the reaction mixture and allowed to incubate at 30 °C for 1 h. Subsequently, the reaction was heated at 90 °C for 5 min to deactivate the enzyme. The RCA reaction mixture was then diluted 5-fold in water and purified by centrifugation using a 100 kDa Nanosep® spin column. The quantity of RCA product synthesized was approximated by assuming 100% conversion of TP into the equivalent amount of RCA product molecules.[258] This assumption is based on the fact that the synthesis of each RCA product molecule is initiated by the extension of the template primer.

Synthesis of poly(oligoethylene glycol methacrylate) polymers

Unfunctionalized poly(oligoethylene glycol methacrylate) (PO) was prepared by adding AIBMe (50 mg, 0.22 mmol), $OEGMA_{475}$ (0.90 g, 1.9 mmol), $M(EO)_2MA$ (3.1g, 16.5 mmol) and TGA (7.5 μL, 0.15 mmol) to a 50 mL Schlenk flask. 1,4-Dioxane (20 mL) was added, and the solution was purged with nitrogen for 30 minutes. The flask was sealed and submerged in a pre-heated oil bath at 75°C for 4 hours under magnetic stirring. After polymerization, the solvent was removed

by rotary evaporation, and the poly($OEGMA_{475}$-co-$M(EO)_2MA$) polymer was purified by dialysis against DIW for 6 cycles (6 hours/cycle) and lyophilized to dryness. The polymer was dissolved in 10 mM PBS at 20 w/w% and stored at 4°C.

Aldehyde-functionalized poly(oligoethylene glycol methacrylate) (POA) was prepared similarly to the unfunctionalized PO polymer above except for the addition of DMEMAm (0.63 g, 3.61 mmol, 15 mol%). Following solvent removal, the acetal groups of the DMEMAm residues were converted to aldehydes via hydrolysis by dissolving the copolymer in 100 mL of 0.25 M HCl and stirring at 300 rpm for 24 hours. The polymer was purified by dialysis against DIW and lyophilized to dryness. POA was dissolved in 10 mM PBS at 20 w/w% and stored at 4°C. The number-average molecular weight was determined to be 14 kDa ($Đ$ = 2.03) from size exclusion chromatography. The aldehyde content was determined to be 12 mol% using ^{1}H-NMR by comparing the integration of the proton signals of the methoxy (O-CH_3, 3H, δ = 3.3 ppm) and aldehyde (CHO, 1H, δ = 9.2 ppm) groups.

Hydrazide-functionalized poly(oligoethylene glycol methacrylate) (POH) was prepared by adding AIBMe (37 mg, 0.16 mmol), $OEGMA_{475}$ (0.90 g, 1.9 mmol), $M(EO)_2MA$ (3.1g, 16.5 mmol), AA (0.55 g, 7.6mmol), and TGA (7.5 μL, 0.15 mmol) to a 50 mL Schlenk flask. Cationic hydrazide-functionalized PO polymer (POH^+) was synthesized using a modified version of this recipe in which the monomer DMAEMA (1.2g, 7.6 mmol, 21 mol%) was also added and the quantity of AA (0.75 g, 10.4 mmol) was increased in order to maintain 30 mol% of AA functional groups, with all other recipe quantities remaining the same Polymerization proceeded similarly to that of PO and POA. Following solvent removal, the copolymer was dissolved in 100 mL DIW. ADH (4.33g, 24.8 mmol, 8.16 mol eq.) was added, and the pH of the solution was adjusted to 4.75. The reaction was initiated by the addition of EDC (1.93 g, 12.4 mmol, 3.80 mol eq.), after which the pH was maintained at 4.75 by the dropwise addition of 0.1 M HCl over 4 hours. The solution was left to stir overnight, dialyzed against DIW over 6 cycles (6 hours/cycle), and lyophilized to dryness. The polymer was dissolved in 10 mM PBS at 20 w/w% and stored at 4°C. The number-average molecular weight was determined using size exclusion chromatography. The degree of hydrazide functionalization was determined by conductometric base-into-acid titration, comparing the carboxylic acid content before and after ADH conjugation

(0.1 M NaOH titrant, 50 mg polymer in 50 mg of 1 mM NaCl titration solution, ManTech automatic titrator). The physical properties of both the neutral and cationic POH polymers produced are listed in Table 5.2.

Table 5.2 Molecular weights and degrees of hydrazide functionalization of hydrazide-functionalized PO polymers

Hydrazide-functionalized PO polymer	Number average molecular weight (M_n, kDa)	Degree of hydrazide-functionalized (mol%)
POH	17 kDa, ($Đ$=2.08)	22 mol%
POH^+	41.3 kDa ($Đ$=2.4)	29 mol%

Printed hydrogel-based RCA microarray

A nitrocellulose microzone plate was fabricated by printing hydrophobic wax barriers onto a nitrocellulose membrane (EMD Millipore) using a Xerox ColorQube 8570N solid wax printer using a 96 well-plate template (3 mm diameter wells, ~9 mm inter-well distance). The wax-printed paper was placed into an oven at 120 °C for 2 minutes to melt the wax through the paper. Polymer inks comprised of 6 w/w% aldehyde-functionalized poly(oligoethylene glycol methacrylate) (POA), hydrazide-functionalized poly(oligoethylene glycol methacrylate) (POH) or cationic hydrazide-functionalized poly(oligoethylene glycol methacrylate) (POH^+) were prepared in 10 mM PBS containing 5 w/w% glycerol as a humectant and viscosity modifier, with the POH and POH^+ ink solutions optionally containing purified RCA product at a concentration of 0.015 μM. A BioJet HR™ non-contact solenoid dispenser was used to sequentially print the inks on the paper microzones. The two reagent lines were charged with POA and POH or POH^+ (prepared with or without RCA product) respectively, the dispenser valve was programmed to stay open for 6 ms, and the frequency was set to 100 Hz. The hydrogel layer was fabricated by dispensing 2 μL POA onto the microzone, immediately followed by 2 μL POH. The samples were dried and stored at room temperature.

RCA product immobilization assay

RCA product was printed in a hydrogel microarray at a density of 0.05 pmol/microzone. The hydrogel-entrapped RCA product samples were dried for 3 hours and washed in 1x PBST containing 0.05% Tween-20 by shaking the samples at 300 rpm on an IKA MS3 Basic Shaker for 10 minutes. The washed samples were stained in 0.8% SYBR Gold in 1x TAE buffer for 2 hours, followed by de-staining in 1x PBST for 2 hours. The samples were imaged through the SYBR Gold channel of the ChemiDoc™ MP System (BioRad). Image processing was performed using Image Lab™ software (BioRad).

RCA product printing reproducibility assay

RCA product was labeled with Alexa Fluor 647 according to the manufacturer's instructions (Ulysis™ Alexa Fluor™ 647 Nucleic Acid Labeling Kit, ThermoFisher Scientific). Alexa Fluor 647-labeled RCA product was purified via centrifugation using a 100 kDa Nanosep® spin column. RCA product was printed in a hydrogel microarray at a density of 0.002 pmol/microzone. The hydrogel-entrapped RCA product array was dried for 3 hours and washed in 1x PBST containing 0.05% Tween-20 by shaking at 300 rpm for 10 minutes. The samples were imaged through the Alexa Fluor 647 channel of the ChemiDoc™ MP System (BioRad). Image processing was performed using Image Lab™ software (BioRad).

Solution-based hybridization assay

An RCA reaction was performed in 100 μL of autoclaved deionized water with 2 pmol of TP (Table 5.1), resulting in the synthesis of ~2 pmol of RCA product (assuming 100% conversion). Next, twelve 5 μL aliquots of the RCA reaction were separated into individual microcentrifuge tubes, resulting in ~0.1 pmol of RCA product in each aliquot. The RCA aliquots were diluted with 1x PBS to a total volume of 10 μL. 1 μL of fluorescein-labeled DNA probe was added to the aliquots in the amounts listed in Table 5.3^{260}. The aliquots were heated at 90 °C for 1 minute, cooled to room temperature for 10 minutes to allow DNA hybridization to occur, and analyzed by 3% agarose gel.

Developing a printed hydrogel-based hybridization assay

RCA product was printed in a hydrogel microarray. DNA probe solutions were prepared in three hybridization buffers: i) 1x PBS; ii) 5x SSC; iii) 6x SSC with the addition of 5x Denhardt's solution, 0.1 mg/mL salmon sperm DNA, 0.3% Tween-20. 5 µL of each DNA probe solution (amounts listed in Table 5.3) were added to each microzone. The DNA probe solutions were incubated with the printed RCA product for 30 minutes or 2 hours under ambient conditions. For the 2 hour incubation period, the printed hydrogels were pre-hydrated in 1x PBS or 6x SSC and stored in a humidity chamber. The microarrays were washed in three wash buffers: i) 1x PBST containing 0.05% Tween-20 for 30 min; ii) 1x SSC containing 0.05% Tween-20 for 1 hour; iii) 2x SSC containing 0.3% Tween-20 for 1 hour. The microarrays were imaged through the fluorescein channel of the ChemiDoc™ MP System (BioRad). Image processing was performed using Image Lab™ software (BioRad).

Hydrogel-based hybridization assay with a DNA probe conjugated to a polystyrene bead

RCA product was printed in a hydrogel microarray. 500 µL of a 1.4 w/v% suspension of streptavidin-coated polystyrene microspheres was diluted in 500 µL of 1x PBS. The beads were washed by centrifuging the suspension at 10,000 x *g* for 5 min, discarding the supernatant, and re-suspending the bead pellet in fresh 1x PBS buffer. Two additional wash steps were performed, after which the bead pellet was re-suspended in 1 mL of PBS/BSA binding buffer (consisting of 100 mL of 20 mM phosphate buffer (pH=7.4), 0.88 g NaCl, and 1 g BSA). To conjugate the DNA probe to the polystyrene beads, 0.67 mg of biotinylated DNA probe was added to the bead suspension in the PBS/BSA binding buffer and incubated at 4°C for 1 hour. The beads were washed three times via centrifugation and re-suspended in the PBS/binding buffer. DNA probe/bead suspensions were prepared in PBS/BSA binding buffer at concentrations corresponding to the DNA probe amounts listed in Table 5.3 (assuming that 100% of the biotinylated DNA probe was conjugated onto the microspheres). The printed hydrogels were pre-hydrated in 1x PBS and stored in a humidity chamber. 5 µL of each DNA probe/bead suspension (amounts listed in Table 5.3) were added to each microzone. The DNA probe/bead suspension was incubated with the printed RCA product for 2 hours in a humidity chamber. The microarray was washed in 1x PBST containing 0.05% Tween-20 for 1 hour. In order to visualize the hybridized DNA/probe beads, the microarray was stained in a 0.02%

solution of biotin-4-fluorescein for 20 minutes and de-stained in 1x PBST for 2 hours. The microarrays were imaged through the fluorescein channel of the ChemiDoc™ MP System (BioRad). Image processing was performed using Image Lab™ software (BioRad).

Table 5.3 DNA probe amounts used in solution-based and printed hydrogel-based hybridization assays

Microzone	DNA probe amount (pmol)
1	0.1
2	0.5
3	1
4	2
5	6
6	8
7	10
8	12
9	16
10	18
11	25
12	30

5.3 Results and Discussion

Entrapping RCA product in the printed hydrogel

The printed hydrogel can entrap RCA product and effectively immobilize it on the nitrocellulose surface. POH ink solutions were prepared with RCA product and subsequently layer-by-layer printed with POA, using POA as the base ink. RCA product remained entrapped in the cross-linked polymer assembly even following vigorous washing of the samples (Fig.5.1, POA+(POH+RCA)), while RCA product printed in non-gelling ink (PO+(POH+RCA)), with only POH-containing ink (i.e. no cross-linker, POH+RCA), or alone with no hydrogel components (RCA) could be either partially or completely removed from the surface.

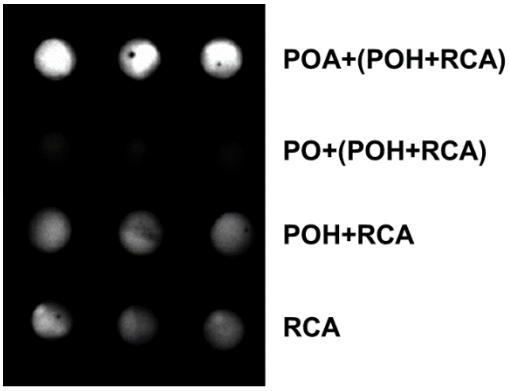

Fig.5.1 Printed hydrogels can immobilize RCA product Retention of fluorescently-labeled RCA product when printed in hydrogel (POA+(POH+RCA)), non-gelling ink (PO+(POH+RCA)), with POH polymer only (POH+RCA) or without any polymer/hydrogel (RCA) following washing in 1x PBST containing 0.05% Tween 20 and staining in 0.8% SYBR Gold solution. The high retained fluorescence signal in the POA+(POH+RCA) samples validates the printable gelling inks as a method for RCA product immobilization. The three adjacent images in each series are replicates, confirming the reproducibility of the result.

Reproducible printing of RCA product entrapped in the hydrogel

The reproducibility of RCA product printing and immobilization was investigated in order to evaluate whether the hydrogel-entrapped RCA product may be useful in microarray hybridization assays. RCA product was labeled with Alexa Fluor 647 and printed in the hydrogel on a multi-well nitrocellulose substrate and the fluorescence intensity of each printed microzone was measured (Fig.5.2a). The coefficient of variation (CV) across all printed microzones was 5.8%, demonstrating that the deposition of RCA product on the multi-well array was uniform. The printed multi-well substrate was vigorously washed in 1x PBST containing 0.05% Tween-20, and the percentage of retained fluorescence was quantified for each microzone (Fig.5.2b). On average, 92±5.3% of the fluorescence was retained in each microzone, indicating that the printed RCA product can be consistently and reproducibly immobilized on the multi-well substrate. It is important to note however that modifying the RCA product with Alexa Fluor 647 likely induces some degree of RCA aggregation due to the hydrophobic nature of the dye. Thus, labeling the RCA product with Alexa Fluor 647 is not suitable for experiments investigating the hybridization capacity of the product, as the dye may promote a collapsed conformation.

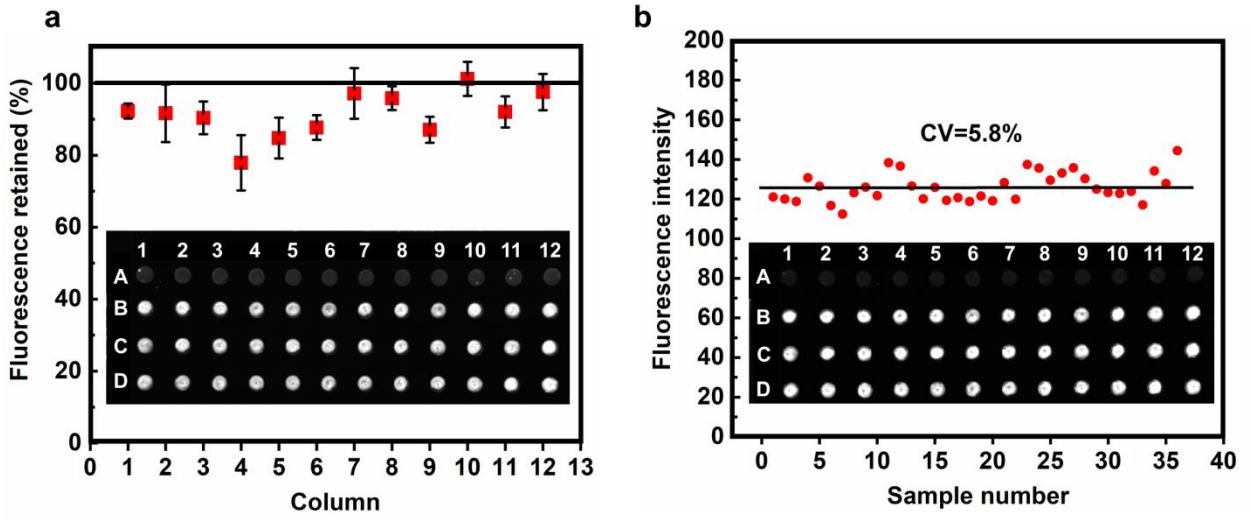

Fig.5.2 RCA product can be reproducibly printed in a hydrogel on a multi-sample array
Alexa Fluor-labeled RCA product was printed in hydrogel on a multi-well nitrocellulose wax printed template. **(a)** The uniform fluorescence signal across the multi-sample substrate (rows B-D) demonstrates the reproducibility of the RCA product printed microzones. Microzones in row A are printed with hydrogel alone. Microzone B1 refers to sample 1, B2 refers to sample 2, etc. Microzones 1 through 12 in each row are replicates. The CV value is the coefficient of variation amongst the samples. **(b)** The multi-sample substrate was washed in 1x PBST containing 0.05% Tween-20. The fluorescence retained across the microzones indicates that the printable gelling inks can consistently immobilize RCA product. Microzones in row A are printed with hydrogel alone. Microzones B1, C1, and D1 refer to column 1, B2, C2 and D2 refer to column 2, etc. Values are represented as mean ± standard deviation (n=3).

Solution-based RCA product hybridization assay

Given the demonstrated capacity to print uniform concentrations of immobilized RCA product in the hydrogel, the utility of RCA product as a substrate for DNA hybridization sensing was next investigated. A fluorescently labeled complementary DNA probe was titrated into a fixed amount of RCA product (0.1 pmol). Following a 10 minute incubation period, the hybridization mixture was run on a 3% agarose gel, and the fluorescence intensities of the hybridized RCA product complexes were quantified (Fig.5.3a). The hybridization titration curve indicates that the accessible binding sites on the RCA product are saturated with 15 pmol of DNA probe (Fig. 5.3b). The titration analysis confirms that RCA product can hybridize with the DNA probe efficiently in solution.

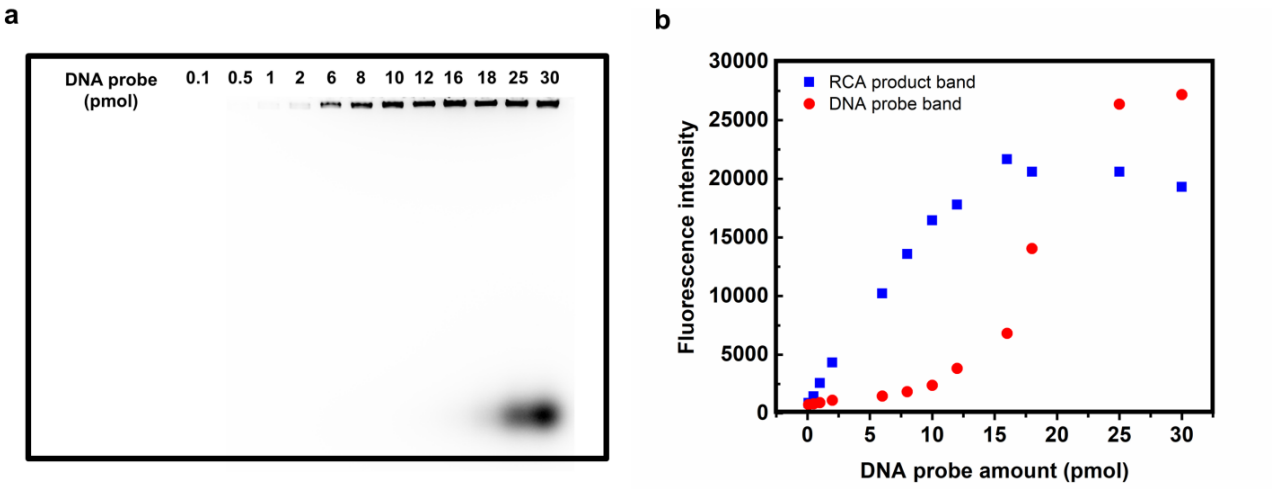

Fig.5.3 RCA product hybridizes with DNA probe in solution **(a)** A 3% agarose gel image of the RCA product mixed with increasing amounts of DNA probe (from 0.1 pmol to 30 pmol). The upper bands represent the RCA product hybridized to the DNA probe, while the lower bands represent any free, unhybridized DNA probe. **(b)** Fluorescence intensities of the RCA product band and the DNA probe band as a function of DNA probe concentration. The RCA product band intensity levels off at ~15 pmol, indicating that 15 pmol of probe saturates the accessible hybridization sites on the RCA product.

Developing a printed hydrogel-based hybridization assay

The printed hydrogel-based microarray was tested for its ability to discriminate specific hybridization events. Modifications to the solution-based hybridization protocol were made to account for limitations associated with solid-phase assays, namely the restricted diffusion of DNA probe[261]. First, to address the mass transport differences between solution and solid-phase hybridization reactions, the incubation period of printed RCA product with the DNA probe was extended to 30 minutes. Hybridization reactions in both hydrogel and planar microarrays encounter diffusional restrictions that can be attributed to the hydrogel barrier in gel-based arrays or the molecular crowding imposed by the high density of immobilized oligonucleotides in most 2-dimensional arrays[247]. Coupled with the lack of convective mixing, these diffusional constraints impair hybridization between the immobilized sensing material and the applied DNA probe and thus demand longer incubation times. For example, traditional 2-dimensional microarrays are typically incubated with DNA probe solutions for time periods ranging from 2-18 hours[262, 263] Intermediate incubation times can be effective for hydrogel-based microarrays since the hydrogel microenvironment can support hybridization kinetics similar to solution-based

systems and the entrapped oligonucleotides are less densely packed in the gel matrix, eliminating potential steric issues.[247] Second, to minimize any potential non-specific interactions between the DNA probe and the hydrogel interface, a DNA probe modified with a PEG spacer group was assessed.

RCA product was printed in a PO-based hydrogel formed from 6 wt% reactive polymer precursors. Incubation of the unmodified DNA probe results in a high background signal in the hydrogel-only control samples and inconsistent fluorescence signals with the hydrogel-entrapped RCA product (Fig.5.4a). Although more consistent fluorescence signals were observed from hybridization assays performed with the PEG modified DNA probe, the high background signal remains visible in the hydrogel control (Fig.5.4b), suggesting that the PEG spacer group was unable to reduce the indiscriminate adsorption of the modified DNA probe onto the PO-based hydrogel. Indeed, in both experiments, the fluorescence signal from the hydrogel controls exceeds those generated from the RCA product microzones. In view of this high background signal, we cannot determine whether hybridization is occurring between the hydrogel-entrapped RCA product and the DNA probe based on these experiments.

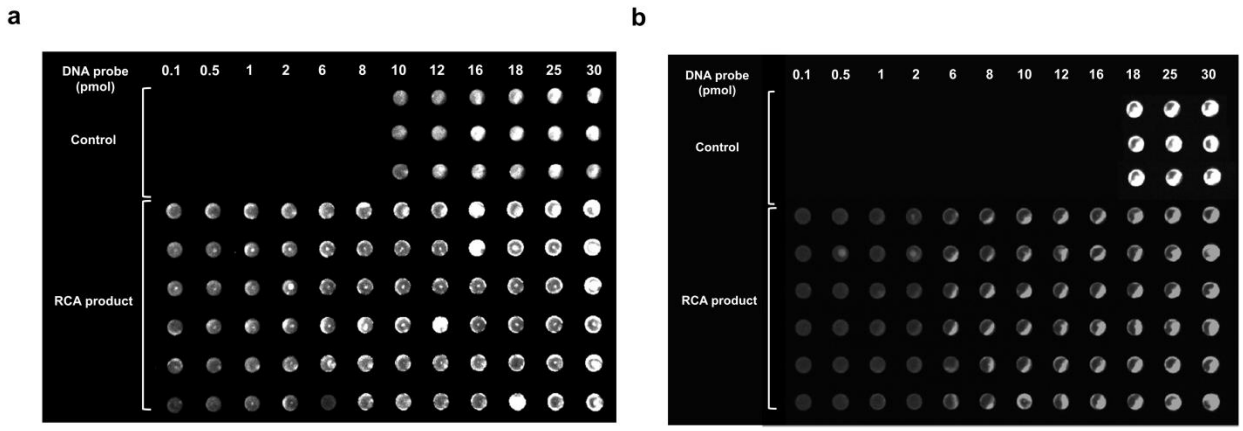

Fig.5.4 Printed hydrogel-based hybridization assays exhibit high background signals RCA product was printed in a hydrogel microarray at a density of 0.1 pmol/microzone. DNA probe solutions were prepared in 1x PBS and incubated with printed RCA product for 30 min under ambient conditions. The microarrays were washed in 1x PBST containing 0.05% Tween-20 for 30 min. **(a)** Hybridization with unmodified DNA probe to both control (non-RCA product containing) hydrogels and RCA product printed hydrogels. Controls were run for DNA probe solutions containing probe amounts ranging from 10 pmol to 30 pmol. **(b)** Hybridization with DNA probe modified with a PEG linker group to both control (non-RCA product containing) hydrogels and RCA product printed hydrogels. Controls were run for DNA probe solutions containing probe amounts ranging from 18 pmol to 30 pmol. In both cases, high background fluorescence is observed in the control microwells that exceeds the signal from the RCA product-printed microwells that have the capacity for specific hybridization.

To attempt to suppress this background signal, we next examined different hydrogel film thicknesses and cross-link densities and their effects on fluorescence signals associated with the hybridization reactions and background hydrogel interactions. In the following assays, the RCA product density was reduced from 0.1 pmol/microzone to 0.05 or 0.03 pmol/microzone. Since the signal is saturated when higher probe concentrations are applied to the microzones, reducing the concentration of RCA product was hypothesized to allow for the detection of a broad range of DNA probe concentrations. Exploiting this advantage of the platform can significantly reduce the amounts of valuable reagents used in the fabrication of this assay.

Three potential solutions to the background challenge were tested. First, RCA product was printed in a double-hydrogel assembly, in which a hydrogel layer containing RCA product was

printed on top of a dried printed hydrogel layer (Fig.5.5a). This assembly was tested to assess if bare or accessible locations on the nitrocellulose paper were causing challenges with non-specific adsorption. Second, RCA product was printed in a hydrogel formed from 5 wt% reactive polymers precursors (Fig.5.5b). This represents a reduction from the 6 wt% reactive polymer precursors used for the previous experiments and was hypothesized to result in both a thinner and a less highly cross-linked hydrogel. Third, hydrogels were prepared by printing the POH+RCA reactive layer on top of a dried POA reactive layer (Fig.5.5c). The POH+RCA reactive layer should re-hydrate the dried POA foundational layer and initiate the formation of hydrazone cross-links, albeit more slowly and inefficiently. Based on these protocols, there is a net reduction in hydrogel layer thickness. Maximum hydrogel thickness is illustrated in Fig. 5a, intermediate hydrogel thickness is illustrated in Fig. 5b and minimal hydrogel thickness is illustrated in Fig. 5c. (Fig.5.5a-c).

The highest background fluorescence signals were observed in the double hydrogel configuration (Fig.5.5a), with the fluorescence signals generated from the hydrogel controls observed to decline with the reduction of hydrogel layer thickness and cross-link density (Fig.5.5a-c). It should be noted that the lack of fluorescence signal observed in the control hydrogel and RCA microzones in Fig.5.5c is likely due to the absence of a minimum number of cross-links between the deposited polymer layers, causing the polymer assembly (and the entrapped RCA product) to be removed from the substrate during the washing step of the assay. To test this hypothesis, Alexa-Fluor labeled RCA was mixed with POH and printed on top of a dried POA foundational layer. The printed multi-sample array was washed in 1x PBST and the loss of fluorescence across the microzones was quantified. On average, a 37±4.0% reduction in fluorescence was observed, demonstrating that this printed hydrogel configuration is weakly cross-linked and cannot efficiently entrap the RCA product (Appendix, Fig.5A1). With all three approaches, fluorescence signals from the control hydrogel still exceeded those generated from the RCA product microzones, leaving the question of whether hybridization is occurring between the RCA product and DNA probe unresolved. That being said, these results do suggest that a hydrogel assembly with a reduced thickness and cross-link density may help mitigate background signals originating from the non-specific adsorption of oligonucleotides onto the hydrogel film. The remaining hybridization assays were thus performed using printed hydrogels fabricated from 5 wt% precursor polymer solutions that resulted in lower non-specific probe binding.

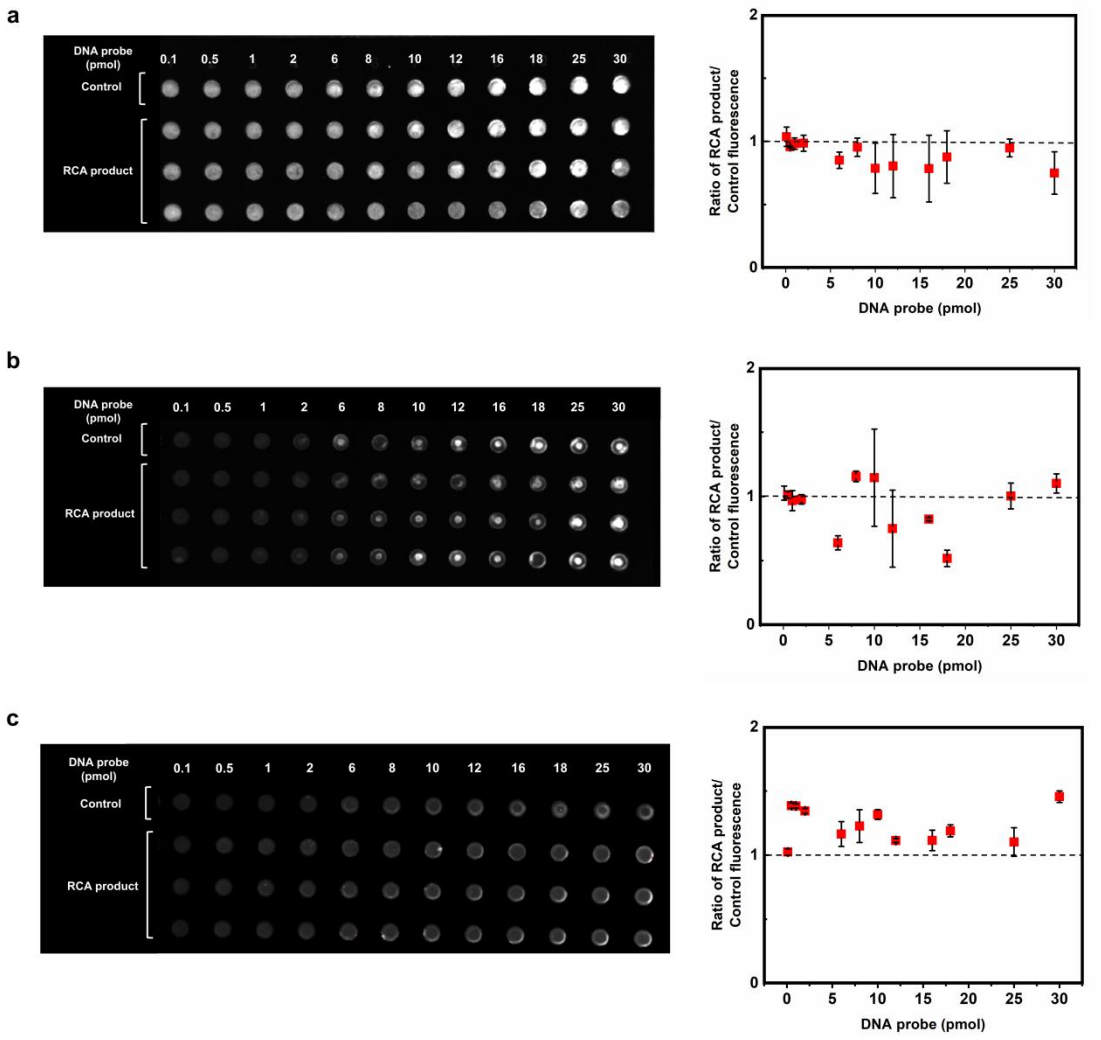

Fig.5.5 Reducing hydrogel thickness reduces non-specific background in the printed hydrogel-based hybridization assay RCA product was printed in a hydrogel microarray at a density of 0.05 pmol/microzone. DNA probe solutions were prepared in 1x PBS and incubated with printed RCA product for 30 min under ambient conditions. Hybridization was performed with DNA probe to both control (non-RCA product containing) hydrogels and RCA product printed hydrogels. The microarrays were washed in 1x PBST containing 0.05% Tween-20 for 30 min. **(a)** RCA product was printed in a double-hydrogel assembly in which a POA/POH hydrogel containing RCA product was printed on top of a dried printed POA/POH hydrogel. **(b)** RCA product was printed in a hydrogel with a reduced cross-link density. Hydrogels were printed with 5 wt% reactive polymers. **(c)** RCA product was printed in a hydrogel with a reduced layer thickness. Hydrogels were prepared by printing the POH+RCA reactive layer on top of a dried POA reactive layer. The ratios of RCA product to control fluorescence signals were plotted on the right of each figure. Values represent means ± standard deviations (n=3).

The unfavourable signal-to-background ratios in this assay may also imply the absence of DNA probe hybridization with the hydrogel-entrapped RCA product. There are two contributing factors that are likely hindering DNA hybridization in the hydrogel-based microarray. First, the assay conditions applied in the hydrogel-based microarray may not be conducive to DNA hybridization. Hybridization conditions have been optimized for solid-phase platforms like Southern blots and DNA microarray technologies.[263, 264, 265] Although there are many aspects that influence DNA hybridization, the specific factors that were investigated in this assay were salt concentration in the hybridization buffer (using 5x SSC buffer for hybridization), the introduction of humid conditions (achieved by pre-incubating the printed hydrogels in 1x PBS), and the increase in the incubation time with the DNA probe (from 30 min. to 2 hours). DNA probe is able to hybridize to the RCA product when it is directly printed onto nitrocellulose in the near absence of a background fluorescence signal (Fig.5.6a). However, the fluorescence signals generated in the RCA-only printed microzones are non-uniform and do not clearly scale with DNA probe concentration. In contrast, significant background noise and inconsistent fluorescence signals are generated from hydrogel-entrapped RCA product that has been incubated with the DNA probe (Fig.5.6b). In the assay containing RCA product alone, an increased availability of DNA binding sites is likely due to the electrostatic interactions between the positively charged nitrocellulose substrate and the negatively charged RCA product. These results suggest that the conformation of the hydrogel-entrapped RCA product may not be conducive to successful hybridization events, in spite of the optimized hybridization conditions (increased humidity, salt concentration and DNA probe incubation time) introduced to this assay.

Second, the polymer-dispersed RCA product may adopt a collapsed morphology within the hydrogel that does not promote the accessibility of DNA binding sites. The aggregative tendency of RCA products has been previously reported and is largely attributed to its size.[260] To address this, RCA product was prepared in a solution of POH polymer copolymerized with cationic functional groups (POH^+). Since DNA is negatively charged, dispersing the RCA product in a positively charged matrix should encourage the RCA product to adopt an extended conformation (and avoid self-collapse) by supporting favourable electrostatic interactions. Following incubation with the DNA probe, inconsistent fluorescence signals were generated from sample microzones printed with a POH^+ + RCA mixture (without POA addition), indicating the absence of hybridization (Fig.5.6c). Given the almost negligible background

fluorescence and the fact that the printed POH+RCA assembly is not efficiently retained on the nitrocellulose surface (Fig.5.1), it is likely that the POH^+ + RCA mixture is washed off of the substrate during the wash step of the assay. In contrast, RCA product entrapped in a printed hydrogel formed with POH^+ generates significantly more consistent and uniform fluorescence signals upon incubation with the DNA probe, although the presence of significant background signals obscures the incidence of successful hybridization events (Fig.5.6d). As such, these results indicate that the addition of POH^+ into the hydrogel system may be a promising step towards promoting DNA probe hybridization to the hydrogel-entrapped RCA product. However, the persistence of non-specific interactions between the DNA probe and the printed hydrogel interface warrants the inclusion of blocking agents into the hybridization buffer.

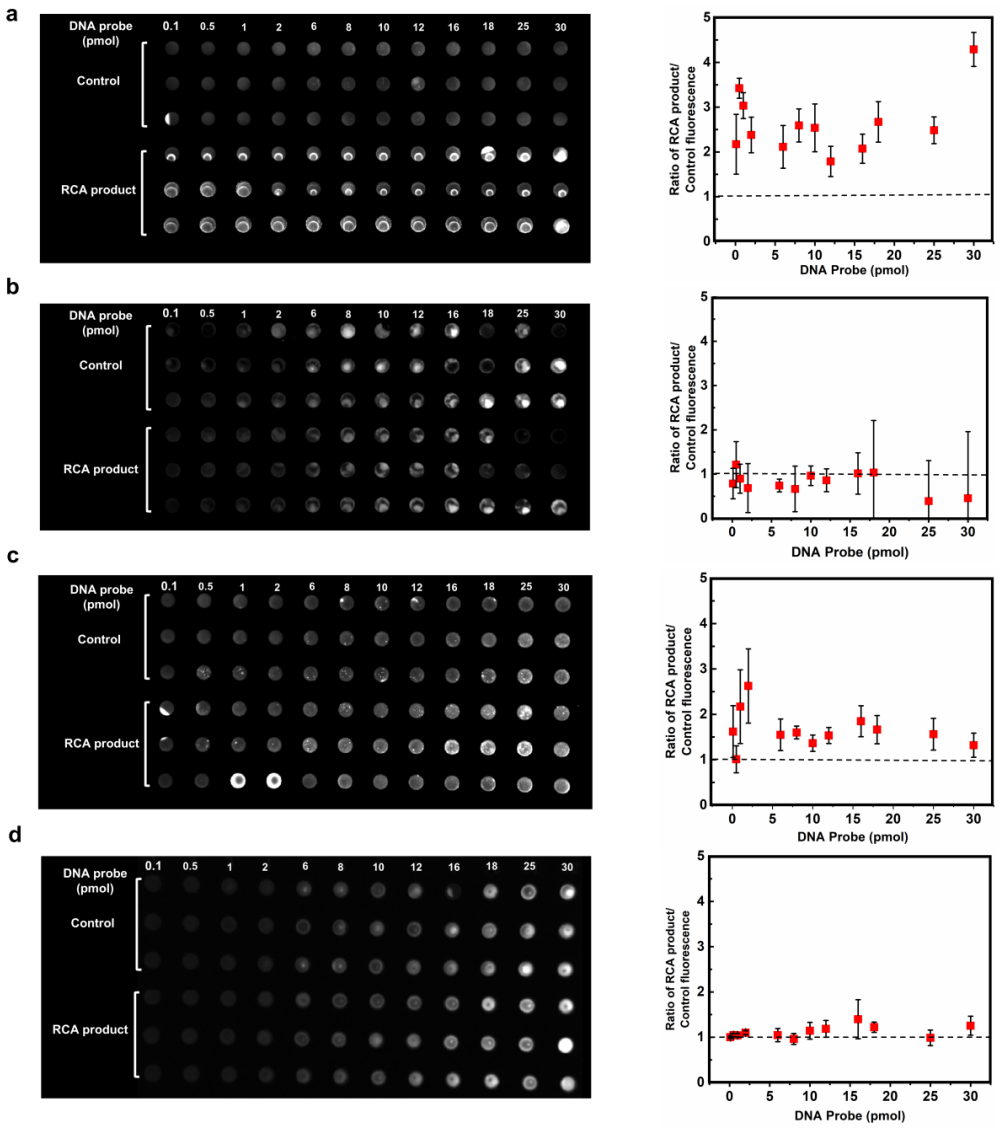

Fig.5.6 The effect of hydrogel charge and optimized DNA hybridization conditions on the printed hydrogel-based hybridization assays RCA product was printed in a microarray at a density of 0.03 pmol/microzone. DNA probe solutions were prepared in 5x SSC and incubated with printed RCA product entrapped in hydrogels pre-hydrated in 1x PBS, for 2 hours in a humidity chamber. Hybridization was performed with DNA probe to both control (non-RCA product containing) hydrogels and RCA product printed hydrogels. The microarrays were washed in 1x SSC containing 0.05% Tween-20 for 1 hour. **(a)** Control: 1x PBS only; RCA product: RCA product printed alone. **(b)** Control: POA/POH hydrogel printed alone; RCA product: RCA product printed in POA/POH hydrogel. **(c)** Control: Cationic POH (POH^+) printed alone; RCA product: POH^+ printed with RCA product. **(d)** Control: Cationic POA/POH^+ hydrogel printed alone; RCA product: RCA product printed in cationic POA/POH^+ hydrogel. The ratios of RCA product to control fluorescence signals were plotted on the right of each figure. Values are represented as mean ± standard deviation (n=3).

To further improve the signal:noise of the assay and suppress non-specific interactions between the DNA probe and the printed hydrogel interface, blocking agents were added into the hybridization buffer. Many commercial hybridization buffers include blocking agents such as salmon sperm DNA and Denhardt's solution, which contains a mixture of polymer-based blocking agents and bovine serum albumin. Both buffer components have been shown to significantly reduce the level of non-specific adsorption of DNA probes in microarray applications[262, 266]. The hybridization conditions applied in the previous set of assays were maintained, with the exception of pre-hydrating the printed hydrogel microarray with 6x SSC in place of 1x PBS; this alteration was made to be consistent with a previous report of in-gel DNA hybridization in which the agarose gel substrate was hydrated in 6x SSC buffer as an equilibration step prior to incubation with the hybridization probe solutions.[267]

Sample microzones printed with cationic hydrogel-entrapped RCA product generated a uniform and consistent signal in the presence of significant background fluorescence (Fig.5.7). Pre-hydration of the printed hydrogel microarray and the addition of blocking agents to the hybridization buffer did little to mitigate background fluorescence signal, suggesting that non-specific *absorption* rather than *adsorption* may be responsible for the low signal-to-background ratios. The non-specific absorption of fluorescently labeled DNA probes in hydrogel-based microarrays is consistent with the report of Xiao et al. with a polyacrylamide-based hydrogel microarray that also indiscriminately absorbed fluorescently labeled DNA probes that could not be displaced by vigorous washing steps[255] but only via the application of an electric field[268].

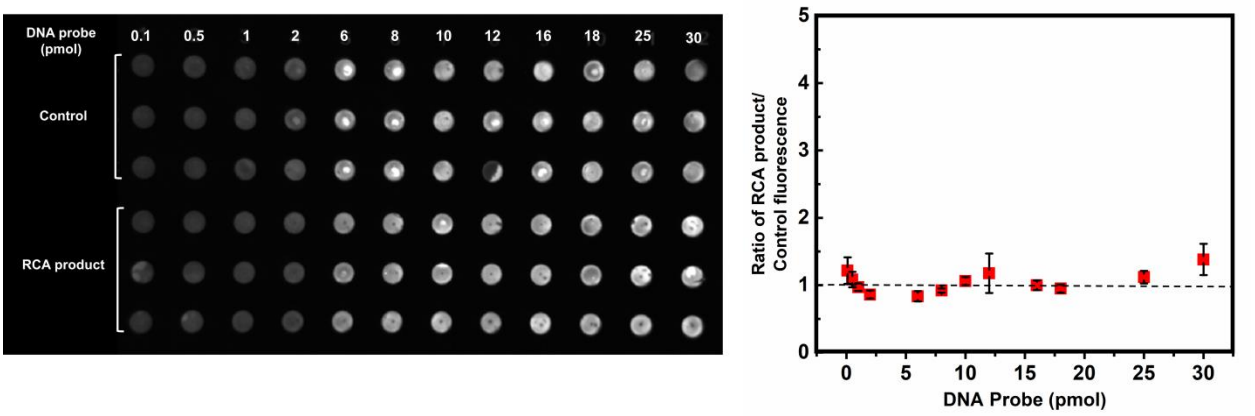

Fig.5.7 The effect of blocking agents on the printed cationic hydrogel-based hybridization assay RCA product was printed in a cationic hydrogel microarray at a density of 0.03 pmol/microzone. DNA probe solutions were prepared in 6x SSC (5x Denhardt's solution, 0.1 mg/mL salmon sperm DNA, 0.3% Tween-20) and incubated for 2 hours in a humidity chamber with printed RCA product entrapped in hydrogels pre-hydrated in 6x SSC. Hybridization was performed with DNA probe to both control (non-RCA product containing) hydrogels and RCA product printed hydrogels. The microarrays were washed in 2x SSC containing 0.3% Tween-20 for 1 hour. Control: Cationic POA/POH^+ hydrogel printed alone; RCA product: RCA product printed in cationic POA/POH^+ hydrogel. The ratios of RCA product to control fluorescence signals were plotted on the right. Values are represented as mean ± standard deviation (n=3).

To investigate whether absorption is responsible for the high background noise in this PO-based microarray system, hybridization was performed with a DNA probe conjugated to a large polystyrene bead (See Appendix, Fig.5A2). The DNA-bead complex has a size of ~6 µm, too large to penetrate the hydrogel interface to facilitate absorption with entrapped RCA product but still sterically available to hybridize with surface-available binding sites. A fluorescent signal was observed throughout both the control and RCA product printed microzones (See Appendix, Fig.5A2). This lack of signal specificity can be attributed to either the non-specific adsorption of the DNA probe/polystyrene bead complex or the biotin-4-fluorescein stain that was used to visualize the presence of the DNA probe/polystyrene bead.

Improving the signal to noise ratio of this assay requires addressing two different problems. The high background noise is likely due to some combination of non-specific adsorption/absorption of the target DNA probe, while the low signal noise can be attributed to the hindered dynamics of the DNA probe that has penetrated the hydrogel. Indeed, the persistence of an unfavourable signal-to-background ratio in this iteration of the assay suggests that the hydrogel itself may be

providing a diffusional barrier to the transport of the DNA probe into the hydrogel to interact with RCA binding sites. In the drug screening application of this printable hydrogel system (Chapter 4), we demonstrated that soluble drugs with molecular weights ranging from ~220 Da to ~320 Da were able to freely diffuse into the hydrogel matrix while insoluble drug aggregates encountered steric restrictions. Given that the size of the fluorescein labeled DNA probe (~6750 Da) is intermediate in size to the drugs and the drug aggregate, the DNA probe may be sufficiently small to enter into the hydrogel pores but too big to experience sufficient diffusional freedom within the printed hydrogel to exhibit effective hybridization. If aldehydes are problematic for limiting probe mobility, the addition of a small molecule thiol of a hydrazide (i.e. a molecule with a thiosemicarbazide functionality) could quench these remaining aldehyde moieties and block any probe-aldehyde interactions.

Collectively, the results of this study suggest that the current printable hydrogel platform must be adapted to fit the requirements of an RCA product-based hybridization assay in the following ways: increase the porosity to allow for the unrestricted diffusional mobility of the DNA probe, and introduce positive charges to the hydrogel matrix in order to promote an extended rather than collapsed RCA product conformation. There are examples of hydrogel-based microarrays that have been fabricated with highly porous hydrogel interfaces in order to facilitate the diffusion of a DNA probe[252, 269]. The porosity of the printable hydrogel can be increased while maintaining the physical entrapment of the RCA product since it is greater than 100 kDa, making the likelihood of leaching low. It is somewhat challenging to increase porosity of the printable hydrogel interface while preserving the minimal degree of cross-linking necessary to uphold the network structure. We determined that the minimum concentration of reactive polymer precursors that can be used to fabricate the printable hydrogel is 5 wt%. In addition to decreasing the polymer precursor concentration, the cross-linking density can also be reduced by lowering the proportions of the functional monomers (aldehyde and hydrazide groups) in the reactive polymer precursors.[270] Optimization of the polymer compositions will be necessary in order to achieve a suitable level of porosity that can accommodate the free diffusion of a 20 bp probe.

Hydrogel-based microarrays can be limited by high fluorescent background signals due to the non-specific absorption of fluorescent DNA probes into the hydrogel film and difficulty of removal through washing alone.[268] Introducing charged moieties to the constituent polymers can impart increased levels of hydrophilicity to the hydrogel network. Both the polarity and charge of these functional groups can increase water uptake in the hydrogel. In particular, the presence of charge promotes the accumulation of counterions, generating an osmotic driving force that pushes more water into the system. Although the addition of cationic charges to the PO-based hydrogel film did not mitigate the non-specific absorption of the DNA probe, the charged interface did help promote a more uniform and consistent fluorescence signal. On this basis, fabricating the printable hydrogel interface with zwitterionic PO-based reactive polymer precursors may confer the advantages of a charged hydrogel environment while incorporating the proven non-fouling capacity of zwitterionic materials.[272, 273] There is precedence for using zwitterionic based polymers for the fabrication of DNA hybridization assays[274, 275]; for example, a quartz crystal microbalance (QCM) based DNA sensing device composed of a zwitterionic hydrogel interface was able to resist the adsorption of noncomplementary oligonucleotides[276]. Introducing zwitterionic functionality to this system holds particular promise in addressing the limitations of the PO-based printable hydrogel interface and should render this platform readily translatable to a DNA hybridization assay.

5.4 Conclusion

The PO-based printable hydrogel described in Chapter 3 was used as a platform to develop a DNA hybridization microarray assay based on the concatameric sensing material, rolling circle amplification product. RCA product was successfully immobilized in the hydrogel on a nitrocellulose substrate and reproducibly printed onto the microzones. Hybridization was performed with a fluorescein-labelled DNA probe. Several assay iterations generated low signal-to-background ratios and the inability of the probe to hybridize to the RCA product due to conformational and diffusional restrictions. Introducing cationic charges to the hydrogel to encourage an elongated RCA product conformation, reducing the degree of hydrogel cross-linking, and the addition of hybridization buffers and blocking agents did little to suppress background noise and encourage hybridization to the sensing material, although cationic hydrogel charge showed some promise for enhancing hybridization potential. The results of this

study strongly suggest that the printable hydrogel platform must be adapted to fit the requirements of a DNA hybridization assay. Recommended changes include an increase in hydrogel porosity and water content as well as imparting an overall positive charge to the hydrogel in order to encourage effective DNA hybridization.

Appendix

Appendix 5A. Supplementary data

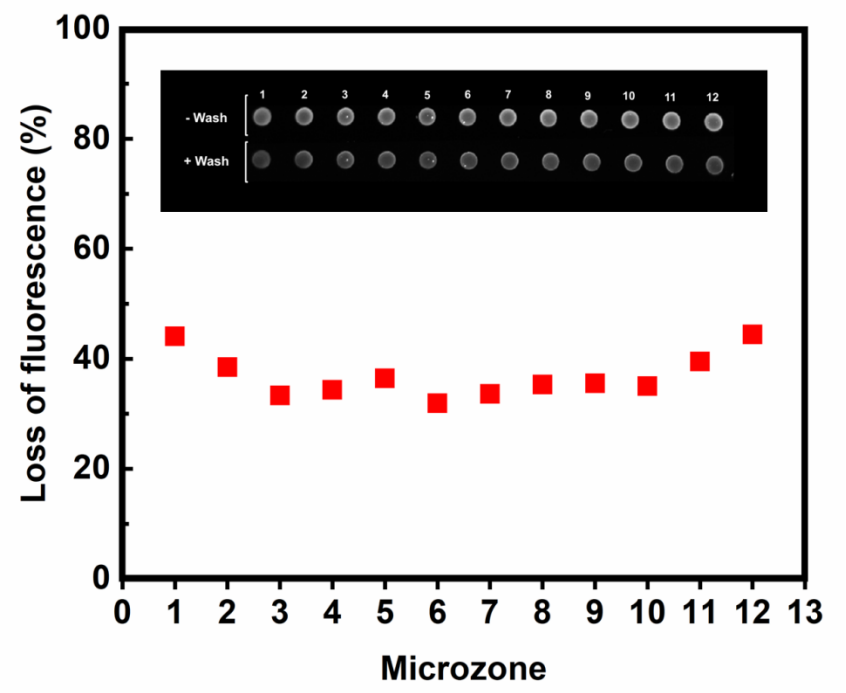

Fig.5A1 RCA product is not efficiently entrapped in printed hydrogels prepared by depositing the POH+RCA layer on top of a dried POA foundational layer Alexa Fluor-labeled RCA product was printed in the hydrogel assembly on a multi-well nitrocellulose wax printed template. The multi-sample substrate was washed in 1x PBST containing 0.05% Tween-20. The loss of fluorescence across the microzones indicates that this particular hydrogel configuration is weakly cross-linked and cannot efficiently entrap the RCA product.

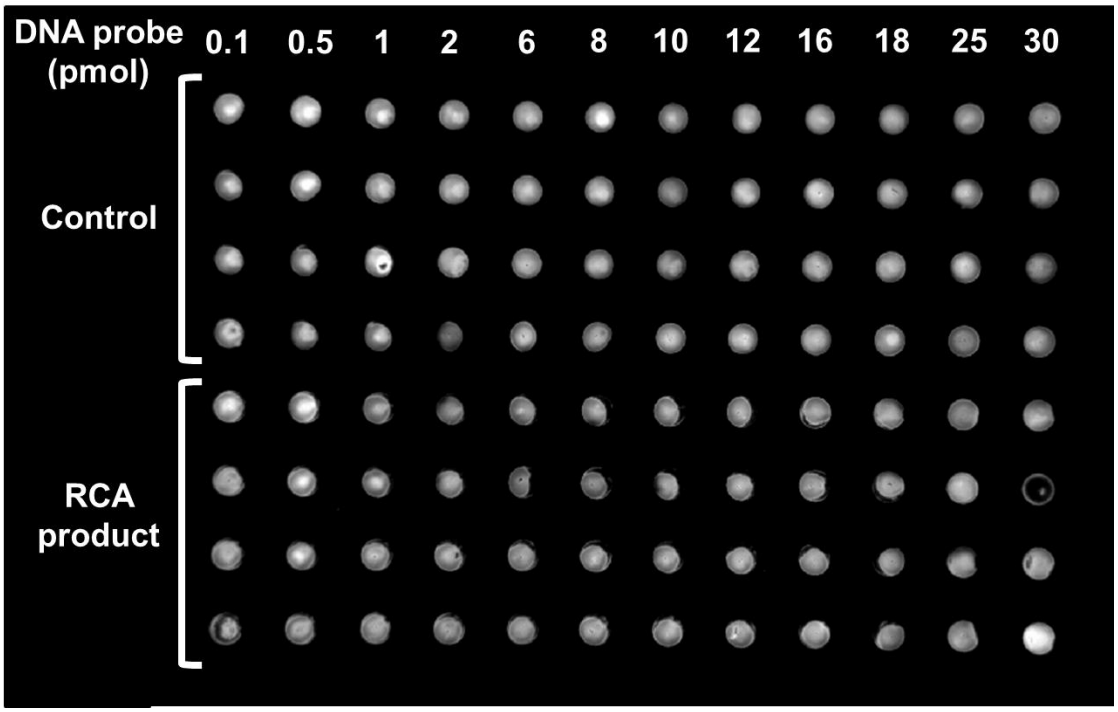

Fig.5A2 Printed hydrogel hybridization assay with DNA probes conjugated to polystyrene beads RCA product was printed in a hydrogel microarray at a density of 0.03 pmol/microzone. DNA probes were conjugated to streptavidin coated polystyrene microspheres. The DNA probe/bead complexes were suspended in a PBS/BSA binding buffer and incubated with printed RCA product entrapped in hydrogels pre-hydrated in 1x PBS for 2 hours in a humidity chamber. Hybridization was performed with the DNA probe/bead complex to both control (non-RCA product containing) hydrogels and RCA product printed hydrogels. The microarrays were washed in 1x PBS containing 0.05% Tween-20 for 1 hour. In order to visualize the hybridized DNA probe/ bead complexes, the microarray was stained in a 0.02% solution of biotin-4-fluorescein for 20 min and de-stained in 1x PBST for 2 hours.

Chapter 6: Conclusions and Recommendations

The research described in this thesis investigates molecular recognition phenomena in polymer-based technologies with applications in drug delivery and biosensing. Complexation behaviours of modified cyclodextrins with the hydrophobic drug, dexamethasone, were studied for the development of optimized controlled release systems that exploit host-guest interactions. A protocol was developed for the fabrication of a printable hydrogel for the immobilization of biomolecules. Enzyme-substrate and enzyme-inhibitor interactions were investigated within the printable hydrogel. A microarray platform based on the printable hydrogel interface was developed for the screening of inhibitors of the model enzyme, β-lactamase. The application of this platform was extended to the detection of nucleic acid hybridization. Properties of the hydrogel interface were modified and investigated in order to support the requirements of a hybridization assay. The major contributions of each chapter are listed below:

In Chapter 2, βCDs were modified with varying densities of a small, negatively charged moiety (carboxymethyls, CM) and a large, neutral moiety (hydrazides, Hzd) and the solubilization capacities, thermodynamic parameters and aggregative potential of these host–guest interactions were studied. CM/βCD and Hzd/βCD derivatives exhibited similar complexation behaviors with dexamethasone including 1:1 stoichiometry, linear phase solubility profiles, and consistent enthalpy changes. Increased functionalization was found to reduce the stability constants of the βCD derivative/dexamethasone complexes as well as the complexation efficiency (CE) of both βCD derivatives. When Hzd/βCD was grafted onto a polymer support, it displayed a CE value and a stability similar to that of a free, monofunctionalized Hzd/βCD derivative, an affinity significantly higher than those of βCD units functionalized with multiple functional groups. These results strongly suggest that polymer-bound βCD groups are optimal drug carriers. CD aggregates were studied for the first time with nanoparticle tracking analysis (NTA), a technique where the displacement of individual particles as a result of their Brownian motion is directly monitored using laser light diffracted from each individual particle. A direct relationship was found between the CE values of the CM/βCD derivatives and the size of aggregates formed when complexed with dexamethasone. Hzd/βCD aggregates were significantly lower in size and did not demonstrate this relationship between aggregate size and CE value. Given the lower aggregation observed for Hzd/βCD derivatives relative to CM/βCD derivatives, Hzd/βCD

derivatives may be utilized as solubilization agents for hydrophobic drugs and as functional sites in drug delivery vehicles.

Chapter 3 described the fabrication of a printable hydrogel based on injectable/*in situ* gelling aldehyde and hydrazide functionalized poly(oligoethylene glycol methacrylate) (PO) polymers. This is the first description of a method to print a covalently cross-linked hydrogel in the absence of ultraviolet (UV) photopolymerization to initiate gelation. This is a significant result as there is interest in developing covalently cross-linked hydrogels that are fabricated under mild synthetic conditions. The printed hydrogel was demonstrated to effectively immobilize the model enzymes alkaline phosphatase, urease, and β-lactamase as well as facilitate the transport of small molecule substrates, consistent with the needs of an immobilized enzyme biosensor system.

Chapter 4 described the investigation of the printable hydrogel as a sensing interface within the context of a microarray. The printable hydrogel was able to stabilize entrapped enzymes against proteases, drying, and time-dependent denaturation. A microarray-based assay was developed for the screening of β-lactamase inhibitors, critical compounds for preserving the activity of antibiotic therapies among many otherwise antibiotic-resistant bacteria. The assay was able to quantify the dose–response relationships of the inhibitors, all while using 95% less sample than required for a solution assay. Moreover, the assay platform prevented the occurrence of false-positive hits by a class of non-specific inhibitors called promiscuous aggregating inhibitors, a result attributed to the size-exclusion property of the printed hydrogel interface. This is the first demonstration of a drug screening assay that can discriminate between true inhibitors and promiscuous aggregating inhibitors of β-lactamase without the addition of detergents and in the absence of complex instrumentation such as nuclear magnetic resonance (NMR) spectroscopy, dynamic light scattering (DLS) or surface plasmon resonance (SPR) devices.

Chapter 5 examined the application of the printable hydrogel-based microarray in a hybridization assay. RCA product was immobilized in the hydrogel and utilized as a sensing material for the detection of a small, fluorophore labeled oligonucleotide. The RCA product was successfully immobilized in the hydrogel and remained immobilized following aggressive washing, suggesting effective non-covalent entrapment of RCA in the hydrogel.

However, despite systematic changes in hydrogel thickness, cross-link density, probe type, hybridization conditions, and blocking strategies, no clear difference was observed in the fluorescence signal generated following the addition of a complementary DNA probe between control and RCA-printed samples. The results of this study strongly suggest that the printable hydrogel platform must be adapted to fit the requirements of a DNA hybridization assay. Increasing hydrogel porosity and hydrophilicity as well as introducing positive charges to the hydrogel are recommendations that can potentially facilitate effective DNA hybridization and prevent non-specific signals.

The printable hydrogel platform developed in this thesis functions optimally in the monitoring of enzyme-substrate and enzyme-inhibitor interactions and exhibits limitations in the detection of DNA hybridization. As addressed in Chapter 5, developing a printable hydrogel with tunable porosity and zwitterionic character should render the microarray platform more amenable to sensing applications involving DNA hybridization. The printable hydrogel demonstrated great potential as a tool in high-throughput drug screening, specifically in its ability to prevent false positive hits by promiscuous aggregating inhibitors. In order to validate the printable hydrogel microarray as an effective platform for drug screening assays, a large library of well-characterized, small molecule inhibitors (typically consisting of 10,000-20,000 compounds) should be tested against a model screening enzyme. If the printable hydrogel microarray is able to prevent inhibition by all of the promiscuous aggregating inhibitors present in the library, this demonstration will support the use of the hydrogel platform as a tool to address the high false positive rates that are frequently encountered during early stage drug discovery campaigns.

To broaden the scope of prospective applications for this platform, a library of printable hydrogels should be developed with a range of tunable properties such as mechanical stiffness, swelling capacity, degradability, and the incorporation of RGD sites in order to promote cell adhesion . With the ability to exert fine control over these material properties, the printable hydrogel can be employed as a platform in cell-laden hydrogel microarrays for phenotypic drug screening applications.[277] In contrast to target-based drug discovery, which focuses on an enzyme or molecular target implicated in a disease pathway, phenotypic screens monitor the drug response of an *in vitro* model by employing assays that test for a desired cellular response.[278] Phenotypic screens offer a more realistic view of the physiological response

triggered by a drug candidate, leading to increased interest in optimizing the platforms that are currently employed in these assays.[279] Since the three-dimensional hydrogel microenvironment has proven to be ideal for culturing cells, incorporating cells in the printable hydrogel described in this thesis would be a natural extension of the microarray platform.[280] Demonstrating that the printable hydrogel is able to promote viability and growth of a robust cell line (such as NIH 3T3 cells) would be a critical first in the development of a cell-laden hydrogel microarray. Thereafter, a model *in vitro* drug screening system can be integrated within the printable hydrogel microarray platform. An ideal example system is the investigation of the toxicity of various drug candidates on primary liver hepatocytes.[281]

The βCD derivatives and printable hydrogel developed and investigated in this thesis can also be extended into additional sensing applications. CDs modified with graphene have been shown to demonstrate enhanced electrochemical reactivity when present in a complexed state.[283] For example, Guo et al. coated a glassy carbon electrode with CD-conjugated graphene and found that the supramolecular interaction of guest molecules with the CD cavity increased the concentration of analytes at the electrode, resulting in an increased peak current. This phenomenon has been exploited in a number of different sensing applications.[284, 285] A paper-based sensor employing βCD as both a hydrogel cross-linker and the sensing component can be developed with the materials described in this thesis. As of yet, a hydrogel film that is covalently cross-linked by a graphene-βCD conjugate has not been reported.[286] Paper-based graphene sensors have previously been designed for gas sensing and were fabricated by transferring thin films of graphene generated via chemical vapour deposition onto paper. [287, 288] A graphene-βCD conjugate can be synthesized by reacting a multi-functionalized hydrazide-βCD with graphene oxide (GO). The GO-βCD conjugate can be reduced by L-ascorbic acid in order to recover its electrically conductive properties. Hydrogel fabrication can proceed through the established printing protocol, with the aldehyde functionalized PO polymer deposited onto the paper substrate, followed by an aqueous dispersion of the graphene-βCD conjugate. There are a variety of analytes that can be investigated. Cholesterol is a suitable choice since it possesses clinical relevance as a metabolite and demonstrates high binding capacity for the CD cavity. Electrical measurements can be made using a multi-meter and electrodes can be drawn onto the paper sensor using a conductive silver ink solution.

References

1. Nakamura T, Kaneko Y, Nishibori E, Nabeshima T. Molecular recognition by multiple metal coordination inside wavy-stacked macrocycles. *Nature Communications* **8**, 129 (2017).

2. Gellman SH. Introduction: molecular recognition. ACS Publications, pp. 1231-1232 (1997).

3. Tang Z, Chang CEA. Binding Thermodynamics and Kinetics Calculations Using Chemical Host and Guest: A Comprehensive Picture of Molecular Recognition. *Journal of Chemical Theory and Computation*, **14** (1), 303-318 (2017).

4. Williams DH, Stephens E, O'Brien DP, Zhou M. Understanding noncovalent interactions: Ligand binding energy and catalytic efficiency from ligand-induced reductions in motion within receptors and enzymes. *Angewandte Chemie International Edition* **43**, 6596-6616 (2004).

5. Pollard TD. A guide to simple and informative binding assays. *Molecular Biology of the Cell* **21**, 4061-4067 (2010).

6. Dam TK, Brewer CF. Applications of Isothermal Titration Calorimetry to Lectin–Carbohydrate Interactions. In: *Lectins* Elsevier, pp. 75-101 (2007).

7. Corzo J. Time, the forgotten dimension of ligand binding teaching. *Biochemistry and Molecular Biology Education* **34**, 413-416 (2006).

8. Kuriyan J, Konforti B, Wemmer D. *The Molecules of Life: Physical and Chemical Principles*. Garland Science (2012).

9. Bongrand P. Ligand-receptor interactions. *Reports on Progress in Physics* **62**, 921 (1999).

10. Stauffer DA, Barrans Jr RE, Dougherty DA. Concerning the thermodynamics of molecular recognition in aqueous and organic media. Evidence for significant heat capacity effects. *The Journal of Organic Chemistry* **55**, 2762-2767 (1990).

11. Fox JM, Zhao M, Fink MJ, Kang K, Whitesides GM. The Molecular Origin of Enthalpy/Entropy Compensation in Biomolecular Recognition. *Annual Review of Biophysics*, **47**, 223-250 (2017).

12. Ryde U. A fundamental view of enthalpy–entropy compensation. *MedChemComm* **5**, 1324-1336 (2014).

13. Hunter CA. Quantifying intermolecular interactions: guidelines for the molecular recognition toolbox. *Angewandte Chemie International Edition* **43**, 5310-5324 (2004).

14. Ben-Naim AY. The Binding Isotherm. In: *Cooperativity and Regulation in Biochemical Processes*, Springer (2001).

15. Hulme EC, Trevethick MA. Ligand binding assays at equilibrium: validation and interpretation. *British Journal of Pharmacology* **161**, 1219-1237 (2010).

16. Mihailescu M, Gilson MK. On the theory of noncovalent binding. *Biophysical Journal* **87**, 23-36 (2004).

17. Meyer-Almes F-J. Kinetic binding assays for the analysis of protein–ligand interactions. *Drug Discovery Today: Technologies* **17**, 1-8 (2015).

18. De Jong LA, Uges DR, Franke JP, Bischoff R. Receptor–ligand binding assays: technologies and applications. *Journal of Chromatography B* **829**, 1-25 (2005).

19. Zhu H, *et al.* d-PET-controlled "off-on" Polarity-sensitive Probes for Reporting Local Hydrophilicity within Lysosomes. *Scientific Reports* **6**, 35627 (2016).

20. Ozers MS, *et al.* Equilibrium binding of estrogen receptor with DNA using fluorescence anisotropy. *Journal of Biological Chemistry* **272**, 30405-30411 (1997).

21. Ma W, Yang L, He L. Overview of the detection methods for equilibrium dissociation constant K_D of drug-receptor interaction. *Journal of Pharmaceutical Analysis* **8**, 147-152 (2018).

22. Catena GC, Bright FV. Thermodynamic study on the effects of. beta.-cyclodextrin inclusion with anilinonaphthalenesulfonates. *Analytical Chemistry* **61**, 905-909 (1989).

23. Brooks HB, *et al.* Basics of Enzymatic Assays for HTS. (2012).

24. Burlingham BT, Widlanski TS. An intuitive look at the relationship of K_i and IC_{50}: A more general use for the Dixon plot. *Journal of Chemical Education* **80**, 214 (2003).

25. Mohan C, Long K, Mutneja M. An Introduction to Inhibitors and Their Biological Applications. *EMD Millipore Corp*, 3-13 (2013).

26. Stepanov I. The Heats of Dilution. Calorimetry and Van't-Hoff. *arXiv preprint physics/0010075*, (2000).

27. Krug R, Hunter W, Grieger R. Enthalpy-entropy compensation. 1. Some fundamental statistical problems associated with the analysis of van't Hoff and Arrhenius data. *The Journal of Physical Chemistry* **80**, 2335-2341 (1976).

28. Freire E, Mayorga OL, Straume M. Isothermal titration calorimetry. *Analytical Chemistry* **62**, 950A-959A (1990).

29. Velázquez-Campoy A, Ohtaka H, Nezami A, Muzammil S, Freire E. Isothermal titration calorimetry. *Current Protocols in Cell Biology* **23**, 17.18. 11-17.18. 24 (2004).

30. Lewis EA, Murphy KP. Isothermal titration calorimetry. In: *Protein-Ligand Interactions*, pp. 1-15 Springer (2005).

31. Freyer MW, Lewis EA. Isothermal titration calorimetry: experimental design, data analysis, and probing macromolecule/ligand binding and kinetic interactions. *Methods in Cell Biology* **84**, 79-113 (2008).

32. Doyle ML. Characterization of binding interactions by isothermal titration calorimetry. *Current Opinion in Biotechnology* **8**, 31-35 (1997).

33. Turnbull WB, Daranas AH. On the value of c: can low affinity systems be studied by isothermal titration calorimetry? *Journal of the American Chemical Society* **125**, 14859-14866 (2003).

34. Dahab AA. Rapid analysis of drug binding to β-cyclodextrin: part II substituents effect on physicochemical and co-conformational stability of drug/cyclodextrin complex. *RSC Advances* **4**, 6624-6637 (2014).

35. Lehn J-M. Supramolecular chemistry: Where from? Where to? *Chemical Society Reviews* **46**, 2378-2379 (2017).

36. Kyba EP, *et al.* Host-guest complexation. 1. Concept and illustration. *Journal of the American Chemical Society* **99**, 2564-2571 (1977).

37. Lehn J-M. *Supramolecular chemistry*. Vch, Weinheim Germany (1995).

38. Lehn JM. Perspectives in supramolecular chemistry—from molecular recognition towards molecular information processing and self-organization. *Angewandte Chemie International Edition* **29**, 1304-1319 (1990).

39. Schneider HJ. Binding mechanisms in supramolecular complexes. *Angewandte Chemie International Edition* **48**, 3924-3977 (2009).

40. Yamabe T, Hori K, Akagi K, Fukui K. Stability of crown ether complexes: a mo theoretical study. *Tetrahedron* **35**, 1065-1072 (1979).

41. Sardjono RE, Rachmawati R. Green Synthesis of Oligomer Calixarenes. In: *Green Chemical Processing and Synthesis*, InTech (2017).

42. Biesaga M, Pyrzyńska K, Trojanowicz M. Porphyrins in analytical chemistry. A review. *Talanta* **51**, 209-224 (2000).

43. Del Valle EM. Cyclodextrins and their uses: a review. *Process Biochemistry* **39**, 1033-1046 (2004).

44. Loftsson T, Duchêne D. Cyclodextrins and their pharmaceutical applications. *International Journal of Pharmaceutics* **329**, 1-11 (2007).

45. Wenz G. Cyclodextrins as building blocks for supramolecular structures and functional units. *Angewandte Chemie International Edition in English* **33**, 803-822 (1994).

46. Brewster ME, Loftsson T. Cyclodextrins as pharmaceutical solubilizers. *Advanced Drug Delivery Reviews* **59**, 645-666 (2007).

47. Biwer A, Antranikian G, Heinzle E. Enzymatic production of cyclodextrins. *Applied Microbiology and Biotechnology* **59**, 609-617 (2002).

48. Eastburn SD, Tao BY. Applications of modified cyclodextrins. *Biotechnology Advances* **12**, 325-339 (1994).

49. Cremer PS, Flood AH, Gibb BC, Mobley DL. Collaborative routes to clarifying the murky waters of aqueous supramolecular chemistry. *Nature Chemistry* **10**, 8 (2018).

50. Szente L, Szemán J. Cyclodextrins in analytical chemistry: Host–guest type molecular recognition. 8024-8030, ACS Publications (2013).

51. Blow DM, Smith JM. Enzyme substrate and inhibitor interactions. *Phil Trans R Soc Lond B* **272**, 87-97 (1975).

52. Lichtenthaler FW. 100 Years "Schlüssel-Schloss-Prinzip": What Made Emil Fischer Use this Analogy? *Angewandte Chemie International Edition in English* **33**, 2364-2374 (1995).

53. Koshland Jr DE. The key–lock theory and the induced fit theory. *Angewandte Chemie International Edition in English* **33**, 2375-2378 (1995).

54. Bosshard HR. Molecular recognition by induced fit: how fit is the concept? *Physiology* **16**, 171-173 (2001).

55. Boehr DD, Nussinov R, Wright PE. The role of dynamic conformational ensembles in biomolecular recognition. *Nature Chemical Biology* **5**, 789 (2009).

56. Marangoni AG. Reversible enzyme inhibition. *Enzyme Kinetics: A Modern Approach*, 61-69 (2002).

57. Williams JW, Morrison JF. The kinetics of reversible tight-binding inhibition. In: *Methods in Enzymology*, Vol. 63, pp. 437-467, Elsevier (1979).

58. Moran LA, Horton HR, Scrimgeour KG, Perry MD. *Principles of Biochemistry*. Pearson Boston (2012).

59. Seidler J, McGovern SL, Doman TN, Shoichet BK. Identification and prediction of promiscuous aggregating inhibitors among known drugs. *Journal of Medicinal Chemistry* **46**, 4477-4486 (2003).

60. McGovern SL, Helfand BT, Feng B, Shoichet BK. A specific mechanism of nonspecific inhibition. *Journal of Medicinal Chemistry* **46**, 4265-4272 (2003).

61. McGovern SL, Caselli E, Grigorieff N, Shoichet BK. A common mechanism underlying promiscuous inhibitors from virtual and high-throughput screening. *Journal of Medicinal Chemistry* **45**, 1712-1722 (2002).

62. Anderson ML. *Nucleic Acid Hybridization*. Bios Scientific Publishers Ltd (1999).

63. Marky LA, Lee HT, Garcia A. Watson–Crick Base Pairs and Nucleic Acids Stability. *e LS*, (2001).

64. Owczarzy R, *et al.* Effects of sodium ions on DNA duplex oligomers: improved predictions of melting temperatures. *Biochemistry* **43**, 3537-3554 (2004).

65. Kessler C. Overview on Factors Influencing Nucleic Acid Hybridization. In: *Nonradioactive Analysis of Biomolecules*, pp.437-442, Springer (2000).

66. Iqbal SS, Mayo MW, Bruno JG, Bronk BV, Batt CA, Chambers JP. A review of molecular recognition technologies for detection of biological threat agents. *Biosensors and Bioelectronics* **15**, 549-578 (2000).

67. Liao X, Chen G, Jiang M. Hydrogels locked by molecular recognition aiming at responsiveness and functionality. *Polymer Chemistry* **4**, 1733-1745 (2013).

68. Nakahata M, Takashima Y, Yamaguchi H, Harada A. Redox-responsive self-healing materials formed from host–guest polymers. *Nature Communications* **2**, 511 (2011).

69. van de Manakker F, van der Pot M, Vermonden T, van Nostrum CF, Hennink WE. Self-assembling hydrogels based on β-cyclodextrin/cholesterol inclusion complexes. *Macromolecules* **41**, 1766-1773 (2008).

70. Tamesue S, Takashima Y, Yamaguchi H, Shinkai S, Harada A. Photoswitchable supramolecular hydrogels formed by cyclodextrins and azobenzene polymers. *Angewandte Chemie International Edition* **49**, 7461-7464 (2010).

71. Koopmans C, Ritter H. Formation of physical hydrogels via host− guest interactions of β-cyclodextrin polymers and copolymers bearing adamantyl groups. *Macromolecules* **41**, 7418-7422 (2008).

72. Harada A, Kobayashi R, Takashima Y, Hashidzume A, Yamaguchi H. Macroscopic self-assembly through molecular recognition. *Nature Chemistry* **3**, 34 (2011).

73. Li J. Self-assembled supramolecular hydrogels based on polymer–cyclodextrin inclusion complexes for drug delivery. *NPG Asia Materials* **2**, 112 (2010).

74. Taylor DL, in het Panhuis M. Self-healing hydrogels. *Advanced Materials* **28**, 9060-9093 (2016).

75. Wang Z, *et al.* A Novel Rapidly Self-healing Host-guest Supramolecular Hydrogel with High Mechanical Strength and Excellent Biocompatibility. *Angewandte Chemie International Edition* **57**, 9008 (2018).

76. Yoshimura I, Miyahara Y, Kasagi N, Yamane H, Ojida A, Hamachi I. Molecular recognition in a supramolecular hydrogel to afford a semi-wet sensor chip. *Journal of the American Chemical Society* **126**, 12204-12205 (2004).

77. Yhaya F, Lim J, Kim Y, Liang M, Gregory AM, Stenzel MH. Development of micellar novel drug carrier utilizing temperature-sensitive block copolymers containing cyclodextrin moieties. *Macromolecules* **44**, 8433-8445 (2011).

78. Hinterdorfer P, Dufrêne YF. Detection and localization of single molecular recognition events using atomic force microscopy. *Nature Methods* **3**, 347 (2006).

79. Cobo I, Li M, Sumerlin BS, Perrier S. Smart hybrid materials by conjugation of responsive polymers to biomacromolecules. *Nature Materials* **14**, 143 (2015).

80. Harris JM, Chess RB. Effect of pegylation on pharmaceuticals. *Nature Reviews Drug Discovery* **2**, 214 (2003).

81. Pelegri-O'Day EM, Lin E-W, Maynard HD. Therapeutic protein–polymer conjugates: advancing beyond PEGylation. *Journal of the American Chemical Society* **136**, 14323-14332 (2014).

82. Duncan R. The dawning era of polymer therapeutics. *Nature Reviews Drug Discovery* **2**, 347 (2003).

83. Hoffman AS, Stayton PS. Conjugates of stimuli-responsive polymers and proteins. *Progress in Polymer Science* **32**, 922-932 (2007).

84. Heredia KL, Maynard HD. Synthesis of protein–polymer conjugates. *Organic & Biomolecular Chemistry* **5**, 45-53 (2006).

85. Vanparijs N, *et al.* Polymer-protein conjugation via a 'grafting to' approach – a comparative study of the performance of protein-reactive RAFT chain transfer agents. *Polymer Chemistry* **6**, 5602-5614 (2015).

86. Grover GN, Maynard HD. Protein-Polymer Conjugates: Synthetic Approaches by Controlled Radical Polymerizations & Interesting Applications. *Current Opinion in Chemical Biology* **14**, 818-827 (2010).

87. Roberts M, Bentley M, Harris J. Chemistry for peptide and protein PEGylation. *Advanced Drug Delivery Reviews* **64**, 116-127 (2012).

88. Bulmus V, Ding Z, Long CJ, Stayton PS, Hoffman AS. Site-specific polymer− streptavidin bioconjugate for pH-controlled binding and triggered release of biotin. *Bioconjugate Chemistry* **11**, 78-83 (2000).

89. Hoffman AS. Bioconjugates of intelligent polymers and recognition proteins for use in diagnostics and affinity separations. *Clinical Chemistry* **46**, 1478-1486 (2000).

90. Stayton PS, *et al.* Control of protein–ligand recognition using a stimuli-responsive polymer. *Nature* **378**, 472 (1995).

91. Ding Z, Long CJ, Hayashi Y, Bulmus EV, Hoffman AS, Stayton PS. Temperature control of biotin binding and release with a streptavidin-poly (N-isopropylacrylamide) site-specific conjugate. *Bioconjugate Chemistry* **10**, 395-400 (1999).

92. Irwin J, *et al.* A Molecular Basis for Innovation in Drug Excipients. *Clinical Pharmacology & Therapeutics* **101**, 320-323 (2017).

93. Akers MJ. Excipient–drug interactions in parenteral formulations. *Journal of Pharmaceutical Sciences* **91**, 2283-2300 (2002).

94. Stegemann S, Leveiller F, Franchi D, De Jong H, Lindén H. When poor solubility becomes an issue: from early stage to proof of concept. *European Journal of Pharmaceutical Sciences* **31**, 249-261 (2007).

95. Gidwani B, Vyas A. A comprehensive review on cyclodextrin-based carriers for delivery of chemotherapeutic cytotoxic anticancer drugs. *BioMed Research International* **2015**, (2015).

96. Larson N, Ghandehari H. Polymeric conjugates for drug delivery. *Chemistry of Materials* **24**, 840-853 (2012).

97. Zhang X, *et al.* A hydrotropic β-cyclodextrin grafted hyperbranched polyglycerol co-polymer for hydrophobic drug delivery. *Acta Biomaterialia* **7**, 585-592 (2011).

98. Namgung R, *et al.* Poly-cyclodextrin and poly-paclitaxel nano-assembly for anticancer therapy. *Nature Communications* **5**, 3702 (2014).

99. Doré K, *et al.* Fluorescent polymeric transducer for the rapid, simple, and specific detection of nucleic acids at the zeptomole level. *Journal of the American Chemical Society* **126**, 4240-4244 (2004).

100. Rahman MA, Kwon N-H, Won M-S, Choe ES, Shim Y-B. Functionalized conducting polymer as an enzyme-immobilizing substrate: an amperometric glutamate microbiosensor for in vivo measurements. *Analytical Chemistry* **77**, 4854-4860 (2005).

101. Lee T-Y, Shim Y-B. Direct DNA hybridization detection based on the oligonucleotide-functionalized conductive polymer. *Analytical Chemistry* **73**, 5629-5632 (2001).

102. Hoare TR, Kohane DS. Hydrogels in drug delivery: Progress and challenges. *Polymer* **49**, 1993-2007 (2008).

103. Hoffman AS. Hydrogels for biomedical applications. *Advanced Drug Delivery Reviews* **64**, 18-23 (2012).

104. Hennink WE, van Nostrum CF. Novel crosslinking methods to design hydrogels. *Advanced Drug Delivery Reviews* **64**, 223-236 (2012).

105. Patenaude M, Smeets NM, Hoare T. Designing Injectable, Covalently Cross-Linked Hydrogels for Biomedical Applications. *Macromolecular Rapid Communications* **35**, 598-617 (2014).

106. Smeets NM, Bakaic E, Patenaude M, Hoare T. Injectable and tunable poly (ethylene glycol) analogue hydrogels based on poly (oligoethylene glycol methacrylate). *Chemical Communications* **50**, 3306-3309 (2014).

107. Xu F, Sheardown H, Hoare T. Reactive electrospinning of degradable poly(oligoethylene glycol methacrylate)-based nanofibrous hydrogel networks. *Chemical Communications* **52**, 1451-1454 (2016).

108. Yoo HS. Photo-cross-linkable and thermo-responsive hydrogels containing chitosan and Pluronic for sustained release of human growth hormone (hGH). *Journal of Biomaterials Science, Polymer Edition* **18**, 1429-1441 (2007).

109. Mateen R, Hoare T. Injectable, in situ gelling, cyclodextrin–dextran hydrogels for the partitioning-driven release of hydrophobic drugs. *Journal of Materials Chemistry B* **2**, 5157-5167 (2014).

110. Larrañeta E, Stewart S, Ervine M, Al-Kasasbeh R, Donnelly RF. Hydrogels for Hydrophobic Drug Delivery. Classification, Synthesis and Applications. *Journal of Functional Biomaterials* **9**, 13 (2018).

111. Guiseppi-Elie A. Electroconductive hydrogels: synthesis, characterization and biomedical applications. *Biomaterials* **31**, 2701-2716 (2010).

112. Wisniewski N, Reichert M. Methods for reducing biosensor membrane biofouling. *Colloids and Surfaces B: Biointerfaces* **18**, 197-219 (2000).

113. White EM, Yatvin J, Grubbs III JB, Bilbrey JA, Locklin J. Advances in smart materials: Stimuli-responsive hydrogel thin films. *Journal of Polymer Science Part B: Polymer Physics* **51**, 1084-1099 (2013).

114. Tokarev I, Minko S. Stimuli-responsive hydrogel thin films. *Soft Matter* **5**, 511-524 (2009).

115. Kuckling D. Responsive hydrogel layers—from synthesis to applications. *Colloid and Polymer Science* **287**, 881-891 (2009).

116. Deng X, *et al.* Poly (oligoethylene glycol methacrylate) dip-coating: turning cellulose paper into a protein-repellent platform for biosensors. *Journal of the American Chemical Society* **136**, 12852-12855 (2014).

117. Shundo A, *et al.* Facile microcapsule fabrication by spray deposition of a supramolecular hydrogel. *RSC Advances* **4**, 36097-36100 (2014).

118. Chollet B, *et al.* Multiscale surface-attached hydrogel thin films with tailored architecture. *ACS Applied Materials & Interfaces* **8**, 11729-11738 (2016).

119. Limem S, McCallum D, Wallace GG, Calvert P. Inkjet printing of self-assembling polyelectrolyte hydrogels. *Soft Matter* **7**, 3818-3826 (2011).

120. Tan Z, Parisi C, Di Silvio L, Dini D, Forte AE. Cryogenic 3D printing of super soft hydrogels. *Scientific Reports* **7**, 16293 (2017).

121. Nakamura M, *et al.* Biocompatible inkjet printing technique for designed seeding of individual living cells. *Tissue Engineering* **11**, 1658-1666 (2005).

122. Farina M, *et al.* Transcutaneously refillable, 3D-printed biopolymeric encapsulation system for the transplantation of endocrine cells. *Biomaterials*, (2018).

123. Lilly JL, Romero G, Xu W, Shin HY, Berron BJ. Characterization of molecular transport in ultrathin hydrogel coatings for cellular immunoprotection. *Biomacromolecules* **16**, 541-549 (2015).

124. Tokarev I, Minko S. Multiresponsive, Hierarchically Structured Membranes: New, Challenging, Biomimetic Materials for Biosensors, Controlled Release, Biochemical Gates, and Nanoreactors. *Advanced Materials* **21**, 241-247 (2009).

125. Suri JT, Cordes DB, Cappuccio FE, Wessling RA, Singaram B. Continuous glucose sensing with a fluorescent thin-film hydrogel. *Angewandte Chemie* **115**, 6037-6039 (2003).

126. Fang H, Kaur G, Wang B. Progress in boronic acid-based fluorescent glucose sensors. *Journal of Fluorescence* **14**, 481-489 (2004).

127. Ikeda M, Ochi R, Hamachi I. Supramolecular hydrogel-based protein and chemosensor array. *Lab on a Chip* **10**, 3325-3334 (2010).

128. Sadeghi I, Yi H, Asatekin A. A Method for Manufacturing Membranes with Ultrathin Hydrogel Selective Layers for Protein Purification: Interfacially Initiated Free Radical Polymerization (IIFRP). *Chemistry of Materials* **30**, 1265-1276 (2018).

129. Yamaguchi N, Zhang L, Chae B-S, Palla CS, Furst EM, Kiick KL. Growth factor mediated assembly of cell receptor-responsive hydrogels. *Journal of the American Chemical Society* **129**, 3040-3041 (2007).

130. Soontornworajit B, Zhou J, Shaw MT, Fan T-H, Wang Y. Hydrogel functionalization with DNA aptamers for sustained PDGF-BB release. *Chemical Communications* **46**, 1857-1859 (2010).

131. Tavakoli J, Tang Y. Hydrogel based sensors for biomedical applications: An updated review. *Polymers* **9**, 364 (2017).

132. Tan B, Zhao H, Du L, Gan X, Quan X. A versatile fluorescent biosensor based on target-responsive graphene oxide hydrogel for antibiotic detection. *Biosensors and Bioelectronics* **83**, 267-273 (2016).

133. Alev-Tuzuner B, Beyler-Cigil A, Vezir Kahraman M, Yarat A. PEG-based hydrogel-coated test strip for on-site urea determination. *International Journal of Polymeric Materials and Polymeric Biomaterials*, 1-10 (2018).

134. Rubina AY, Kolchinsky A, Makarov AA, Zasedatelev AS. Why 3-D? Gel-based microarrays in proteomics. *Proteomics* **8**, 817-831 (2008).

135. Gumuscu B, Bomer JG, van den Berg A, Eijkel JC. Photopatterning of hydrogel microarrays in closed microchips. *Biomacromolecules* **16**, 3802-3810 (2015).

136. Kiyonaka S, Sada K, Yoshimura I, Shinkai S, Kato N, Hamachi I. Semi-wet peptide/protein array using supramolecular hydrogel. *Nature Materials* **3**, 58 (2003).

137. Beyer A, Pollok S, Berg A, Weber K, Popp J. Easy daylight fabricated hydrogel array for colorimetric DNA analysis. *Macromolecular Bioscience* **14**, 889-898 (2014).

138. Jansook P, Kurkov SV, Loftsson T. Cyclodextrins as solubilizers: formation of complex aggregates. *Journal of Pharmaceutical Sciences* **99**, 719-729 (2010).

139. Kurkov SV, Loftsson T. Cyclodextrins. *International Journal of Pharmaceutics* **453**, 167-180 (2013).

140. Davis ME, Brewster ME. Cyclodextrin-based pharmaceutics: past, present and future. *Nature Reviews Drug Discovery* **3**, 1023 (2004).

141. Uekama K, Hirayama F, Irie T. Cyclodextrin Drug Carrier Systems. *Chemical Reviews* **98**, 2045-2076 (1998).

142. Szejtli J. The properties and potential uses of cyclodextrin derivatives. *Journal of Inclusion Phenomena and Molecular Recognition in Chemistry* **14**, 25-36 (1992).

143. Çırpanlı Y, *et al.* Antitumoral activity of camptothecin-loaded nanoparticles in 9L rat glioma model. *International Journal of Pharmaceutics* **403**, 201-206 (2011).

144. dos Santos J-FR, Torres-Labandeira J-J, Matthijs N, Coenye T, Concheiro A, Alvarez-Lorenzo C. Functionalization of acrylic hydrogels with α-, β- or γ-cyclodextrin modulates protein adsorption and antifungal delivery. *Acta Biomaterialia* **6**, 3919-3926 (2010).

145. Sajomsang W, *et al.* Water-soluble β-cyclodextrin grafted with chitosan and its inclusion complex as a mucoadhesive eugenol carrier. *Carbohydrate Polymers* **89**, 623-631 (2012).

146. Khan AR, Forgo P, Stine KJ, D'Souza VT. Methods for Selective Modifications of Cyclodextrins. *Chemical Reviews* **98**, 1977-1996 (1998).

147. Szente L, Szejtli J. Highly soluble cyclodextrin derivatives: chemistry, properties, and trends in development. *Advanced Drug Delivery Reviews* **36**, 17-28 (1999).

148. Loftsson T, Brewster ME. Pharmaceutical Applications of Cyclodextrins. 1. Drug Solubilization and Stabilization. *Journal of Pharmaceutical Sciences* **85**, 1017-1025 (1996).

149. Kurkov SV, Ukhatskaya EV, Loftsson T. Drug/cyclodextrin: beyond inclusion complexation. *Journal of Inclusion Phenomena and Macrocyclic Chemistry* **69**, 297-301 (2011).

150. Puskás I, Schrott M, Malanga M, Szente L. Characterization and control of the aggregation behavior of cyclodextrins. *Journal of Inclusion Phenomena and Macrocyclic Chemistry* **75**, 269-276 (2013).

151. Müller BW, Brauns U. Solubilization of drugs by modified β-cyclodextrins. *International Journal of Pharmaceutics* **26**, 77-88 (1985).

152. Arima H, Adachi H, Irie T, Uekama K, Pitha J. Enhancement of the antiinflammatory effect of ethyl 4-biphenylyl acetate in ointment by β-cyclodextrin derivatives: increased absorption and localized activation of the prodrug in rats. *Pharmaceutical Research* **7**, 1152-1156 (1990).

153. Kompantseva E, Gavrilin M, Ushakova L. β-Cyclodextrin derivatives and their applications in pharmacology (a review). *Pharmaceutical Chemistry Journal* **30**, 258-262 (1996).

154. Marques HMC, Hadgraft J, Kellaway IW. Studies of cyclodextrin inclusion complexes. I. The salbutamol-cyclodextrin complex as studied by phase solubility and DSC. *International Journal of Pharmaceutics* **63**, 259-266 (1990).

155. Stojanov M, Nielsen HM, Larsen KL. Cyclodextrins: Efficient biocompatible solubilizing excipients for bromhexine liquid and semi-solid drug delivery systems. *International Journal of Pharmaceutics* **422**, 349-355 (2012).

156. Sun HY, *et al.* New cyclodextrin derivative 6-O-(2-hydroxybutyl)-β-cyclodextrin: preparation and its application in molecular binding and recognition. *Carbohydrate Research* **344**, 1999-2004 (2009).

157. Moya-Ortega MD, Alvarez-Lorenzo C, Sigurdsson HH, Concheiro A, Loftsson T. γ-Cyclodextrin hydrogels and semi-interpenetrating networks for sustained delivery of dexamethasone. *Carbohydrate Polymers* **80**, 900-907 (2010).

158. Stella VJ, Rao VM, Zannou EA, Zia V. Mechanisms of drug release from cyclodextrin complexes. *Advanced Drug Delivery Reviews* **36**, 3-16 (1999).

159. Patenaude M, Hoare T. Injectable, Degradable Thermoresponsive Poly(N-isopropylacrylamide) Hydrogels. *ACS Macro Letters* **1**, 409-413 (2012).

160. Zhang J, Ma PX. Cyclodextrin-based supramolecular systems for drug delivery: Recent progress and future perspective. *Advanced Drug Delivery Reviews* **65**, 1215-1233 (2013).

161. Rivera VA. *Carboxymethylation of Dextran for Surface Modification of Magnetite Nanoparticles*. ProQuest (2009).

162. Zhao L, Xu L, Mitomo H, Yoshii F. Synthesis of pH-sensitive PVP/CM-chitosan hydrogels with improved surface property by irradiation. *Carbohydrate Polymers* **64**, 473-480 (2006).

163. Thomason SC, Kubler DG. Acids as derivatives of aldehydes prepared with silver oxides. *Journal of Chemical Education* **45**, 546 (1968).

164. Wagner BD, Fitzpatrick SJ. A comparison of the host–guest inclusion complexes of 1, 8-ANS and 2, 6-ANS in parent and modified cyclodextrins. *Journal of Inclusion Phenomena and Macrocyclic Chemistry* **38**, 467-478 (2000).

165. Higuchi T, Connors K. Adv anal chem instrum. *Phase-solubility Techniques* **4**, 117-212 (1965).

166. Job P. Formation and stability of inorganic complexes in solution. *Annali di Chimica* **9,** 113 (1928).

167. Velazquez-Campoy A, Freire E. Isothermal titration calorimetry to determine association constants for high-affinity ligands. *Nature Protocols* **1**, 186 (2006).

168. Turnbull WB, Daranas AH. On the Value of c: Can Low Affinity Systems Be Studied by Isothermal Titration Calorimetry? *Journal of the American Chemical Society* **125**, 14859-14866 (2003).

169. Wiseman T, Williston S, Brandts JF, Lin L-N. Rapid measurement of binding constants and heats of binding using a new titration calorimeter. *Analytical Biochemistry* **179**, 131-137 (1989).

170. Wedig M, Holzgrabe U. Resolution of ephedrine derivatives by means of neutral and sulfated heptakis(2,3-di-O-acetyl)β-cyclodextrins using capillary electrophoresis and nuclear magnetic resonance spectroscopy. *Electrophoresis* **20**, 2698-2704 (1999).

171. Soto AM, Kankia BI, Dande P, Gold B, Marky LA. Thermodynamic and hydration effects for the incorporation of a cationic 3-aminopropyl chain into DNA. *Nucleic Acids Research* **30**, 3171-3180 (2002).

172. Sideris EE, Valsami GN, Koupparis MA, Macheras PE. Determination of association constants in cyclodextrin/drug complexation using the Scatchard plot: Application to β-cyclodextrin-anilinonaphthalenesulfonates. *Pharmaceutical Research* **9**, 1568-1574 (1992).

173. Grant DJW, Higuchi T. *Solubility behavior of organic compounds*. John Wiley & Sons (1990).

174. Zhang Z, Wu G, Gao J, Song T. Inclusion Complex of a Bcl-2 Inhibitor with Cyclodextrin: Characterization, Cellular Accumulation, and in Vivo Antitumor Activity. *Molecular Pharmaceutics* **7**, 1348-1354 (2010).

175. Loftsson T, Hreinsdóttir D, Másson M. Evaluation of cyclodextrin solubilization of drugs. *International Journal of Pharmaceutics* **302**, 18-28 (2005).

176. Usayapant A, Karara AH, Narurkar MM. Effect of 2-hydroxypropyl-β-cyclodextrin on the ocular absorption of dexamethasone and dexamethasone acetate. *Pharmaceutical Research* **8**, 1495-1499 (1991).

177. Zia V, Rajewski R, Stella V. Effect of cyclodextrin charge on complexation of neutral and charged substrates: comparison of (SBE) 7M-β-CD to HP-β-CD. *Pharmaceutical Research* **18**, 667-673 (2001).

178. Botsi A, Yannakopoulou K, Perly B, Hadjoudis E. Positive or Adverse Effects of Methylation on the Inclusion Behavior of Cyclodextrins. A Comparative NMR Study Using Pheromone Constituents of the Olive Fruit Fly. *The Journal of Organic Chemistry* **60**, 4017-4023 (1995).

179. Nielsen TT, Wintgens V, Amiel C, Wimmer R, Larsen KL. Facile Synthesis of β-Cyclodextrin-Dextran Polymers by "Click" Chemistry. *Biomacromolecules* **11**, 1710-1715 (2010).

180. Messner M, Kurkov SV, Flavià-Piera R, Brewster ME, Loftsson T. Self-assembly of cyclodextrins: The effect of the guest molecule. *International Journal of Pharmaceutics* **408**, 235-247 (2011).

181. Echezarreta-López MM, Perdomo-López I, Estrada E, Vila-Jato JL, Torres-Labandeira JJ. Utility of nuclear magnetic resonance spectroscopy to characterize the structure of dexamethasone sodium phosphate inclusion complexes with cyclodextrins in solution and to analyze potential competitive effects. *Journal of Pharmaceutical Sciences* **91**, 1536-1547 (2002).

182. Fülöp Z, Nielsen TT, Larsen KL, Loftsson T. Dextran-based cyclodextrin polymers: Their solubilizing effect and self-association. *Carbohydrate Polymers* **97**, 635-642 (2013).

183. Ridley BL, Spiro MD, Glushka J, Albersheim P, Darvill A, Mohnen D. A Method for Biotin Labeling of Biologically Active Oligogalacturonides Using a Chemically Stable Hydrazide Linkage. *Analytical Biochemistry* **249**, 10-19 (1997).

184. Rekharsky MV, Inoue Y. Complexation Thermodynamics of Cyclodextrins. *Chemical Reviews* **98**, 1875-1918 (1998).

185. Liu L, Guo Q-X. The Driving Forces in the Inclusion Complexation of Cyclodextrins. *Journal of Inclusion Phenomena and Macrocyclic Chemistry* **42**, 1-14 (2002).

186. Moreau D, Chauvet C, Etienne F, Rannou FP, Corté L. Hydrogel films and coatings by swelling-induced gelation. *Proceedings of the National Academy of Sciences* **113**, 13295-13300 (2016).

187. De Gans B-J, Schubert US. Inkjet printing of well-defined polymer dots and arrays. *Langmuir* **20**, 7789-7793 (2004).

188. Andres CM, Kotov NA. Inkjet deposition of layer-by-layer assembled films. *Journal of the American Chemical Society* **132**, 14496-14502 (2010).

189. Derby B. Inkjet printing of functional and structural materials: fluid property requirements, feature stability, and resolution. *Annual Review of Materials Research* **40**, 395-414 (2010).

190. Kim B, Lee Y, Lee K, Koh W-G. Immobilization of enzymes within hydrogel microparticles to create optical biosensors for the detection of organophosphorus compounds. *Current Applied Physics* **9**, e225-e228 (2009).

191. Zhu X, *et al.* A mild strategy to encapsulate enzyme into hydrogel layer grafted on polymeric substrate. *Langmuir* **30**, 15229-15237 (2014).

192. Yan J, Sun Y, Zhu H, Marcu L, Revzin A. Enzyme-containing hydrogel micropatterns serving a dual purpose of cell sequestration and metabolite detection. *Biosensors and Bioelectronics* **24**, 2604-2610 (2009).

193. Murphy SV, Skardal A, Atala A. Evaluation of hydrogels for bio-printing applications. *Journal of Biomedical Materials Research Part A* **101**, 272-284 (2013).

194. Di Risio S, Yan N. Piezoelectric ink-jet printing of horseradish peroxidase: effect of ink viscosity modifiers on activity. *Macromolecular Rapid Communications* **28**, 1934-1940 (2007).

195. Lesch A, Cortés-Salazar F, Amstutz Vr, Tacchini P, Girault HH. Inkjet printed nanohydrogel coated carbon nanotubes electrodes for matrix independent sensing. *Analytical chemistry* **87**, 1026-1033 (2015).

196. Baroli B. Photopolymerization of biomaterials: issues and potentialities in drug delivery, tissue engineering, and cell encapsulation applications. *Journal of Chemical Technology & Biotechnology: International Research in Process, Environmental & Clean Technology* **81**, 491-499 (2006).

197. Wong I, Lohman TM. A double-filter method for nitrocellulose-filter binding: application to protein-nucleic acid interactions. *Proceedings of the National Academy of Sciences* **90**, 5428-5432 (1993).

198. Segura JL, Mancheno MJ, Zamora F. Covalent organic frameworks based on Schiff-base chemistry: synthesis, properties and potential applications. *Chemical Society Reviews* **45**, (20):5635-71 (2016).

199. Liang, H.C., Chang, W.H., Liang, H.F., Lee, M.H. and Sung, H.W. Crosslinking structures of gelatin hydrogels crosslinked with genipin or a water-soluble carbodiimide. *Journal of Applied Polymer Science* **91**(6),.4017-4026 (2004).

200. Patenaude, M., Campbell, S., Kinio, D., & Hoare, T. Tuning gelation time and morphology of injectable hydrogels using ketone–hydrazide cross-linking. *Biomacromolecules* **15**(3), 781-790 (2014).

201. Bleicher KH, Böhm H-J, Müller K, Alanine AI. A guide to drug discovery: hit and lead generation: beyond high-throughput screening. *Nature Reviews Drug Discovery* **2**, 369 (2003).

202. Butler MS, Blaskovich MA, Cooper MA. Antibiotics in the clinical pipeline at the end of 2015. *The Journal of Antibiotics* **70**, 3 (2017).

203. King AM, *et al.* Aspergillomarasmine A overcomes metallo-β-lactamase antibiotic resistance. *Nature* **510**, 503 (2014).

204. Mitchell P. A perspective on protein microarrays. *Nature Biotechnology* **20**, 225 (2002).

205. Sun H, Chen GY, Yao SQ. Recent advances in microarray technologies for proteomics. *Chemistry & Biology* **20**, 685-699 (2013).

206. van Langen LM, Oosthoek NH, van Rantwijk F, Sheldon RA. Penicillin acylase catalysed synthesis of ampicillin in hydrophilic organic solvents. *Advanced Synthesis & Catalysis* **345**, 797-801 (2003).

207. Palomo JM, Muñoz G, Fernández-Lorente G, Mateo C, Fernández-Lafuente R, Guisán JM. Interfacial adsorption of lipases on very hydrophobic support (octadecyl–Sepabeads): immobilization, hyperactivation and stabilization of the open form of lipases. *Journal of Molecular Catalysis B: Enzymatic* **19**, 279-286 (2002).

208. Dos Santos JC, *et al.* Characterization of supports activated with divinyl sulfone as a tool to immobilize and stabilize enzymes via multipoint covalent attachment. Application to chymotrypsin. *RSC Advances* **5**, 20639-20649 (2015).

209. Bruns N, Tiller JC. Amphiphilic network as nanoreactor for enzymes in organic solvents. *Nano letters* **5**, 45-48 (2005).

210. Wang J, Bowie D, Zhang X, Filipe C, Pelton R, Brennan JD. Morphology and entrapped enzyme performance in inkjet-printed sol–gel coatings on paper. *Chemistry of Materials* **26**, 1941-1947 (2014).

211. Feng D, *et al.* Stable metal-organic frameworks containing single-molecule traps for enzyme encapsulation. *Nature Communications* **6**, 5979 (2015).

212. Romanov V, Davidoff SN, Miles AR, Grainger DW, Gale BK, Brooks BD. A critical comparison of protein microarray fabrication technologies. *Analyst* **139**, 1303-1326 (2014).

213. Shoichet BK. Screening in a spirit haunted world. *Drug Discovery Today* **11**, 607-615 (2006).

214. Rishton GM. Nonleadlikeness and leadlikeness in biochemical screening. *Drug Discovery Today* **8**, 86-96 (2003).

215. Coan KE, Maltby DA, Burlingame AL, Shoichet BK. Promiscuous aggregate-based inhibitors promote enzyme unfolding. *Journal of Medicinal Chemistry* **52**, 2067-2075 (2009).

216. McGovern SL, Shoichet BK. Kinase inhibitors: not just for kinases anymore. *Journal of Medicinal Chemistry* **46**, 1478-1483 (2003).

217. Ryan AJ, Gray NM, Lowe PN, Chung C-w. Effect of detergent on "promiscuous" inhibitors. *Journal of Medicinal Chemistry* **46**, 3448-3451 (2003).

218. Irwin JJ, *et al.* An aggregation advisor for ligand discovery. *Journal of Medicinal Chemistry* **58**, 7076-7087 (2015).

219. Feng BY, Shoichet BK. A detergent-based assay for the detection of promiscuous inhibitors. *Nature Protocols* **1**, 550 (2006).

220. Ferreira RS, *et al.* Complementarity between a docking and a high-throughput screen in discovering new cruzain inhibitors. *Journal of Medicinal Chemistry* **53**, 4891-4905 (2010).

221. Wang Q, Yang Z, Wang L, Ma M, Xu B. Molecular hydrogel-immobilized enzymes exhibit superactivity and high stability in organic solvents. *Chemical Communications*, 1032-1034 (2007).

222. Mariani AM, Natoli ME, Kofinas P. Enzymatic activity preservation and protection through entrapment within degradable hydrogels. *Biotechnology and Bioengineering* **110**, 2994-3002 (2013).

223. Kutcherlapati SR, Yeole N, Jana T. Urease immobilized polymer hydrogel: Long-term stability and enhancement of enzymatic activity. *Journal of Colloid and Interface Science* **463**, 164-172 (2016).

224. Qian Y-C, Chen P-C, Zhu X-Y, Huang X-J. Click synthesis of ionic strength-responsive polyphosphazene hydrogel for reversible binding of enzymes. *RSC Advances* **5**, 44031-44040 (2015).

225. Yang Q, Adrus N, Tomicki F, Ulbricht M. Composites of functional polymeric hydrogels and porous membranes. *Journal of Materials Chemistry* **21**, 2783-2811 (2011).

226. McComb RB, Bowers Jr GN, Posen S. *Alkaline phosphatase*. Springer Science & Business Media (2013).

227. Cicerone MT, Soles CL. Fast dynamics and stabilization of proteins: binary glasses of trehalose and glycerol. *Biophysical Journal* **86**, 3836-3845 (2004).

228. Payne DJ, Cramp R, Winstanley DJ, Knowles D. Comparative activities of clavulanic acid, sulbactam, and tazobactam against clinically important beta-lactamases. *Antimicrobial Agents and Chemotherapy* **38**, 767-772 (1994).

229. Smeets NM, Bakaic E, Yavitt FM, Yang F-C, Rheinstädter MC, Hoare T. Probing the internal morphology of injectable poly (oligoethylene glycol methacrylate) hydrogels by light and small-angle neutron scattering. *Macromolecules* **47**, 6017-6027 (2014).

230. Liu B, *et al.* Parts-per-million of polyethylene glycol as a non-interfering blocking agent for homogeneous biosensor development. *Analytical Chemistry* **85**, 10045-10050 (2013).

231. Feng BY, *et al.* A high-throughput screen for aggregation-based inhibition in a large compound library. *Journal of Medicinal Chemistry* **50**, 2385-2390 (2007).

232. LaPlante SR, *et al.* Compound aggregation in drug discovery: implementing a practical NMR assay for medicinal chemists. *Journal of Medicinal Chemistry* **56**, 5142-5150 (2013).

233. Drummond TG, Hill MG, Barton JK. Electrochemical DNA sensors. *Nature Biotechnology* **21**, 1192 (2003).

234. Schena M, Shalon D, Davis RW, Brown PO. Quantitative monitoring of gene expression patterns with a complementary DNA microarray. *Science* **270**, 467-470 (1995).

235. Jobling MA, Gill P. Encoded evidence: DNA in forensic analysis. *Nature Reviews Genetics* **5**, 739 (2004).

236. Southern EM. DNA microarrays. In: *DNA Arrays*, pp.1-15, Springer (2001).

237. Hardiman G. Microarray technologies–an overview. *Pharmacogenomics* **3**, 293-297 (2002).

238. Wolcott MJ. Advances in nucleic acid-based detection methods. *Clinical Microbiology Reviews* **5**, 370-386 (1992).

239. Hoheisel JD. Microarray technology: beyond transcript profiling and genotype analysis. *Nature Reviews Genetics* **7**, 200 (2006).

240. Heller MJ. DNA microarray technology: devices, systems, and applications. *Annual Review of Biomedical Engineering* **4**, 129-153 (2002).

241. Chan V, Graves DJ, McKenzie SE. The biophysics of DNA hybridization with immobilized oligonucleotide probes. *Biophysical Journal* **69**, 2243-2255 (1995).

242. Liu J. Oligonucleotide-functionalized hydrogels as stimuli responsive materials and biosensors. *Soft Matter* **7**, 6757-6767 (2011).

243. Mabic S, Kano I. Impact of purified water quality on molecular biology experiments. *Clinical Chemistry and Laboratory Medicine* **41**, 486-491 (2003).

244. Draghici S, Khatri P, Eklund AC, Szallasi Z. Reliability and reproducibility issues in DNA microarray measurements. *TRENDS in Genetics* **22**, 101-109 (2006).

245. Diehl F, Grahlmann S, Beier M, Hoheisel JD. Manufacturing DNA microarrays of high spot homogeneity and reduced background signal. *Nucleic Acids Research* **29**, e38-e38 (2001).

246. Jung IY, Kim JS, Choi BR, Lee K, Lee H. Hydrogel Based Biosensors for In Vitro Diagnostics of Biochemicals, Proteins, and Genes. *Advanced Healthcare Materials* **6**, 1601475 (2017).

247. Le Goff GC, Srinivas RL, Hill WA, Doyle PS. Hydrogel microparticles for biosensing. *European Polymer Journal* **72**, 386-412 (2015).

248. Proudnikov D, Timofeev E, Mirzabekov A. Immobilization of DNA in polyacrylamide gel for the manufacture of DNA and DNA–oligonucleotide microchips. *Analytical Biochemistry* **259**, 34-41 (1998).

249. Sorokin N, Chechetkin V, Livshits M, Vasiliskov V, Turygin A, Mirzabekov A. Kinetics of hybridization on the oligonucleotide microchips with gel pads. *Journal of Biomolecular Structure and Dynamics* **21**, 279-288 (2003).

250. Rubina AY, *et al.* Hydrogel drop microchips with immobilized DNA: properties and methods for large-scale production. *Analytical Biochemistry* **325**, 92-106 (2004).

251. Le Goff GC, Blum LJ, Marquette CA. Shrinking Hydrogel-DNA Spots Generates 3D Microdots Arrays. *Macromolecular Bioscience* **13**, 227-233 (2013).

252. Soto CM, Patterson CH, Charles PT, Martin BD, Spector MS. Immobilization and hybridization of DNA in a sugar polyacrylate hydrogel. *Biotechnology and Bioengineering* **92**, 934-942 (2005).

253. Gryadunov D, *et al.* Gel-based microarrays in clinical diagnostics in Russia. *Expert Review of Molecular Diagnostics* **11**, 839-853 (2011).

254. Tanase CP, Albulescu R, Neagu M. Application of 3D hydrogel microarrays in molecular diagnostics: advantages and limitations. *Expert Review of Molecular Diagnostics* **11**, 461-464 (2011).

255. Tang J, Xiao P. Polymerizing immobilization of acrylamide-modified nucleic acids and its application. *Biosensors and Bioelectronics* **24**, 1817-1824 (2009).

256. Meiring JE, *et al.* Hydrogel biosensor array platform indexed by shape. *Chemistry of Materials* **16**, 5574-5580 (2004).

257. Ali MM, *et al.* Rolling circle amplification: a versatile tool for chemical biology, materials science and medicine. *Chemical Society Reviews* **43**, 3324-3341 (2014).

258. Zhao W, Ali MM, Brook MA, Li Y. Rolling circle amplification: applications in nanotechnology and biodetection with functional nucleic acids. *Angewandte Chemie International Edition* **47**, 6330-6337 (2008).

259. Nallur G, *et al.* Signal amplification by rolling circle amplification on DNA microarrays. *Nucleic Acids Research* **29**, e118-e118 (2001).

260. Clausson C-M, *et al.* Compaction of rolling circle amplification products increases signal integrity and signal-to-noise ratio. *Scientific Reports* **5**, 12317 (2015).

261. Borden JR, Paredes CJ, Papoutsakis ET. Diffusion, Mixing, and Associated Dye Effects in DNA-Microarray Hybridizations. *Biophysical Journal* **89**, 3277-3284 (2005).

262. Belosludtsev Y, *et al.* DNA microarrays based on noncovalent oligonucleotide attachment and hybridization in two dimensions. *Analytical Biochemistry* **292**, 250-256 (2001).

263. Han T, *et al.* Improvement in the reproducibility and accuracy of DNA microarray quantification by optimizing hybridization conditions. In: *BMC Bioinformatics*, Vol.7, No.2, p.S17, BioMed Central (2006).

264. Relógio A, Schwager C, Richter A, Ansorge W, Valcárcel J. Optimization of oligonucleotide-based DNA microarrays. *Nucleic Acids Research* **30**, e51-e51 (2002).

265. Leary JJ, Brigati DJ, Ward DC. Rapid and sensitive colorimetric method for visualizing biotin-labeled DNA probes hybridized to DNA or RNA immobilized on nitrocellulose: Bio-blots. *Proceedings of the National Academy of Sciences* **80**, 4045-4049 (1983).

266. Ghindilis AL, *et al.* Sensor Array: Impedimetric Label-Free Sensing of DNA Hybridization in Real Time for Rapid, PCR-Based Detection of Microorganisms. *Electroanalysis* **21**, 1459-1468 (2009).

267. Wöhl T, Brecht M, Lottspeich F, Ammer H. The use of genomic DNA probes for in-gel hybridization. *Electrophoresis* **16**, 739-741 (1995).

268. Xiao PF, *et al.* An improved gel-based DNA microarray method for detecting single nucleotide mismatch. *Electrophoresis* **27**, 3904-3915 (2006).

269. Beyer A, Cialla-May D, Weber K, Popp J. Hydrogel Decorated Chips for Convenient DNA Test. *Macromolecular Chemistry and Physics* **217**, 959-965 (2016).

270. Mateescu A, Wang Y, Dostalek J, Jonas U. Thin hydrogel films for optical biosensor applications. *Membranes* **2**, 40-69 (2012).

271. Charles PT, Stubbs VR, Soto CM, Martin BD, White BJ, Taitt CR. Reduction of non-specific protein adsorption using poly (ethylene) glycol (PEG) modified polyacrylate hydrogels in immunoassays for staphylococcal enterotoxin B detection. *Sensors* **9**, 645-655 (2009).

272. Jain P, *et al.* Poly(ectoine) Hydrogels Resist Nonspecific Protein Adsorption. *Langmuir* **33**, 11264-11269 (2017).

273. Carr LR, Zhou Y, Krause JE, Xue H, Jiang S. Uniform zwitterionic polymer hydrogels with a nonfouling and functionalizable crosslinker using photopolymerization. *Biomaterials* **32**, 6893-6899 (2011).

274. Nilsson KPR, Inganäs O. Chip and solution detection of DNA hybridization using a luminescent zwitterionic polythiophene derivative. *Nature Materials* **2**, 419 (2003).

275. Ho H-A, Najari A, Leclerc M. Optical Detection of DNA and Proteins with Cationic Polythiophenes. *Accounts of Chemical Research* **41**, 168-178 (2008).

276. Åsberg P, Björk P, Höök F, Inganäs O. Hydrogels from a water-soluble zwitterionic polythiophene: Dynamics under pH change and biomolecular interactions observed using quartz crystal microbalance with dissipation monitoring. *Langmuir* **21**, 7292-7298 (2005).

277. Hosseinkhani H, Hosseinkhani M, Khademhosseini A. Emerging technology of hydrogels in drug discovery. *Topics in Multifunctional Biomaterials and Devices*, (2008).

278. Moffat JG, Vincent F, Lee JA, Eder J, Prunotto M. Opportunities and challenges in phenotypic drug discovery: an industry perspective. *Nature Reviews Drug Discovery* **16**, 531 (2017).

279. Esch EW, Bahinski A, Huh D. Organs-on-chips at the frontiers of drug discovery. *Nature Reviews Drug Discovery* **14**, 248 (2015).

280. Tibbitt MW, Anseth KS. Hydrogels as extracellular matrix mimics for 3D cell culture. *Biotechnology and Bioengineering* **103**, 655-663 (2009).

281. Underhill GH, Khetani SR. Bioengineered Liver Models for Drug Testing and Cell Differentiation Studies. *Cellular and Molecular Gastroenterology and Hepatology* **5**, 426-439. e421 (2018).

282. Li Y, Kumacheva E. Hydrogel microenvironments for cancer spheroid growth and drug screening. *Science Advances* **4**, eeaas8998 (2018).

283. Guo Y, Guo S, Ren J, Zhai Y, Dong S, Wang E. Cyclodextrin functionalized graphene nanosheets with high supramolecular recognition capability: synthesis and host− guest inclusion for enhanced electrochemical performance. *ACS Nano* **4**, 4001-4010 (2010).

284. Soylemez S, Hacioglu SO, Kesik M, Unay H, Cirpan A, Toppare L. A Novel and Effective Surface Design: Conducting Polymer/β-Cyclodextrin Host–Guest System for Cholesterol Biosensor. *ACS Applied Materials & Interfaces* **6**, 18290-18300 (2014).

285. Zor E, Bingol H, Ramanaviciene A, Ramanavicius A, Ersoz M. An electrochemical and computational study for discrimination of d-and l-cystine by reduced graphene oxide/β-cyclodextrin. *Analyst* **140**, 313-321 (2015).

286. Li C, Shi G. Functional gels based on chemically modified graphenes. *Advanced Materials* **26**, 3992-4012 (2014).

287. Yang G, Lee C, Kim J, Ren F, Pearton SJ. Flexible graphene-based chemical sensors on paper substrates. *Physical Chemistry Chemical Physics* **15**, 1798-1801 (2013).

288. Kumar S, Kaushik S, Pratap R, Raghavan S. Graphene on Paper: A simple, low-cost chemical sensing platform. *ACS Applied Materials & Interfaces* **7**, 2189-2194 (2015).